ARTIFICIAL ROAD INPUT DATA GENERATION TOOL FOR VEHICLE DURABILITY ASSESSMENT USING ARTIFICIAL INTELLIGENCE

BY

ADEBOLA OLUWASEYI OGUNOIKI

UNIVERSITY OF BIRMINGHAM

A thesis submitted to the College of Engineering and Physical Sciences

of the University of Birmingham for the degree of

DOCTOR OF PHILOSOPHY

School of Mechanical Engineering

College of Engineering and Physical Sciences

The University of Birmingham

May 2015

UNIVERSITY OF BIRMINGHAM

ABSTRACT

Vehicle durability assessment in the automotive industry requires a good knowledge of the road load input the vehicle will experience while in service. This research explored the approach of artificial intelligence for predicting the road load input for road load simulation in the CAE environment prior to the development of a vehicle prototype.

The multi-body dynamics (MBD) simulation of a quarter vehicle test rig, built with the specification of a commercial SUV, and the full vehicle of the same SUV were modelled and validated in SIMPACK using a simple tyre model developed using the tri-axial tyre test rig at the University of Birmingham. The models were used to carry out a road load data characterisation based on the variation in vehicle parameters.

An artificial road input tool (ARIT) based on an optimised NARX artificial neural network architecture was developed to predict the road input for variants of vehicle for a particular vehicle behaviour over a road event. The results of the ARIT were used to run MBD simulations and compared with those from drive file iteration. The results of this research show a successful method of artificial intelligence for the generation of road load data from CAE simulations.

UNIVERSITY OF BIRMINGHAM

Now all glory to God, who is able, through his mighty power at work within us, to accomplish infinitely more than we might ask or think.

To Strive, To Seek, To Find and Not To Yield

Per Ardua Ad Alta

UNIVERSITY OF BIRMINGHAM

ACKNOWLEDGEMENTS

I would like to express my sincere gratitude to my supervisor, Dr O.A. Olatunbosun, for his valuable support, guidance, encouragement and mentorship during the course of this research project.

I would also like to express my thanks to my colleagues: Mohammad Esgandari, Chongfeng Wei and Samaneh Arabi for their helpful suggestions and support in the course of the project. My appreciation also goes to Carl Hingley, Peter Thornton, Lee Gauntlett and Jack Garrod of the Vehicle Technology Laboratory at the University of Birmingham for their technical support during my experiments.

I would like to express my profound gratitude to my parents: Chief and Mrs Ogunoiki and my siblings: Oyepero, Adenike, Afolake and Morenike for their constant support, prayers and encouragement.

My sincere gratitude also goes to my fiancée, Adefunke, for her constant support, encouragement, love and understanding.

Finally, I would like to thank the very many people, whom I can't exhaustively mention here, who encouraged and supported me in various ways during my research.

UNIVERSITY OF BIRMINGHAM

TABLE OF CONTENTS

UNIVERSITY OF BIRMINGHAM

LIST OF FIGURES

UNIVERSITY OF BIRMINGHAM

LIST OF TABLES

UNIVERSITY OF BIRMINGHAM

LIST OF SYMBOLS

p	Network Input
w	Neuron weight
f	Transfer function
a	Network output
b	Bias
n	Sum of Network input
$e(r)$	Response Error
$R_{des}(r)$	Desired Response
$R_{ach}(r)$	Achieved Response
Q_{er}	QanTiM Error
F_s	Spring Force
K	Spring Stiffness Constant
d	Spring Compression Displacement
M_T	Total Moving Mass
M_w	Mass of Wheel-tyre Assembly
M_a	Mass of Axle

M_f	Mass of Moveable Fork
K_t	Stiffness of Tyre
C_t	Damping of Tyre
F	Tyre Vertical Force
x	Tyre Vertical Displacement
F_0	Tyre Force Amplitude
f_0	Frequency of excitation
ω	Angular Frequency of Excitation
t	Time
i	Complex Number Operator
X	Amplitude of Tyre Displacement
$e(s)$	Error in Signal
n_s	Number of Samples in Signal
T	Target Output
$y(t)$	Network Output Time Series
$u(t)$	Network Input Time Series
r	Correlation Coefficient
g	Reference Signal
m	Correlated Signal

UNIVERSITY OF BIRMINGHAM

LIST OF PUBLICATIONS

1. Ogunoiki, A. Olatunbosun, O. Copeta, A "*Artificial Road Load Generation: A Quarter Car Model for Road Load Simulation*" JSAE Annual Congress, Japan, 2013
2. Ogunoiki, A. and Olatunbosun, O., "*Characterisation of the Effects of Vehicle Parameter Variations on Vehicle Road Load Data*," SAE Technical Paper 2015-01-0634, 2015, doi:10.4271/2015-01-0634
3. Ogunoiki, A. and Olatunbosun, O., "*Artificial Road Load Generation Using Artificial Neural Networks*," SAE Technical Paper 2015-01-0639, 2015, doi:10.4271/2015-01-0639
4. Ogunoiki, A. Olatunbosun, O. "*Artificial Road Input Data Synthesis - A Full Car Model Case Study*" (Writing in progress)

UNIVERSITY OF BIRMINGHAM

CHAPTER ONE: INTRODUCTION

1.1 INTRODUCTION

Durability assessment in the automotive industry refers to procedures that are taken to ensure the service life span of a component or system of components meet a predetermined specification with a minimal likelihood of failure. Considering the vehicle as a system of various sub-systems with each sub-system comprising its own components, a vehicle can be said to be a system of components. Hence, the durability assessment of a vehicle would involve the individual durability assessment of each of the sub-systems it comprises. In the early days of the automotive industry, vehicles were manufactured without much knowledge of how the customers would use them and hence, the durability testing of these vehicles did not consider the customer usage but in the last two decades, much work has been carried out on durability testing in vehicles in order to ensure they meet specific industry standards or government legislative requirements. The earliest and most common method for carrying out this vehicle durability assessment is the physical vehicle test where a prototype of the final production vehicle is driven in conditions similar to those it would experience in its service life. The physical vehicle testing involved the driving of the vehicles on chosen road tracks for a pre-determined mileage or until a component in the vehicle failed while different types of data were collected from various locations in the vehicle. This method has been proven to provide useful information which could be used to optimise the vehicle design and configuration. The main disadvantages of this method were the huge cost and time requirement.

Even with the huge cost and time requirements for accurate durability testing, the automotive industry, similar to many modern industries, is under the pressure to design and manufacture state-of-the-art vehicles and to also release them to the market at a minimal cost and in good time to leverage on the build technology while it is still relevant [1]. In order to meet these targets, many processes in the design cycle would need to change to accommodate the shorter design and manufacture cycles. The vehicle durability testing is one of the processes in the design cycle which if not gotten right could lead to huge loss if the affected vehicles were to be recalled from the market. Hence, even though the market of today requires that the automotive industry has a shorter product cycle time, it would not tolerate an unreliable product in terms of durability.

The development of computers came with an advantage for the durability assessment of vehicles in the automotive industry; Computer Aided Engineering (CAE). The early implementations of CAE in product design [2] showed how effective the techniques were in reducing the product development period. Further down the time line and with advances in the speed and robustness of computers, it is clear that CAE is the future of product design with many industries aiming for a *zero-prototype product design cycle* [3] where the design goes directly from the CAE phase to the manufacturing lines.

Even with the advent of CAE, the place of physical vehicle testing has not been removed in the automotive industry for the following reasons:

1. The inaccuracy of some results from CAE modelling
2. Government Legislation

The motivation for this research comes from the first reason. The accuracy of any CAE modelling is dependent on the accuracy of the components that make up the model. So also, the accuracy of a durability assessment from a CAE model is dependent on the accuracy of the knowledge of the road load (which is the forces and moments experienced by the vehicle from its interaction with the road surface) the vehicle would experience in its service life. The prediction of the road load the vehicle would experience is particularly difficult when the vehicle has not been built, i.e. in the early stages of the vehicle programme. This is because the road load is influenced by the design and performance characteristics of the various systems in the vehicle. A change in one component or system could result in unexpected changes in the vehicle's reaction to the road input as a result of the dynamic nature of the loads generated.

Though there have been a number of endeavours at artificially generating road load data from the road loads of predecessor models of vehicles [4-10], which is made possible by the evolutionary nature of vehicle design in the automotive industry where many characteristics are carried over from a predecessor model to the newer model, there is currently no method that takes the effect of the various vehicle configuration setups into consideration in predicting the input for artificial road load.

The service loads the vehicle experiences in its operational life is known to be affected by different vehicle parameters such as the wheel diameter, spindle load, the suspension spring stiffness and the damping characteristics to mention a few. Hence, the knowledge of the road input that the vehicle would experience in service is therefore important to engineering design and development teams in order to ensure that the vehicle is not over designed or under designed. This is especially

useful in the early stage of the vehicle development when a physical test cannot be carried out because a prototype hasn't been built. All these were the precursor for the research question of this thesis which is:

"*How can accurate road input data be predicted for a new vehicle variant durability test in CAE from the road load data collected from predecessor models of the vehicle while considering the differences in the configuration parameters of the new vehicle variant?*"

With all the aforementioned in mind, this research proposes the use of an artificial intelligence system [11]; artificial neural network (ANN), which is capable of accurately predicting the road input for a vehicle in order to generate road load data. The advantage of the ANN is its capacity to gain implicit knowledge from training and to accurately generalise when presented with similar problems from which it has been trained. The artificial intelligence system is able to solve problems in a similar way as the natural human nervous system, hence its name; artificial neural network. With the application of ANNs, the huge amount of road load data collected by vehicle original equipment manufacturers (OEMs) in the course of durability testing over the years, and used for the optimisation of the durability performance for predecessor vehicles for which they were collected, can be put to use in generating realistic road load data which can be used for durability assessments in the pre-prototype stage.

The aim of the research work presented in this thesis is to develop an ANN based Artificial Road Input Tool, which is capable of modelling the effects of the different

vehicle configurations and design parameters on the road input signal for driving vehicle models in the pre-prototype stage.

In order to achieve the aim of this research project, the following objectives are defined:

1. Develop and Validate CAE models of the target vehicle
2. Characterise the effects of the vehicle parameters on the road load data statistically
3. Select a suitable ANN Architecture
4. Train and Optimise the ANN to produce the Artificial Road Input Tool

1.2 THESIS OUTLINE

This thesis comprises the work carried out to meet the objectives of this research as stated in the preceding section and is laid out as follows:

Chapter 1 sets the scene with an introduction to the research and an outline of the objectives and motivation.

Chapter 2 is a review of relevant literature on the subject of durability assessment, road load data acquisition and artificial neural networks.

Chapter 3 discusses the modelling hardware and software tools used in this current research. This chapter contains the details of the laboratory test equipment and software used for the modelling of the target vehicle as well as its validation.

Chapter 4 describes the development and validation process of the CAE models of the quarter and full vehicles. The various components of the models are discussed and the details of a simple tyre model are also presented.

In *Chapter 5*, the effects of the variation in the quarter vehicle and full vehicle configuration parameters are presented to describe the variation in road load data. The variation in road input as the vehicle parameters are modified is also presented and the hypothesis of variation in road input for different vehicle configuration parameter setups is presented.

Chapter 6 presents the development, training and optimisation of the ANN architecture for the prediction of road input with the vehicle configuration taken into account. Results from the application of the Artificial Road Input Tool are also presented.

The conclusions and recommendations for future works from this project are discussed in *Chapter 7*.

CHAPTER TWO: LITERATURE SURVEY

2.1 INTRODUCTION

This chapter contains a review of various literatures on road load data, vehicle variants and artificial intelligence. The literatures are by no means exhaustive but provide a basis for the ideas implemented in this current research.

2.2 ROAD LOAD DATA

Road Load Data is the data collected from various locations on a vehicle as it traverses road profiles. These data are a direct result of the effect of the road a vehicle traverses on the chassis and various components of the vehicle as well as the load transfer path from the road surface. These road load data include wheel spindle moment, wheel spindle acceleration, wheel spindle force, sprung mass acceleration, unsprung mass acceleration, strain etc.

Road load data provides information on the prospective customer usage of the vehicle, how the vehicle components respond to the use of the vehicle and most importantly how much fatigue and damage the usage imposes on the vehicle components. Road load data is important to the design engineer as it enables the engineer to make informed decisions for modifications to the design of a vehicle in order to ensure that it meets the durability performance level chosen by the manufacturer and in some cases, the legislation of the country the vehicle would be used in.

Therefore, the aim of a road load data acquisition exercise is to obtain information that would be used to optimise both the behaviour of the various components of the vehicle and the interaction of these components and ultimately, the overall performance of the vehicle while in service. Examples of useful information obtained from road load data include the work of Backer et al. [12] who discovered the effect of the low gear on the yaw mode of a new bus type from the road load data collected in the early testing phase. Similarly, Haq et al. [13] were able to quantify the variability effects in a vehicle as a result of an increase in the unsprung mass from the use of Wheel Force Transducers instead of standard tyres as a result of the analysis of the road load data collected from testing the different vehicle configurations. Reddy et al. [14] were also able to discover statistical trends in the spindle loads for vehicles with variants using the road load data acquired. More recently, Babu et al. [15] used the road load data acquired from testing as well as CAE to optimise the design of the steering system of a mini-truck. So, it is quite clear that the road load data plays an important role in the design and optimisation of a vehicle design.

2.2.1 Application of Road Load Data

As highlighted in previous sections, Road Load Data is needed for the accurate optimisation of the design of a vehicle before it is released to the commercial market for the customers' use and the following explain how the road load data is used to achieve the optimisation:

2.2.1.1 Road Test Simulator (RTS)

A primary application of road load data is in the road test simulator (RTS). The use of RTS was made popular in the early 1950s with the invention of W.C. Moog's servo valves [16] and has developed from 4-post simulators which could replicate only the vertical displacement of the wheel to very advanced 6-degree-of-freedom simulators which are able to replicate the displacement, forces and moments in the wheel. These simulators have become very good alternatives to running the vehicle on a proving ground as they can be run in a controlled environment such as a laboratory for long periods of time. The use of the RTS relies directly on the availability of road load data from physical vehicle testing or other methods as these are the quantities that are back-calculated into displacement inputs to drive the simulators. The aim of using these measured road load data is that they represent some sort of damaging effect which could impact on the vehicle's durability and hence, a play back of those damaging road scenarios are quite useful for optimising the durability of the vehicle in the laboratory.

2.2.1.1.1 Types of RTS

There are mainly two types of road test simulators [17] and this classification is based on the method in which the vehicle is coupled to the simulator.

a) **Tyre Coupled RTS**: In this simulator setup, the vehicle's tyres sit on a pan on top of servo-hydraulic actuators with vertical strokes and the drive signal is sent via a controller to the actuator to excite the tyres in the vertical direction. Because of this setup, only the vertical displacement of the tyre can be controlled using this simulator type. Moreover, the simulator is only able to

capture events that occur when the tyre contact patch is in contact with the road but not events where the tyre of the vehicle loses contact with the road surface. Figure 2.1 is an example of a Tyre Coupled RTS.

Figure 2.1: A Tyre-Coupled RTS courtesy of MTS Systems Corporation

b) **Spindle Coupled RTS**: This simulator setup is able to replicate the longitudinal, lateral and vertical displacements of the wheel. It is also able to replicate acceleration and braking events via the spindle connection. The most sophisticated spindle coupled RTS can produce up to 6 degrees freedom at each wheel. In this case, an event where the tyre is not in contact with road surface can be accurately simulated. Figure 2.2 is an example of a Spindle Coupled RTS

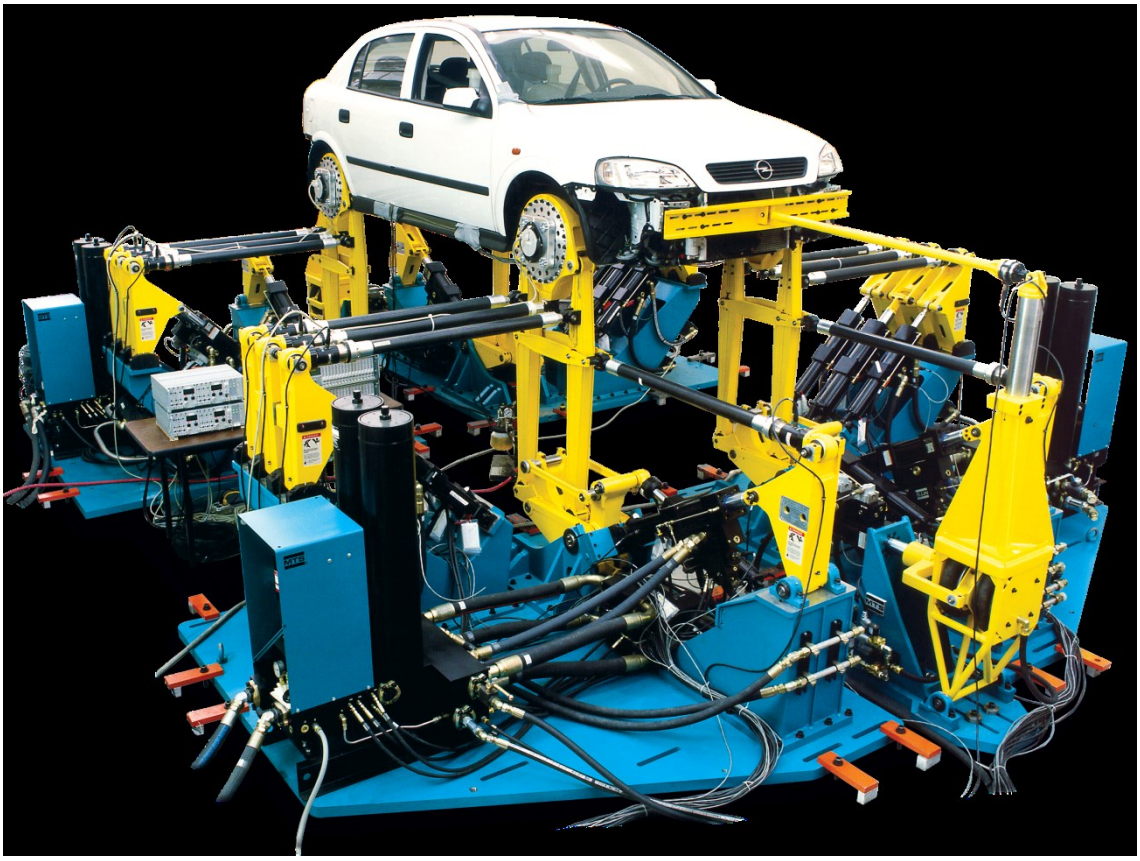

Figure 2.2: Spindle Coupled RST Courtesy of MTS Systems Corporation

2.2.1.1.2 RTS Procedure

The procedure for running a Road Test Simulator for durability testing is a systematic one and is illustrated in figure 2.3 overleaf.

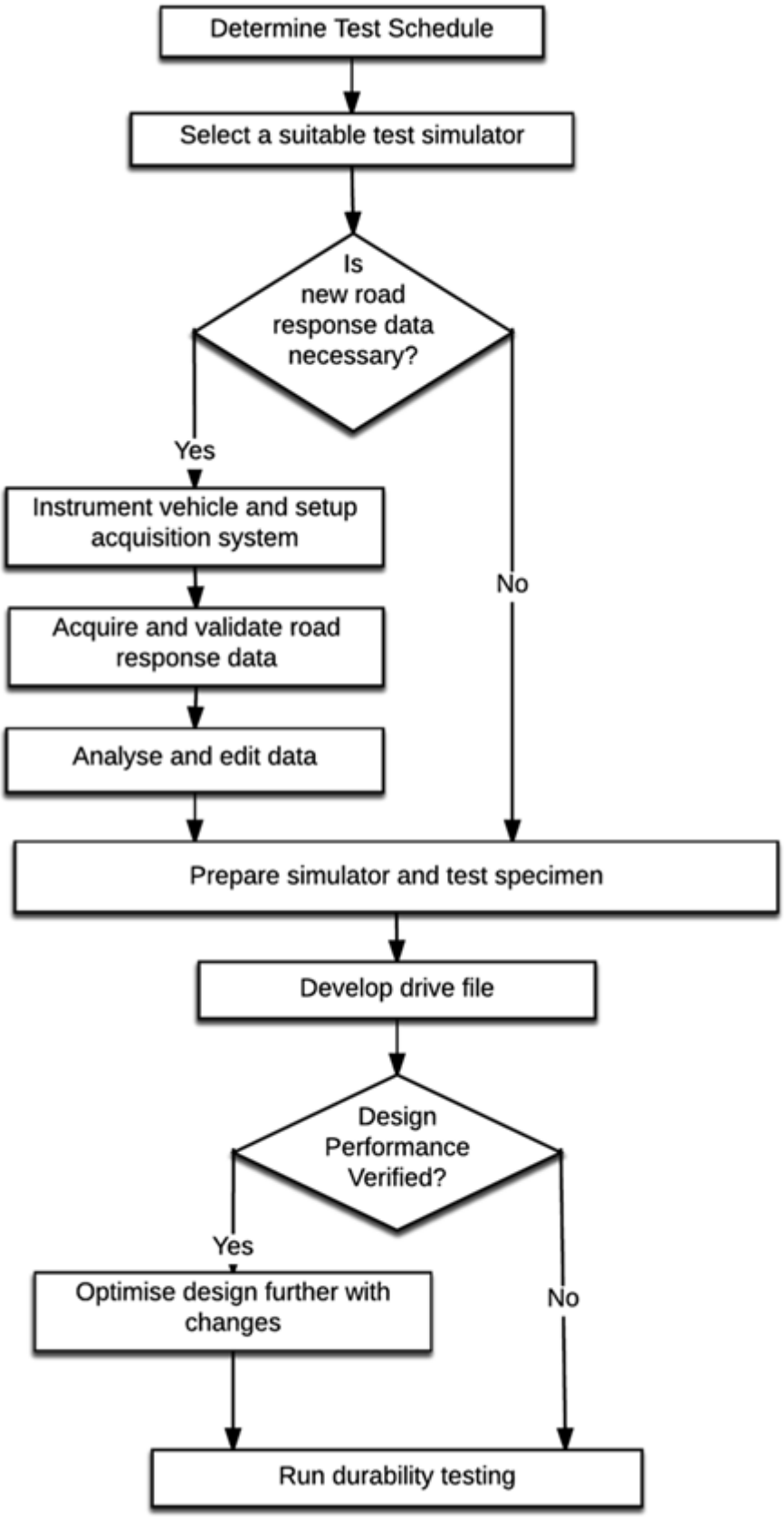

Figure 2.3: Road Test Simulation Process [17]

2.2.1.1.3 Drive File Development

The drive file development process is an iterative method where the measure road load data from a physical vehicle test or simulation is back-calculated into displacement signals to drive the durability test of a vehicle or vehicle component on a road test simulator [16]. The back-calculation is necessary in order to develop drive signals with which the road test simulators can excite the target vehicle. The back-calculation is usually carried out to vehicle responses which are classed as damaging hence, reproducing them on an RTS can be used to study and accelerate the durability performance of the vehicle. The stages of the drive file development are highlighted as follows:

1. **System Identification**: The vehicle is excited with a white noise and a mathematical model is fitted to the known input actuator drive signal and the measured vehicle responses.
2. **Model Inversion**: The model identified in step 1 is inverted so the model generates as output, the actuator drive signal to a measured vehicle response.
3. **Drive Signal Calculation**: The actuator drive signal for a chosen target vehicle response signal is calculated by running the response signal through the inverted system model. The output of the model generates the first drive signal which can be used to drive the target vehicle.
4. **Drive File Generation**: The generated first drive signal in step 3 is used to drive the actuator for the target vehicle while the vehicle's responses are collected and the errors between the expected vehicle responses and actual vehicle responses are calculated.

5. **Drive File Iteration**: The response errors calculated in step 4 are passed through the inverted system model and the drive signal generated from the errors is added to the first drive signal to generate the second drive file.
6. Steps 4 and 5 are repeated until the response errors reach an acceptably small value.

The drive file development process is illustrated in the diagram in figure 2.4.

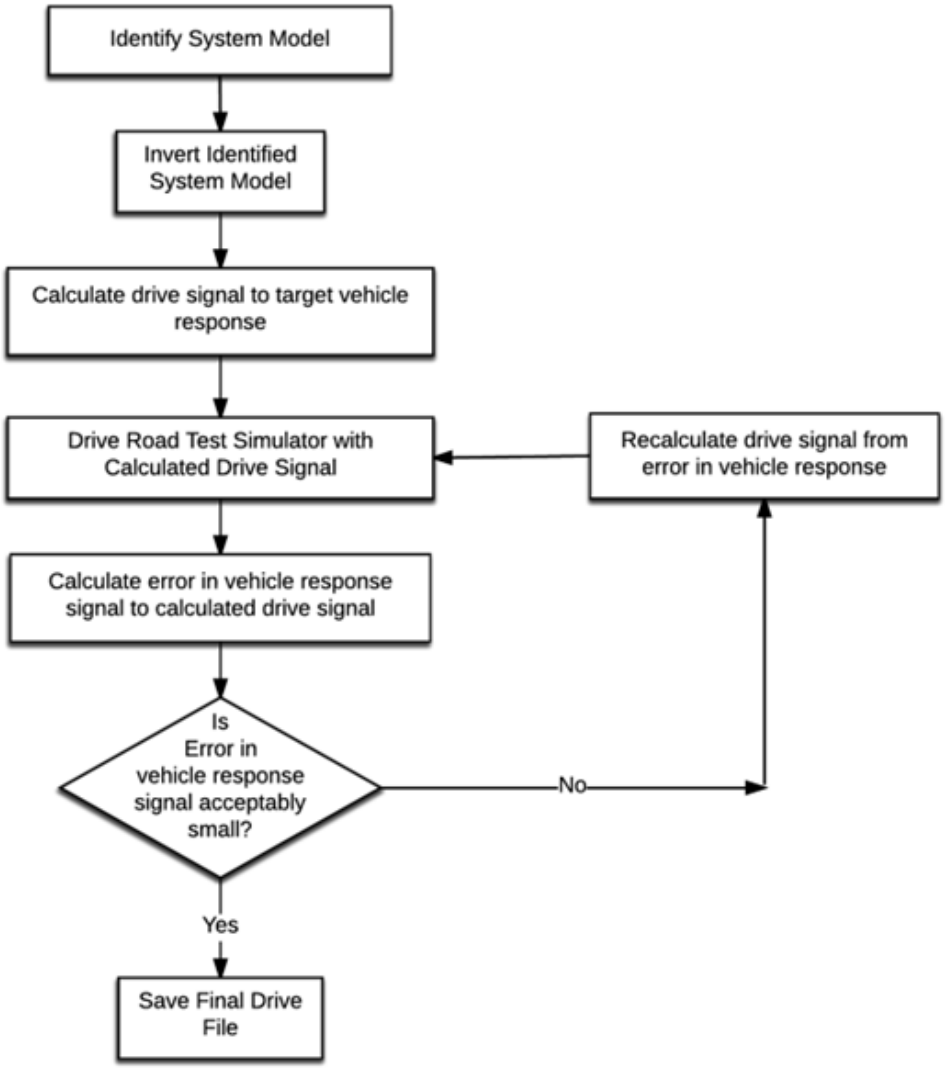

Figure 2.4: Drive File Development Process

2.2.1.2 Other Applications

Besides the use of road load data in the Road Test Simulator for play-back of road events in full vehicle road simulation, road load data is also used in other vehicle optimisation such as those described in the works of Yang et al. [18] where the loading of suspension components were studied from the back-calculation of wheel spindle loads from previously collected road load data, Reddy et al. [14] where the road load data is used to characterise the effects of vehicle variation on the spindle loads and Babu et al. [15] where the road load data collected from customer usage is used to optimise the design of the steering system. An additional example is Kim et al. [19] who used the acquired road load data to validate a simulation programme for the estimation of cumulative damage to an automatic transmission. Similarly, You and Joo [20] used the collected road load data to validate their method of virtual testing.

2.2.2 Acquisition of Road Load Data

A search through literature has revealed different methods of collecting road load data and these can be classified into three groups as follows:

- Empirical Methods
- Analytical Methods
- Semi-Analytical Methods

2.2.2.1 Empirical Methods

Empirical methods of road load data acquisition involve actual testing of the vehicle on a road surface to collect the response data to the road input. This method is divided into the following:

- Customer Usage Road Load Data Acquisition
- Proving Ground Road Load Data Acquisition

2.2.2.1.1 Customer Usage Road Load Data Acquisition

Collection of road load data from customer usage is carried out in two ways.

The first is the active customer usage road load data which is carried out by placing transducers in various points in the vehicle and running the vehicle over the road surface types the customer would use the vehicle on in service while the data from the transducers is collected. In order to accurately determine the road surface types a customer would use the vehicle on, data is gathered from the experiences of the customers as done by *Backer et al.* [12] where customer questionnaires provided an insight into the customer usage profile for the test vehicle. The information gathered was processed so that it showed the customer usage profile in terms of the percentage of usage on each road type. This method of road load data acquisition process usually includes the use of bulky data acquisition loggers with various wires and transducer running around various parts of the vehicle and can be said to be obtrusive [21] as additional components that would not be present in a normal customer usage scenario are installed into the vehicle just for the purpose of the road load data acquisition. Furthermore, this method doesn't accurately represent the driving style of the customer and the effects of the severity or placidity of the

driving style as these cannot be replicated by mere filling of questionnaires by customers.

The second method is the passive customer usage road load data where the road load data is collected via the data loggers installed into customer vehicles such that the logging is done without altering the way the driver interacts with the vehicle or without a reminder that the vehicle is instrumented for data collection [21]. The purpose of this method is to collect the normal usage data from the driver without altering the driver's style of driving.

In the past, collection of road load data from active customer usage was the only way of collecting data and this data collection continued for a predetermined range, typically 100,000km, which is the limit of the mileage most manufactures would provide a warranty cover for. In order to achieve the predetermined distance range, the vehicle had to be driven by trained test drivers on the selected road surfaces till the target mileage was met or till a component failed. The advantage of this method of road load data acquisition is that it is the most detailed way of collecting road load data from actual customer usage. The disadvantages of such method of road load data acquisition are the large amount of time required for data acquisition; such as time for transducer installation setup on the test vehicle, transducer calibration and data logger testing apart from the time required to run the acquisition itself, the high cost of running the acquisition and the inability to control the data acquisition environment to ensure the security and safety of the test vehicle. Of great importance to the success of the data acquisition exercise also is the availability of representative vehicle hardware. In the case where the vehicle setup is not representative of the final vehicle in production, the collection of data prior to the

availability of a hardware that represents the final vehicle on the production line would jeopardize the accuracy and fidelity of the road load data collected.

2.2.2.1.2 Proving Ground Road Load Data Acquisition

This method of road load data collection also involves instrumenting the test vehicle with transducers as in the case of the active customer usage method and thereafter, the vehicle is run on a proving ground. A vehicle proving ground is an area specifically reserved and laid out for running a variety of vehicle road tests. Commercial proving grounds such as IDIADA[1] (figure 2.5) have a variety of test track courses such as washboard road, comfort road, pave road (figure 2.6), repaired asphalt road, gravel road and cobblestones road (figure 2.7) among others. The test vehicle is run severally on a combination of two or more test track courses which represents the most damaging effects similar to those from the customer usage profile. The data from the run is collected and post-processed in order to make design modifications, such as a change in spring stiffness etc., to the vehicle.

[1] Applus IDIADA is a commercial proving ground in Spain with over 12 test track courses

Figure 2.5: An Overview of the Proving Ground in IDIADA Spain

Figure 2.6: A Belgian Pave Road in IDIADA

Figure 2.7: A Cobblestone Road in IDIADA

The advantage of this method is the reduced time it offers compared with the customer usage methods as the data acquisition environment is controlled and much more mileage can be attained in a shorter time. In addition, the security and safety of the test vehicle is much more assured compared with the customer usage methods. As more data is being collected in the same period as a customer usage method, it is possible to fix errors in the collected data due to failed transducers much faster than in the customer usage methods as the data is collected and checked at more regular time intervals. The data collected from proving ground road load data acquisition is a good representation of the road load the vehicle would experience in service and a good number of studies in automotive engineering have had to depend to a great extent on the data collected from proving grounds for durability analysis and prediction [22] [14, 23-25]

The major drawbacks of proving ground method are the high cost, large time consumption and time delay associated with it as with any method of physical

vehicle testing. Though, compared with customer usage methods, the proving ground method has better time scales.

In summary, physical vehicle testing whether via the customer road load data acquisition or proving ground data acquisition, are known to be time and cost consuming [26] because the test vehicle needs to be first built before any road load data measurement can take place and this in turn leads to delays in obtaining the data required for making cost and time efficient changes in the early stages of the vehicle development programme. This road load data acquisition process also involves heavy instrumentation of the vehicle in order to ensure that every important data is collected [27]. Furthermore, a proving ground road load data acquisition, like the customer usage method, would require a trained driver or drivers driving the vehicle for long periods of time till sufficient data is collected which in some vehicle development programmes could be from a few weeks to several months.

2.2.2.2 Analytical Methods

The analytical methods of road load data collection involve the use of mathematical equations to model the behaviour of a vehicle as it traverses a road profile. These analytical methods have proven to be cost and time efficient as no physical vehicle needs to be tested in order to collect the needed road load data for the vehicle's durability and performance optimisation.

Olatunbosun & Dunn [28], Tianbing et al. [29] and Andersen et al. [30] developed vehicle models by using forms of the Lagrange equation to derive the equations of motion. Olatunbosun & Dunn created a full vehicle model to study ride performance under both steady-state and transient conditions and this model was created as a

rigid body model with 2-degree-of-freedom suspension systems. Tianbing *et al*.'s quarter vehicle model was able to represent the dynamic behaviour of a quarter vehicle as it traversed a road profile and was used to study the ride quality and vibration characteristics. Tianbing et al. furthermore, investigated the effect of the sprung/unsprung mass ratio, tyre/suspension spring stiffness and damping coefficient ratio of the suspension system on the response of the quarter vehicle to the input from the road. Andersen et al. developed a multi-body dynamics models of a McPherson strut suspension for a quarter-car rig using the Lagrange form of the equation of motion to derive a set of differential algebraic equations (DAE) which were used to predict the dynamic behaviour of the model. The aforementioned examples express the use of analytical methods to model and study the vehicle's behaviour without the use of a physical vehicle.

The recent advances in computing technology have made it possible to harness the power of computers in vehicle engineering analyses. Computer Aided Engineering (CAE) techniques have made the development time of products shorter in various fields of engineering and this advantage is applied in the automotive industry. CAE now allows engineers to model, simulate and investigate the effect of vehicle parameters and other external constraints on the vehicle systems. CAE methods have made deriving and solving modelled mathematical equations less time consuming and therefore more cost efficient. CAE is now being applied much more in the areas of road load prediction, analyses of suspension systems[23], durability evaluations [27], NVH analyses [31], handling performance [32] etc. CAE in road data acquisition is especially important in the early stages of a vehicle development programme where the prototype of the vehicle has not yet been built.

The application of CAE in automotive durability assessment can be classified into two groups; Finite Element Analysis (FEA) and Multi-Body Dynamics Simulation (MBDS).

2.2.2.2.1 Finite Element Analysis (FEA)

Finite Element Analysis, as the name implies, is a numerical method that discretizes the domain of a continuous structure [33]. Continuous structures such as vehicle chassis components can be modelled with *finite elements* in order to investigate the effects of loading on the deflection and therefore, the fatigue and damage effects of such loading. The results from the fatigue analysis provide engineers with information on the service life of the structure. Some examples of commercial FEA software packages are ABAQUS, Nastran, ANSYS, LS-DYNA and COMSOL Multiphysics®. The accuracy of the finite element model depends on factors such as the size of the mesh, the geometry of the finite elements, the physical characterisation of the component to be analysed and the boundary conditions for the component among others. The use of FEA has expanded in the automotive industries over the last decade. For example, Zhang et al. [34] modelled a full vehicle four-post analysis using FEA. The model comprised the tyre, wheel, body and the suspension system. Similarly, Shahidi et al. [35] used a finite element method to model the interaction between connected components in a vehicle with the aim to understanding the boundary interaction between them and hence, optimise the design of such components. More recently, Bakir et al. [36] used FEA to optimise the design of a leaf spring for a heavy duty truck.

2.2.2.2.2 Multi-Body Dynamics Simulation (MBDS)

The MBDS is used to model the dynamic behaviour of the different interconnected bodies in the vehicle system [37]. The interconnected bodies can be modelled as either rigid body components; where the body has a defined mass and a stiffness of infinity and hence, would not deform under loading or a flexible body component; where the body has a mass and a stiffness matrix defined from pre-processing from Finite Element Analysis. These flexible body MBDS models are referred to as Hybrid MBDS [38]. Multi-Body systems have been in existence and used in vehicle engineering for over forty years [39] [40] [41] [42]. Hence, they have evolved from simple MBD simulations solving a few equations of motion to much more robust ones which are able to model complex systems.

Commonly used commercial MBDS software packages are ADAMS™, SIMPACK, CarSIM®, LMS Virtual.Lab, Recur-Dyn and COMSOL Multiphysics®. An example of the application of MBDS is seen in the work of Subramanyam et al.[43] who developed an All-Wheel Drive minivan model using ADAMS and compared the results of simulation with that from the suspension kinematics and compliance testing. This study showed that a good static correlation could be obtained from the MBDS modelling with the only short coming being that some of the results of dynamic test of the model didn't show as good a correlation as the static case.

In spite of the progress made by MBDS in reducing the time and cost of road load data acquisition, it is necessary to state that the accuracy of the MBDS relies on the modelling data provided to the MBDS software. The masses and inertia for the rigid bodies, the masses and stiffness of the flexible bodies and the characterisation of

other linear and non-linear components and the fidelity of the representation of these components determine the accuracy of the model and the reliability of the results from the simulation. Components such as shock absorbers, bushes and the tyre which play an important part in the MBDS modelling are in real life non-linear components with hysteretic behaviours. Hence, the better the accuracy of the MBDS representation of each of the components, the better the vehicle model obtained. Shawn and Sang-Gun [20] reported in their study, the MBDS method to complete virtual durability evaluations on a passenger car coupled to a spindle-coupled test system. Their work involved building both a vehicle model and the spindle-coupled test system in ADAMS™, reproducing road load data collected from physical vehicle testing on the road in the simulation environment and comparing the results obtained from the 4 degree-of-freedom virtual test rig with that from the 6 degree-of-freedom virtual test rig. In their simulation, a good correlation of the simulation with physical test data was achieved even though the study did not consider the flexibility of the vehicle body. Also, the results showed that the 6 degree-of-freedom system simulates the road loads better than the 4 degree-of-freedom test system when compared with physical test results though the acceleration response in a case showed a bad correlation in both magnitude and phase. Lin *et al.* [23]in their study went further by developing a flexible body vehicle model to perform a CAE based analyses using FEA; a full vehicle model using LS-DYNA was developed. The collected road load data from physical testing was used to validate the accuracy of the model and fatigue damage estimation carried out thereafter with the validated model. The work of Dannbauer et al. [44] also discussed a method of integrating virtual tests and physical tests in order to achieve

a reduction in time and effort towards vehicle development. The results of their work on the fatigue life prediction for physical test rig data and simulation were compared and these showed better prediction from the simulation than from the test rig measured forces.

The summary of these is that the development of an accurate CAE model is reliant on the accuracy of the individual components in the model and the test scenario the model is aimed at simulating.

As mentioned earlier, one of the most important components in the CAE modelling of a vehicle is the tyre as it is the only part of the vehicle that interacts with the road surface. The next section examines the role of the tyre model in CAE accuracy and fidelity.

2.2.2.2.3 Tyre Models

The tyre is a very important part of the vehicle as it is the only component of the vehicle that connects the rest of the vehicle to the road. The tyre functions as the support to the vehicle's weight to provide sufficient tractive and braking force and also dampen out the effects of an irregular road surface on the vehicle [45]. Various tyre models have been developed up to date to capture the non-linear and dynamic characteristics of the tyre and of particular importance to this work are those developed and optimised for use in road load analyses when prediction of durability loads are important. The models are able to predict the forces in the vertical, longitudinal and lateral tyre directions. These models are cited by Li et al. [46] as Ring on Elastic Foundation Model [47], Mousseau's Model [48], Zegelaar's Model [49], RMOD-K Model [50], Kao's BAT Model [51], Schmeitz's Model [52], MF-SWIFT

[53], FTire Model [54], CD-Tire [55], Baecker's Model [56], ABAQUS-Based Surrogate Tire Model [57]. These tyre models have been developed for use in conjunction with FEA and MBDS and each has a test scenario for which it performs best. The important thing is to choose the most suitable model for a particular simulation application. In this current research, a simple tyre model and the FTire model were used for the MBD simulations. The choice of the FTire and simple tyre models was based on the ability to use both of them with the chosen MBDS package and the scope of this current research which included only the prediction of the vertical loads from the tyre model.

2.2.2.3 Semi-Analytical Method

This method of road load data acquisition combines both the analytical method and the empirical method to create a hybrid. These hybrid methods make use of some data collected via physical testing and combine these with those from CAE simulation to generate the required road load data. Various researchers have used this method and they include Schdut et al. [58] who showed how road load data generated from CAE could be used to supplement those from physical road tests in General Motors. Similarly, da Cruz et al. [3] presented a typical procedural example of the semi-analytic method. In their study, the wheels of a sport utility vehicle (SUV) were instrumented with Wheel Force Transducers and the vehicle ran over a road track sequence, selected particularly to study the vehicle's durablity performance, to acquire the spindle forces and moments to drive a Rigid body MBDS model in ADAMS. The data collected from the physical test was also used to validate the fidelity of the results from the ADAM model while further simulations were carried out using the validated model in order to minimise the time and costs associated

with the physical test. Bäcker *et al.* [26] also used a similar method referred to as the Hybrid road approach to generate road load data for a new generation model of a vehicle by back-calculating the effective road profile from the data collected from a predecessor model and running an MBDS model of the new generation model of the vehicle with the longitudinal and lateral spindle forces as well as the back-calculated effective road profile iterated from the vertical spindle force. The results of the use of this hybrid road approach showed a good correlation with the road load data measured from the new vehicle after its manufacture. Also, Liu et al. [59] used a semi-analytic method by developing and validating an MBDS model of a vehicle in ADAMS and validating the fidelity of the model with data from the kinematic testing of the physical vehicle. Once the validation was complete, the model was used to generate chassis loads and the results of the data collected from the model showed a very good correlation with those from the proving ground test of the physical vehicle.

As the capabilities and accuracy of CAE improves, more automotive manufacturers would favour CAE road load data acquisition especially in the early development stages of the vehicle over physical testing. At the current stage of the development of CAE, the *virtual* road load data collected cannot yet be used to completely replace those from physical testing but would be good enough to provide very useful information needed to carry out a vehicle durability and performance optimisation.

2.2.3 Efforts at Artificial Road Load Data Acquisition

An apparent conclusion from the review of the various methods of road load data acquisition is that though the physical test provides the most accurate and reliable

source of the data, the cost and time required for the acquisition of the data is much higher than the other methods of data acquisition. Also, the method of physically testing the vehicle either on the road as in the customer usage methods or on the test tracks as in the proving ground method is only possible when a representative prototype of the vehicle has been manufactured. As this is not the case in the very early stages of the vehicle development programme, it is necessary to explore other methods of road load acquisition. From the various aforementioned methods of road load data acquisition, the analytic and semi-analytical methods are the feasible options in the pre-prototype stage of the vehicle development, hence recent studies on artificial road load data acquisition methods are reviewed here.

One of the earliest methods used the effective road profile method for the simulation of road load data. Rui et al. [60] presented the concept of the use of the effective road profile iterated from the spindle responses of the vehicle on the road and a tyre model in the frequency domain. The study assumed that the new vehicle would have the same simplifications as the preceding model and that the longitudinal and lateral effective road profiles were the same. The results of spindle vertical acceleration as well as the radius arm force produced a good correlation in the frequency domain. This method showed the effectiveness of the road profile provided the new variant of the vehicle had a very similar configuration to the predecessor, thereby limiting the application of this method to a new variant if it was significantly different in configuration.

Similar to the effective road profile method is the hybrid road approach [26] where the effective road profile was calculated and transferred to the next generation design of the target vehicle. The method presented by Backer et al. included the use

of an unconstrained vehicle for a full vehicle simulation. The effective road profile was calculated only in the vertical direction while the measured longitudinal and lateral loads were transferred directly from measurement to the MBDS model of the next generation target vehicle. A simple linear tyre model was used in this process. The back-calculation of the effective road profile is similar to the method of drive file iteration used on Road Test Simulators for accelerated durability testing of vehicles in the laboratory. The results produced by using this method showed a good correlation with the measured loads from the physical testing of the next generation vehicle. The accuracy of this method depends, to a good extent, on how different the next generation vehicle is from the predecessor. The bigger the difference, the less accurate this method would be as the longitudinal and lateral spindle forces were transferred directly from the preceding vehicle to the new one.

Kang et al. [61] developed a virtual road profile using the spindle loads collected via a wheel force transducer on an SUV which ran on a Belgian and Washboard road. The collected load data was back-calculated to a road profile using an iterative method in the frequency domain and was used as an input to run an MBDS model of the vehicle in ADAMS/Car and using the FTire tyre model. The method of the road profile iteration is similar to that used in the hybrid road approach by Backer et al. [26] with its difference being the use of a dynamic tyre model; FTire. Though the results showed a good correlation between the measured road load data and the simulated load, the effect of the changes in vehicle parameter configuration was not taken into account.

Scime's [9] approach was different from the aforementioned methods in that a 4-post durability simulation using a tire coupled setup without measuring any road

load data from a physical vehicle was carried out. This was done by using digitized road surfaces representative of the durability schedules of a proving ground test, creating 4-post displacement signals via an algorithm that accounts for the tyre enveloping effect on the digitized road surface and then running a fully analytic 4-post simulation. The enveloping effect of the tyre is the variation in the vertical force and its deformation as the tyre traverses an uneven road surface as a result of its flexibility hence, the tyre can be said to envelop the road surface. The results indicated a good correlation of the spindle acceleration from the simulation with that collected from the physical test in the frequency domain and the time history shape and peak also indicated a good correlation. The challenge of this approach is reliance on the accuracy of the digitized road surface. Digitization of road surfaces requires high technical and cost resources. The work of Tasci et al. [62] indicate how a significant cost and time investment are required in developing accurate and efficient road surface profiles for use in simulation.

Schudt et al. [7] implemented a virtual road load data acquisition which allowed the switching of the measured data for synthetic data in the development of vehicles at General Motors. This method was also used for the virtual acquisition of road load data for a rear suspension of a vehicle under development [8]. The implementation of this method was successful because of the amount of time spent in the development of the processes involved with the significant ones being the development and generation of digital road surfaces and development. This method would pose a big challenge to a smaller volume manufacturer because of the huge costs and time required for acquiring adequate digital road profile information.

Having reviewed the various methods of road load data acquisition and various procedures of implementing them, the import of these as regards vehicles with variants is considered in the next section.

2.2.4 Vehicle Variants

In order to reduce vehicle development time, the associated costs and in order to be able to also transfer the knowledge gained from the development of a predecessor vehicle model, automobile manufacturers design some of their newer vehicles based on already existing models. These next generation models are here described as the vehicle variants and would generally have similar properties such as body shape, engine type, aerodynamics etc. as the existing model with some modifications to other configuration parameters. In other cases, variants of vehicles are developed in order to meet a custom design requirement as in the work of Sivashankar et al. [63] where their commercial vehicles were developed to customer specifications for the loading and usage of the vehicle. Traditionally, the measured data and knowledge gained from the development of the predecessor vehicle are transferred and used for the development of the newer model during the pre-prototype stage because of the similarities in both vehicle architectures but the configuration modifications in the new vehicle reduce the accuracy of data collected from predecessor model when used for the new vehicle. The introduction of new or modified components into a vehicle have been known to cause an increase in the reliability problems [1] and hence, being able to determine the effects of the changes in the vehicle configuration on the service loading of the vehicle is of great benefit.

Not many studies have been carried out on the effect of variation of vehicle configuration parameters on the road load data. One of the earliest studies was carried out by Reddy et al. [14] where the trends in the wheel spindle loads for vehicle variants were examined. This was based on the data collected from different variants of the same vehicle. The variants had different types of leaf spring shackles, loading conditions and number of mounting points from the frame to the body. The road load data was collected by running the variants of the vehicle on the same road track and at a single vehicle speed. The results from this study showed the variation in the spindle forces, moments, acceleration and the associated pseudo damage for each of the vehicle variants. This was a first step in understanding the effects of the parameter changes on the road load data. This work was carried out successfully primarily because the variants of the vehicles already existed and could be run on a track and road load data collected and analysed. As mentioned earlier in this chapter, the associated costs with physical testing are much higher than other means of vehicle testing. Hence, a cost saving method such as the analytical or semi-analytical method of vehicle testing would be a preference for many manufacturers. This was the motivation for Backer et al. [26] when they implemented the hybrid road approach for a vehicle variant using the wheel spindle load from the predecessor model of the vehicle as described in the earlier section above and though this yielded some success, the effect of the changes in the new vehicle parameters were not accounted for in the back-calculated vertical road input.

All the CAE methods covered in this literature survey, though they provide plausible solutions to road load data prediction, either do not account for the parameter

variations in the variants of the vehicle or are very cost and time intensive especially at the pre-prototype stage where vehicle optimisation is much more cost effective.

Hence, this research proposes the use an Artificial Intelligence method for the generation of road load data. The Artificial Intelligence method will take into consideration, the configuration variations in predicting the road input for generating the road load data. The following section details the Artificial Intelligence methods.

2.3 ARTIFICIAL INTELLIGENCE SYSTEMS

Artificial Intelligence (AI) is a method of providing solutions to problems that would require human intelligence. AI has been applied in various fields of engineering and has proven to reliably provide solutions [64]. The aim of Artificial Intelligence systems is to be able to model the human intelligence and the method of human learning. Examples of the implementation of artificial intelligence systems are artificial neural networks, fuzzy logic systems, expert systems, inductive learning and genetic algorithm [11]. One of the many implementation of AI in automotive engineering is the Artificial Neural Network.

2.3.1 Artificial Neural Networks

Artificial neural networks are systems of artificial neurons interconnected in such a way that they imitate the behaviour of the human nervous system and are able to solve problems which have characteristics or behaviours that have not been fully understood yet and hence, cannot be modelled accurately.

The history of Artificial Neural Networks dates back to the development of the concept of neural networks in the late 19th century [65] by scientists in the fields of

physics, neurophysiology and psychology. The development involved the general establishment of theories on the operation of human functions such as vision, learning etc. Further into the 20th Century, the works of various scientists such as Warren McCulloch and Walter Pitts [66], Donald Hebb [67], Frank Rosenblatt [68], Windrow and Hoff [69], Minsky and Papert [70], Teuvo Kohonen [71], Rumelhart and McClelland [72] as described by Downes [73] and Hagan et al. [65] highlighted the capability of artificial neural networks in solving both logical and arithmetic problems. The benefit of artificial neural networks is their capacity to solve problems in a similar way as the human brain does [64]. Though the full functional behaviours of the human brain are not completely understood yet, the main characteristics of learning and adaptation, generalization, robustness among others have been assembled for the development of artificial neural networks. The ability of artificial neural networks to learn in a similar way as the human brain, by training to impart implicit knowledge, has made them popular in a variety of fields in the last decade. Examples of the application of neural networks include input-output and curve fitting, pattern recognition and classification, dynamic time series prediction and clustering.

An example of a popular neural network type is the Multilayer Perceptron Network. The multilayer perceptron network comprises 3 layers of artificial neurons viz. the input layer, the hidden layer and the output layer. The flow of data in the multilayer perceptron network is forward from the input layer, through the hidden layer, to the output layer. Each neuron comprises a weight, a summer, a transfer function and an offset often referred to as a “bias.” The training of the multilayer perceptron network is carried out by a training method where a training data set consisting of both inputs and the corresponding target outputs are presented to the network. The neurons’

weights and biases in the network are by default randomly initiated and are modified via an error back propagation algorithm until the error from the output of the neural network reaches a satisfactory level. The back propagation algorithm feeds backwards the error, between the network's output and the expected corresponding output, to an input through the neural network so the weights and biases are modified in accordance with the error from the network's output. A schematic of the multilayer perceptron is shown in figure 2.8.

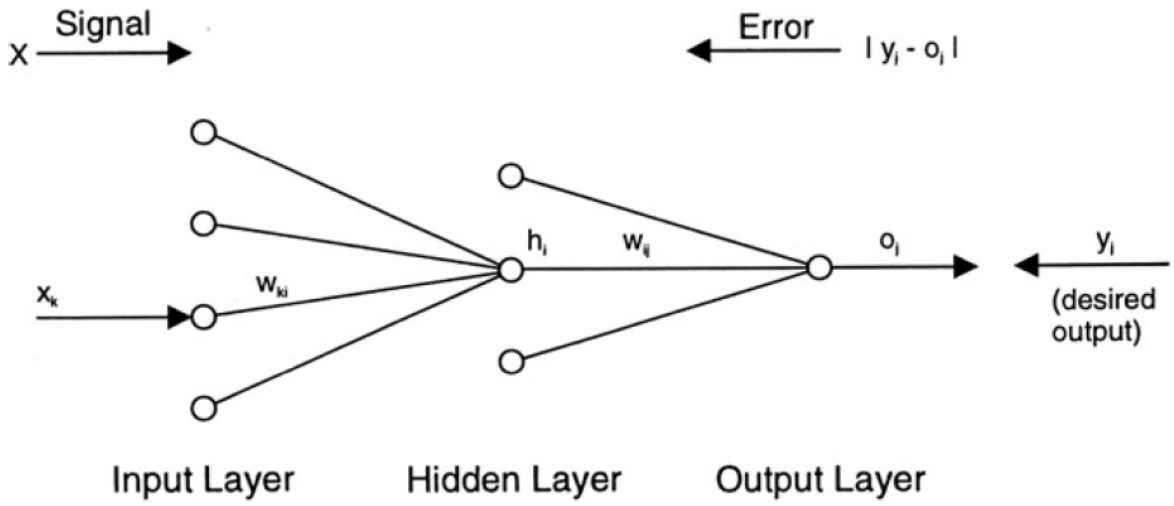

Figure 2.8: Schematic of a Multilayer Perceptron Network [64]

Besides automotive engineering, various other fields have put to use the capabilities of the artificial neural networks such as Material Engineering [74] where neural networks were used to model fatigue behaviour and predict the fatigue life of a composite, Hydrology [75] where the capabilities of an artificial neural network were used to estimate the safe pumping rate in order to maintain the groundwater's salt content and Oil and Gas exploration [76] where artificial neural networks were used

to estimate the parameters of a reservoir from the well test data and these are just a few of the many applications of artificial neural networks.

A number of neural network architectures exist to solve different problems depending on the requirements of the problem.

2.3.1.1 Artificial Neural Network Architectures

Artificial Neural Network Architectures can be defined by the types of neurons they are made up of, the arrangement of the connections among the neurons, the training algorithm and other components [64].

2.3.1.1.1 Neurons

The artificial neurons in the network comprises an input, *p;* an associated weight, *w*; a summing function, a singular input to the summer with a value of 1 and an associated weight referred to as the bias, *b* and a transfer function, *f* which is activated by the sum of the inputs, *n* to produce an output, *a*. The transfer function could be a linear or non-linear function of the input signal. The figure 2.9 below represents a neuron with a single input.

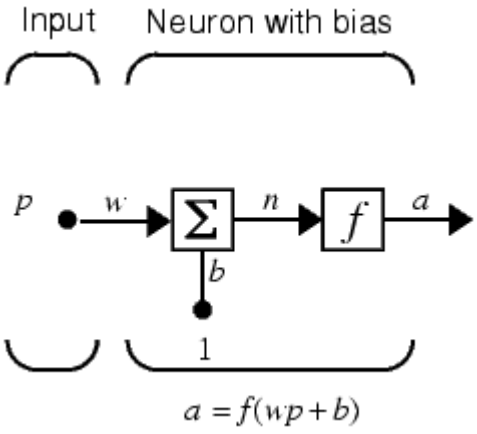

Figure 2.9: A Single-Input Neuron [77]

In training a neural network, the associated weight parameter, *w* and the bias, *b* are those that are adjustable by a learning rule.

Some common examples of the types of transfer function are described as follows:

1. **Hard Limit Transfer Function** (Figure 2.10)

   This transfer function produces an output of zero below a certain input threshold value or an output of one at and above the input threshold value.

$$a = 0 \; for \; n < 0 \tag{2.1}$$

$$a = 1 \; for \; n \geq 0 \tag{2.2}$$

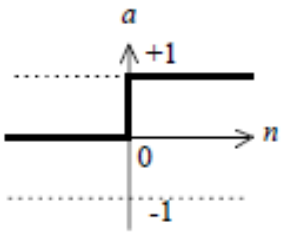

Figure 2.10: Hard Limit Transfer Function [77]

2. **Linear Transfer Function** (Figure 2.11)

   The linear transfer function produces an output that is exactly the same as the input value.

$$a = n \tag{2.3}$$

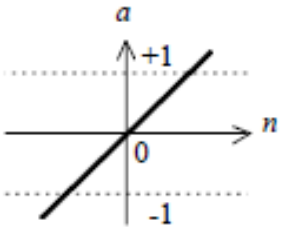

Figure 2.11: Linear Transfer Function [77]

3. **Log Sigmoid Transfer Function** (Figure 2.12)

   This transfer function produces an output according to equation 2.4.

$$a = \frac{1}{1 + e^{-n}} \tag{2.4}$$

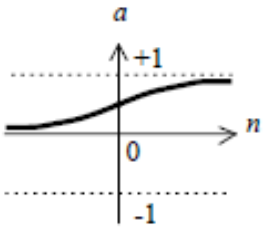

Figure 2.12: Log Sigmoid Transfer Function [77]

4. **Hyperbolic Tangent Sigmoid** (Figure 2.13)

   The output of this transfer function is according to equation 2.5.

$$a = \frac{e^{n} - e^{-n}}{e^{n} + e^{-n}} \tag{2.5}$$

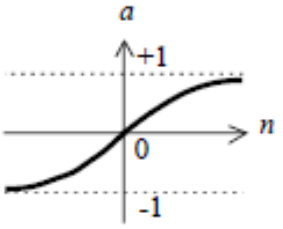

Figure 2.13: Hyperbolic Tangent Sigmoid Transfer Function [77]

2.3.1.1.2 Arrangement of Neuron Connections

The arrangement of the connections of the neuron in an artificial neural network defines if neurons are connected, partially connected or not connected at all as identified by Kasabov [64]. The connectivity of the neurons also depends on the number of input and output neurons. A network that has the input neurons serving as the output neurons as well is termed an associative network (Figure 2.14) while one which has the input neurons separate from the output neurons is termed a heteroassociative network (Figure 2.15).

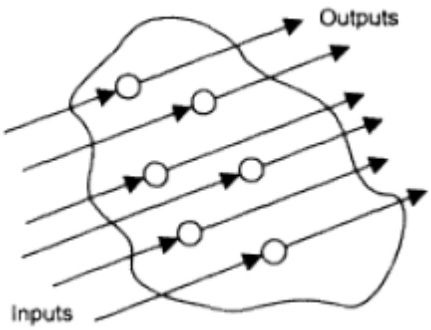

Figure 2.14: Autoassociative Network [64]

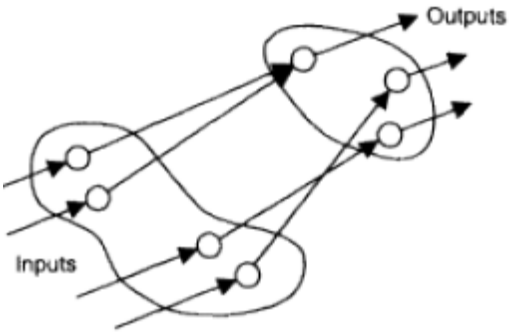

Figure 2.15: Heteroassociative Network [64]

2.3.1.1.3 Training Algorithm

The Training algorithm refers to the method of updating the associated input weights and biases of the artificial neural network. As the name suggests, the training algorithm imparts implicit knowledge into the neural network so it can carry out a predetermined operation [11]. This is also referred to as the learning rule. Examples of Training Algorithm are as follows:

1. **Gradient descent**: The weights and biases are modified with training in the direction of the negative gradient of the network's performance.
2. **Gradient descent with momentum**: This is similar to the gradient descent but in addition, has the ability to allow the network ignore local minimums; like a low pass filter acting on the error surface.
3. **Variable Learning Rate**: This algorithm is similar to the gradient descent with the exception that the learning rate parameter is adjusted as the training proceeds. This ensures that the algorithm doesn't become unstable and it converges fast.
4. **Resilient Backpropagation:** This algorithm eliminates the problems associated with partial derivatives which occur when gradient descent algorithms are used on sigmoid transfer functions multilayer networks. Because the sigmoid transfer function normalise a large range of input to a finite range in the output, gradient descent algorithms tend to reflect very small changes in the magnitude of the gradient hence, not accurately optimising the weights and biases.

5. **Broyden–Fletcher–Goldfarb–Shanno (BFGS) Quasi-Newton:** This algorithm is based on the Newton method of optimisation but unlike the Newton method, doesn't require the computation of the second derivatives of the network's performance index in the course of the training. Hence, this algorithm produces fast optimisations but its performance diminishes as the network becomes larger.
6. **Levenberg-Marquardt:** This algorithm is similar to the BFGS method and was developed for minimising functions that are sums of squares of some other non-linear functions [65]. The main drawback of this algorithm is that it requires quite a large memory than other algorithms for some problems.
7. **Bayesian Regularization:** This algorithm updates the weights and biases according to the Levenberg-Marquardt optimisation and in addition, minimises the linear combination of squared errors and weights so the network has good generalisation [78].

The speed of each algorithm for a given problem could be difficult to know as these depend on factors such as the size of the training data set, the size of the input, hidden and output layers, the complexity of the problem and the problem type. Though these algorithms are usually chosen by trial, the works of various researchers seem to favour the Levenberg-Marquardt and Bayesian Regularization for an application such the drive signal prediction carried out in this current research.

Training algorithms can be classified into three groups: supervised training, unsupervised training and reinforcement training [64, 65].

2.3.1.1.3.1 Supervised Training

The implementation of this training algorithm requires that sample inputs and targets which represent the system or phenomenon the network is being trained for be presented to the neural network. As the training proceeds, the outputs from the network are compared with the targets presented and the difference is used via the training algorithm to modify the associated weights of the inputs and the biases.

2.3.1.1.3.2 Unsupervised Training

This training algorithm requires that only the training inputs to the network be presented. The associated input weights and biases are modified only by reason of the training inputs. This type of training is mainly used for pattern recognition and classification applications [79]

2.3.1.1.3.3 Reinforcement Training

The reinforcement training can be said to be somewhat similar to the supervised training in that instead of presenting the network with the correct training set of input and output as the case of the supervised training, the network is scored based on its performance to the input. The implication of this score it that the network weights are either increased for a good score or decreased for a poor score.

2.3.1.1.4 Other Components

A number of other components help in defining the structure of the artificial neural network and an important one to this current research is the time delay block. The block could be either on an input line where it functions as an input delay block or on the feedback line where it functions as a feedback delay block. The function of the

delay block is to delay its output by a specified number of time steps. The illustration in figure 2.16 shows a time delay for one time step.

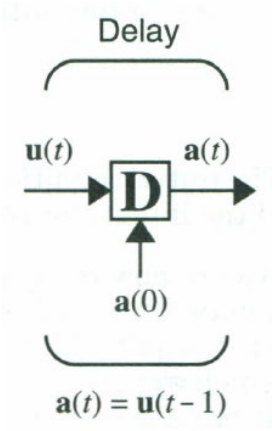

Figure 2.16: Delay Block [77]

2.3.2 Application of ANN in Automotive Engineering

Artificial Neural networks have found many applications in the area of automotive engineering. Kurniawan et al. [80] used a back-propagation artificial neural network to predict the engine performance and the CO and NO levels from a compressed natural gas spark ignited engine. The results from the neural network show very good correlation with those obtained from the Computational Flow Dynamics simulation. Johrendt et al. [81] as well used a neural network in conjunction with a multi-body dynamics simulation model in representing the non-linear damping force in a one degree-of-freedom system. In their case study, the damping force and velocity were collected from a proving ground durability road load data acquisition and normalised for use in a neural network. A co-simulation of the MBDS system in ADAMS and the neural network in MATLAB was carried out with the results showing very good correlations with the ADAMS simulation using an approximated damper

behaviour characterisation. Similarly, Leser et al. [82] achieved a significant improvement in the modelling of shock absorbers with the use of neural network which was trained with data collected from physical vehicle testing. The results from their study showed very good prediction of the damping force in the time domain and also an excellent fatigue life prediction.

Lolas & Olatunbosun [1] as well developed a vehicle reliability performance system using artificial neural networks. This system was capable of predicting the reliability behaviours of the target vehicles at 6000km using information available at 0km. The success of their neural network can be attributed to the network optimisation methods which explored the sensitivity of various components in the network architecture such as the training algorithm, the size of the hidden layer, the number of hidden layers etc. Particularly clear from their study is the importance of a large amount of training data in obtaining a minimum network error

Recently, Balakrishnan et al. [83] used an artificial neural network to predict the strain time histories in various locations in a two-wheel vehicle from data measured from a few other channels. In their study, road load data was collected from transducers installed to various components on the two-wheeler during a proving ground measurement. A comparison of the actual measured data from the target locations on the two-wheeler with the prediction from the neural network used indicated a very good correlation.

2.4 SUMMARY

The literature survey has revealed the significance of road load data acquisition in vehicle durability testing and its various applications. The survey also identified three methods of acquiring the road load data; empirical, analytical and semi-analytical. In addition, the efforts at artificially generating road load data and their limitation with regards to vehicle variants and cost implications were examined and this led to the review of the efforts of various researchers towards the artificial road load data generation prior to the availability of representative vehicle hardware. This revealed that the current methods do not account for the parameter variation in the final production vehicle.

The novelty in this current research is based on these reviewed literatures which showed very little consideration for variation in the input drive signal for vehicles with different configuration parameters. Therefore, this research examines the changes in input drive signal as the vehicle's suspension configuration parameters change and also prediction of the road input data using an artificial intelligence method.

The application of artificial intelligence (AI) methods examined in the literature survey revealed a plethora of applications and particularly, its application in automotive engineering. The AI method of artificial neural network and its application by various researchers also revealed the possibility of its application for the generation of road input data which can be used to accurately generate road load input for use in the pre-prototype stage of a vehicle programme and particularly for vehicles variants.

With the successes of the methods of implementing neural networks highlighted in literature survey in mind, the choice of neural networks in the implementation of road load data input prediction is a leap forward in the application of artificial intelligence in the engineering design process.

CHAPTER THREE: MODELLING AND VALIDATION TOOLS

3.1 INTRODUCTION

The cost and time saving advantages of CAE in automotive engineering are achieved through the elimination of long and costly vehicle test procedures in the vehicle development programme and such CAE methods are the first points of call in the vehicle development process. The advantages of CAE are made possible by the advances in computing technology which has led to the development of high speed computers as well as robust CAE modelling tools.

This chapter presents the hardware and software tools used for the development and validation of the CAE model used in this current research. These tools comprise the instrumentation and features of a laboratory test rig – the Quarter Vehicle test rig, the CAE Modelling software platform implemented in this research and the validation of the CAE models using the data collected from the laboratory test rig and a proving ground road load data acquisition.

3.2 HARDWARE TOOLS

3.2.1 The Quarter Vehicle Test Rig

The quarter vehicle test rig was designed and manufactured in the Vehicle Dynamics Laboratory at the University of Birmingham with the specifications and parts for a popular commercial SUV. The test rig comprises the left hand front side suspension of the target vehicle and removable steel blocks to represent the weight of the chassis on the suspension. The original configuration of the test rig has a Continental Cross Contact 235/60R18 107V tyre inflated to a pressure of 234kPa.

The test rig comprises three units: the *Quarter Vehicle and Suspension Unit*, the *Hydraulic Power Unit* and the *Control System Unit*. The Quarter Vehicle was used for the generation of correlation data for the validation of the MBD model.

3.2.1.1 Quarter Vehicle and Suspension Unit

As highlighted in the preceding section, the Quarter Vehicle and Suspension unit stand alone as a functional unit adapted from a commercial SUV. This unit is instrumented with the following transducers:

1. **Accelerometer**: At the outset of this research, a piezoelectric accelerometer was attached to the centre of the wheel hub of the test rig to measure the vertical acceleration at the wheel hub but this was replaced with a variable capacitance accelerometer further into the research. The change from the piezoelectric to the variable capacitance accelerometer was implemented in order to take advantage of the high sensitivity of the variable capacitance accelerometer and its low frequency response which goes down to zero Hz. Table 3.1 shows the different sensitivities of both accelerometer types used in this research. The accelerometers have a range of up to ±50g.

Table 3.1: Accelerometer Types

Accelerometer	Sensitivity	Frequency Response (Hz)	Mass (grams)	Case Material
Piezoelectric	7.86 (pC/g)	1 – 10000	3.5	Titanium Grade 2
Variable Capacitance	80 (mV/g)	0 – 1500	10.0	Anodized Aluminium

2. **Load Cell**: A flat load cell is installed between the top of the actuator and the base of the tyre contact plate. The cell contains sealed strain gauges which generate electrical signals as the magnitude of the force on them varies. The full scale capacity of the load cell installed on the test rig is 33kN for both tension and compression and is able to accurately measure forces in the range of 0.1% of the full scale (33kN) to 100% of the full scale.
3. **Linear Variable Differential Transformer (LVDT)**: An LVDT measures the displacement via changes in electrical signals. These electrical signals are proportional to the displacements and a constant gain factor. An LVDT is installed in the casing of the Actuator at the bottom of tyre contact. The LVDT provides displacement feedback to the control system during the signal excitation.

The locations of these transducers are shown in the image of the Quarter Vehicle and Suspension Unit in figure 3.1.

Figure 3.1: Quarter Vehicle and Suspension Unit

3.2.1.2 Hydraulic Power Unit (HPU)

The hydraulic power unit comprises the components that generate the oil pressure needed to drive the Quarter Vehicle and Suspension unit. This unit consists of the following parts:

1. **Oil Tank:** The tank contains about 1000 litres of Nuto™ H32 oil which is circulated through the HPU by the hydraulic pump.
2. **Hydraulic Pump:** The function of the Bucher Hydraulics Pump is to convert mechanical energy to hydraulic energy in the HPU. The pump has an effective displacement 80cm^3/rev and is powered with a Brook Crompton electric motor with a 3-phase connection (415V @50Hz) to the electricity grid and is rated at 55kW and 1475rpm.
3. **Piping:** The piping of the HPU comprises both pipes and hoses. The hoses are SAE 100R13 Size ¾" with a working pressure of up to 35MPa and carry the oil from the oil tank outlet to the suction of the hydraulic pump, out through the discharge, through the entire HPU and back to the oil tank.
4. **Servo Valves:** The MOOG servo valves control the in-flow and out-flow of the oil to the actuator cylinder chamber in response to the electrical signal sent from the controller. The opening and closing of the valves produces the vertical upwards and downwards displacement of the actuator.
5. **Hydraulic Actuator:** The actuator is the part of the HPU that converts the hydraulic energy from the unit to displacement. The displacement is controlled by signals sent to the servo valves via the controller. The total length of the actuator stroke is 150mm.

3.2.1.3 Control System Unit

This unit comprises the Digital servo controller and the Test Rig Computer. Both devices are connected to each other via Registered Jack (RJ) – 45 ports located on their main processor boards. The detail of each device is as follows:

1. **Digital Servo Controller**: The digital servo controller is the Control Cube developed by CaTs[3] UK and it monitors, records and processes analogue transducer feedback signals from the test rig; controls and generates the digital input to the test rig's servo valves via a software interface on the test rig computer. The Control Cube is capable of generating simple constant amplitude tests, static ramp test and external signals generated from external software.
2. **Test Computer**: A computer system equipped with an Intel® Core™ 2 Quad CPU Q9400@2.66GHz Processor, 6GB of RAM and running Microsoft Windows 7 was used in conjunction with the digital controller software for the execution of dynamic tests, control of the test rig and analysis of the data acquired from tests. The computer's configuration was adequate in processor computing power, memory capacity and storage for running all the test experiments.

3.2.2 Tri-Axial Tyre Test Rig

The Tri-axial tyre test rig at the University of Birmingham was used for the determination of the stiffness and damping of the tyre installed on the Quarter Vehicle test rig. The rig comprises a 2.44 meter drum, two hydraulic actuators in the vertical and longitudinal tyre axes and some instrumentation for the collection of test

data. The instrumentation on the tri-axial tyre test rig are the same as those on the quarter vehicle test rig; accelerometer, load cell and LVDT. The digital servo controller connected to the test rig generates displacement drive signals as the input to the tyre-wheel assembly in either the longitudinal or vertical tyre axis while the data from the transducers; acceleration time history from the accelerometer, force time history from the load cell and displacement time history from the LVDT, were the outputs from the test rig. The stiffness and damping data calculated from the tyre test was used for the definition of the tyre properties in the MBD simulation of the Quarter Vehicle test rig.

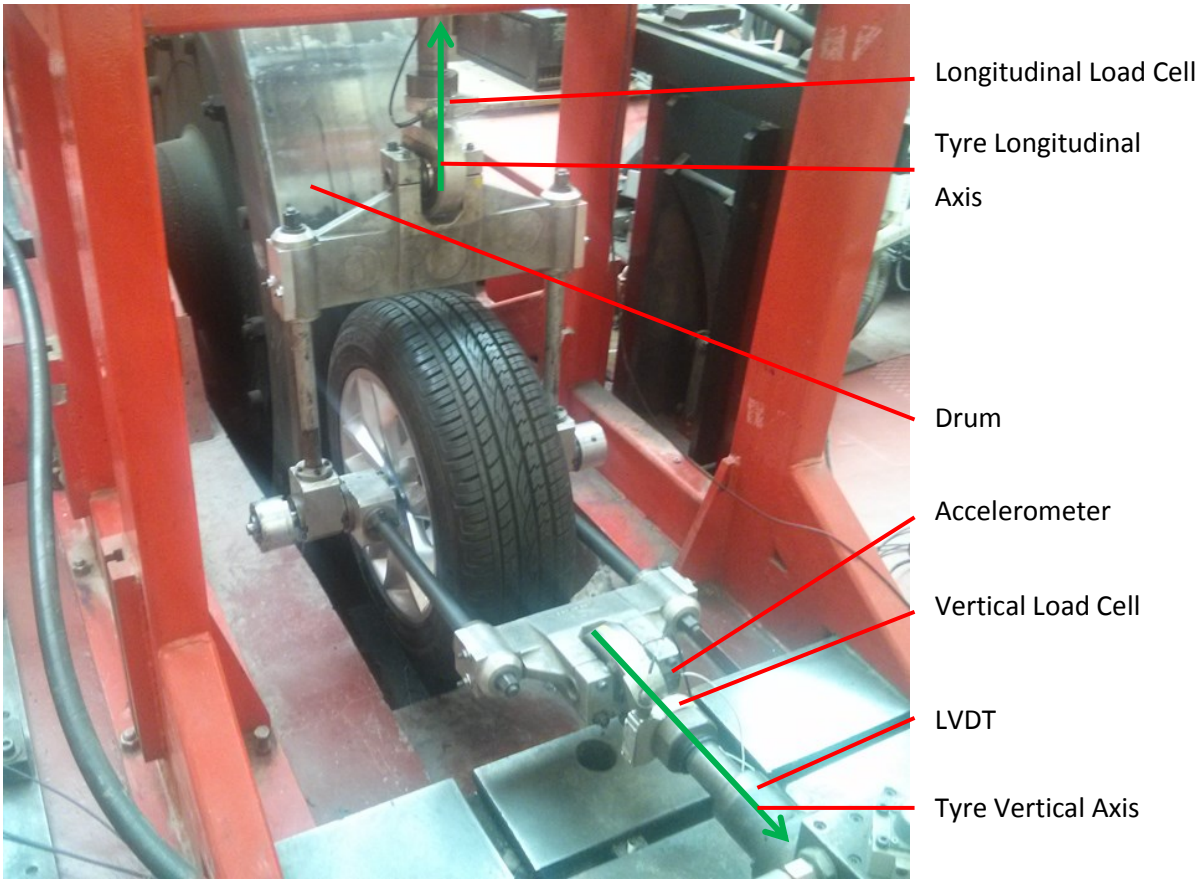

Figure 3.2: Tri-axial Tyre Test Rig

3.2.3 Simulation Computer

The Simulation computer was equipped with an Intel® Core™ i7 CPU 870@2.93GHz Processor, 14GB of RAM and ran the Microsoft Windows 7 operating system. The configuration of the simulation computer was found to be adequate for the execution of the Multi-Body Dynamics simulations, Drive File Generation and MATLAB Simulations.

3.3 SOFTWARE TOOLS

3.3.1 Digital Controller Software

The digital controller required a control interface where various test configurations could be setup in order to carry out a specific test procedure on the Quarter Vehicle test rig. The digital controller software also provides the electronic means of setting the gain, polarity, offset on the input and output signals from the controller in addition to the execution of a variety of experimental tests. The Digital Controller Software programmes used in this current research were Cubus, QanTiM and LabVIEW.

3.3.1.1 CUBUS

Cubus is the computer software that interacts with the Digital Controller (Cube) for sending and retrieving signals from the test rig. The Cubus interface is divided into 3 modules: Rig, Data and Test.

The Rig module is for the configuration of the test rig and the transducers attached to the test rig. The data module provides the tools for the configuration of data sampling rate and the acquisition of the data measured by the transducers. The test

module enables the user to run a simple test such as cyclic constant amplitude sine input or to give the digital controller access to an external test software package.

Cubus directly controls the drive signal to the actuator via the digital controller to produce the displacement on the test rig while the LVDT, load and acceleration channels provide the feedback of measured signals.

3.3.1.2 QanTiM®

QanTiM is a time domain based software tool for the laboratory reconstruction of the input loads required to generate the dynamic response on a structure as measured in its operating environment. QanTiM works using a state space model in the time domain using the method called: "*the parametric dynamic system identification*." The state space model in QanTiM is able to generate a displacement time history drive signal as an output to a measured dynamic response, which in this research is the acceleration response of the wheel. The generated output displacement drive signal is thereafter used to drive the quarter vehicle test rig and model from the tyre contact patch. The advantage of using the time domain for the identification is the significant reduction in the amount of system identification data required compared with the same process in the frequency domain [84].

The QanTiM simulation steps are as follows[85]:

1. **Acquisition of Road Load Data**

   In order to reconstruct the load input to the vehicle, road load data of the representative service usage of the vehicle is collected either through an

empirical, analytical or semi-analytical method as discussed in the literature survey section in chapter 2.

2. **Preparation of Road Load Data**

   This step requires that the collected road load data be transferred to QanTiM via its data acquisition system. The data is pre-processed by filters to remove the spikes and other noisy sections from the data and thereafter resampled to the chosen sampling rate.

3. **System Modelling**

   The dynamic system in a laboratory test rig setup comprises the hydraulic actuator, the digital controller, the test vehicle and the transducer. In order to identify this system, a short white noise signal which covers the frequency spectrum of the acquired road load data is generated in QanTiM and used to drive the test rig while the output data is collected from the connected transducers. QanTiM then calculates an inverse dynamic system model which is capable of producing displacement inputs commensurate with the measured output signal.

4. **Generation of Linear Drive File**

   Once the system modelling is complete, QanTiM is ready to generate a drive file using the identified dynamic system model and the previously acquired road load data. The output from the model is the displacement time history which corresponds to the road load data acquired. Exciting the test rig with this generated drive file would produce a laboratory simulated road load data response. The comparison of the laboratory simulated response and the acquired response would usually contain some errors as the dynamic system

model identified doesn't account for the non-linearity that may exist in the test rig setup. The error in the response from the use of the linear drive file is defined by a quantity referred to as the QanTiM error (Q_{er}).

The error in the response is defined in Eq. 3.1

$$e(r) = R_{des}(r) - R_{ach}(r) \tag{3.1}$$

Where

$R_{des}(r)$ = desired response

$R_{ach}(r)$ = achieved response

The QanTiM error is the percentage of the error in response to the desired signal, Eq. (3.2)

$$Q_{er} = \frac{\sum|e(r)|}{\sum|R_{des}|} \times 100\% \tag{3.2}$$

5. **Iteration of Drive file**

In order to eliminate the errors in the response generated from the laboratory simulation, the error from the comparison of the simulated and acquired road load data responses are processed through the identified dynamic system model and added to the linear drive file to create the next generation drive file. The responses from exciting the test rig with the next generation drive file are also compared with the acquired road load data responses and any

errors are processed through the identified system model. This process continues until the errors reach an acceptable level when the final drive file is saved for use in the durability testing.

3.3.1.3 LabVIEW

LabVIEW is an intuitive graphical programming language for the development and implementation of laboratory test routines as well as processing data from the tests into useful information. A programme developed in LabVIEW is referred to as a virtual instrument (VI) because it has the resemblance and emulates the operational behaviour of physical instruments. LabVIEW comprises two user interfaces; the front panel where the test input controls such as knobs, dials, numeric input boxes etc. as well as indicators such as LEDs, graphs and numeric indicators are located and the block diagram where the various components of the programming code can be added and connected in order to execute the overall VI's function.

LabVIEW was used in this current research for the design of the control and data processing interface for the characterisation of the simple tyre model. The advantage of LabVIEW is the intuitive, simple and user friendly programming environment which allows the programmer to easily visualise and implement an experimental procedure. The front panels from the simple tyre model characterisation test are shown in figures 3.3 and 3.4.

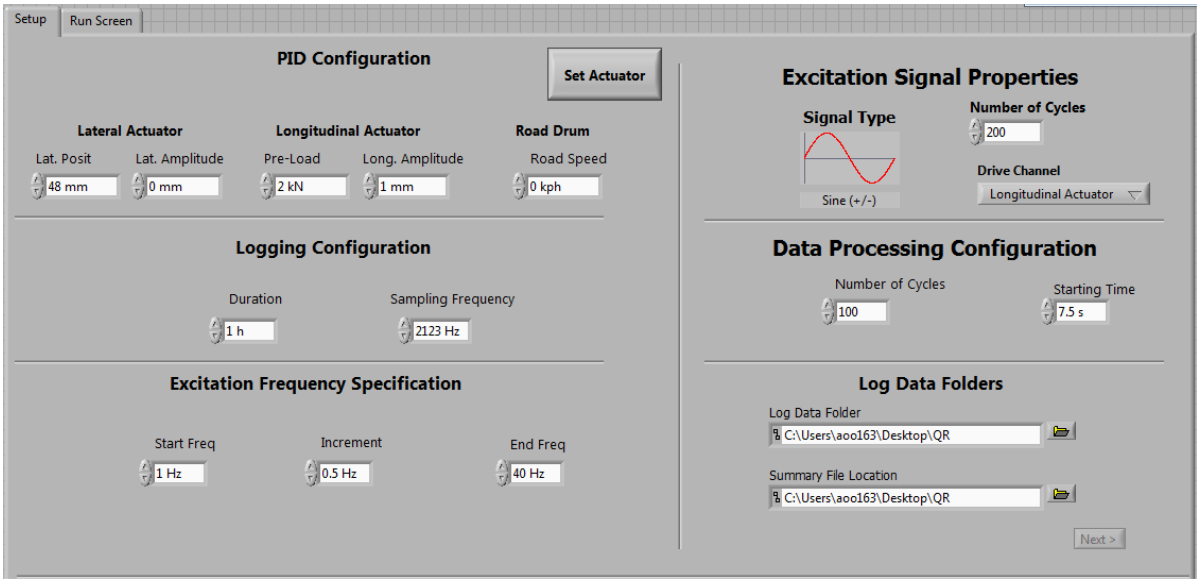

Figure 3.3: Simple Tyre Characterisation Test Setup Front Panel

Figure 3.4: Simple Tyre Characterisation Test Control and Result Front Panel

3.3.2 SIMPACK

SIMPACK is a Multi-Body Dynamics Simulation software which has applications in various industries such as railway technology, oil and gas, renewable energy as well as automotive engineering. SIMPACK is divided into two parts: SIMPACK/Pre where the modelling of the components takes place and SIMPACK/Post where the simulated information is processed and viewed.

SIMPACK solver works by converting the elements of the model into ordinary differential equations. The inclusion of a constraint in the model requires an additional set of differential-algebraic equations (DAE) [86].

In this current research, SIMPACK 9.6 was used for the modelling of the Quarter Vehicle Rig and a Full Car model. Both models were used in conjunction with QanTiM in the latter part of the research for the iteration of virtual drive files. The properties of the components in SIMPACK were populated with data collected from the Quarter Vehicle and Tri-axial Tyre Test rigs.

A Basic SIMPACK MBD model comprises the following:

1. **Body**: This is where all the mass and inertia properties of the structure being modelled are defined. The body can be modelled as a rigid or flexible structural body.
2. **Joint**: The joint is a massless element which connects bodies to each other. The joint provides degrees of freedom.
3. **Constraint**: A constraint is a massless element used to connect bodies to each other kinematically. Unlike the joints which give degrees of freedom, constraints restrain degrees of freedom.

4. **Force Element**: The force element introduces force and torque into the MBD model. Like the joint and constraint, they are also massless components.

3.3.3 MATLAB

MATLAB is high-level computing language with a user friendly interactive environment used for numerical calculation, data analysis, signal processing and various other analyses. The tools built into MATLAB enable faster solving of problems compared with other programming languages such as C++ and Java [87].

The Neural Network Design Toolbox™ in MATLAB R2014a was used in this current research for the development and deployment of a neural network architecture for the generation of artificial road load inputs for use in the MBD simulation. The toolbox provides functions for the modelling of nonlinear and complex systems.

3.4 SUMMARY

The details of the various hardware and software tools used in this current research were presented in this chapter. Of particular importance were the Quarter Vehicle and the Tri-axial Tyre Test rigs which provided information for the modelling of the components of the Quarter Vehicle in SIMPACK. The identified computer hardware was also determined to be adequate for running both experimental tests and computer simulations. The drive file iteration software, QanTiM, was used for the development of drive files for the Quarter Vehicle test rig as well as the virtual drive files for the Quarter Vehicle model. QanTiM was particularly chosen because of the

speed it offers in generating drive files as well as its ability to model dynamic systems with few data samples.

SIMPACK 9.6 was identified as the MBD software platform for the development of the CAE models used in this research. The advantage of SIMPACK is its ability to integrate easily with QanTiM for the development of virtual drive files. Finally, MATLAB, alongside the Neural Network Toolbox, was used for the implementation of the artificial neural network architecture.

CHAPTER FOUR: CAE MODEL DEVELOPMENT

4.1 INTRODUCTION

There are two major methods of CAE modelling for durability analysis as discussed in the literature survey; Multi-Body Dynamics Simulation (MBDS) and Finite Element Analysis (FEA) with MBDS being used for road load analysis and FEA for fatigue life analysis [88]. In the last decade, researchers have implemented both methods of CAE modelling using various software platforms with much success. [4, 12, 24, 34, 89]. In executing this research, MBDS was chosen as the method for CAE modelling. Although there are a good number of commercial MBDS software such as those mentioned in the literature survey, SIMPACK was chosen as the preferred option because of the ease of integrating the development of the virtual drive file from QanTiM with the MBDS in the latter section of this thesis.

As the reliability of the MBDS model is dependent, to a great extent, on the accuracy and quality of the representation of the physical properties of each component that makes up the model and their interactions [17], it is important that the physical properties of the components are accurately characterised for use in the MBDS. In this chapter, the MBDS model of the Quarter vehicle test rig is developed as well as a Full vehicle model. The characterisation of its various components and validation of the accuracy of the model are also presented.

4.2 QUARTER VEHICLE MODELLING

The procedure for the development of the quarter vehicle model is divided into the following sections.

4.2.1 Components Modelling

The development of the model starts with the modelling of each individual component of the Quarter vehicle test rig and thereafter, an assembly of these components with the appropriate joints and constraints to give degrees of freedom to the model. The test rig comprises a MacPherson strut suspension system (as shown in Figure 4.1) with the following components:

1. 18-inch wheel
2. 235/60R18 107V tyre
3. Brake Disk
4. Brake Calliper
5. Knuckle and Hub Assembly
6. Shock Absorber
7. Spring
8. Steering Tie Rod
9. Lower Control Arm
10. Chassis Frame
11. Chassis Mass

For an accurate representation of the test rig in the SIMPACK model environment, the physical properties of each component part of test rig was collected and used to define the model properties in SIMPACK. The properties of these components are divided into *Geometry*, *Mass* and *Force Element Characteristics*.

4.2.1.1 Geometry

The geometry of a component is only as important as the information of the physical properties of the component it can provide. It is known that in FEA, an accurate geometrical representation of a component is usually necessary [90] but this is only true for MBDS modelling if the model consists of a flexible body structure which would have been pre-processed in an FEA environment. In the case of this current research, the body structures were modelled as rigid bodies hence, approximate geometrical representation were used for most of the components. In SIMPACK, the geometry enables the user to visually inspect the interactions of the components but does not contribute to the computation of the results for a fully rigid body structure model.

The geometry information of some of the components of the test rig was obtained from the computer aided design (CAD) data of the individual components while the other components were represented by simple geometrical shapes. The figure 4.1 shows the exploded view of the quarter vehicle test rig model.

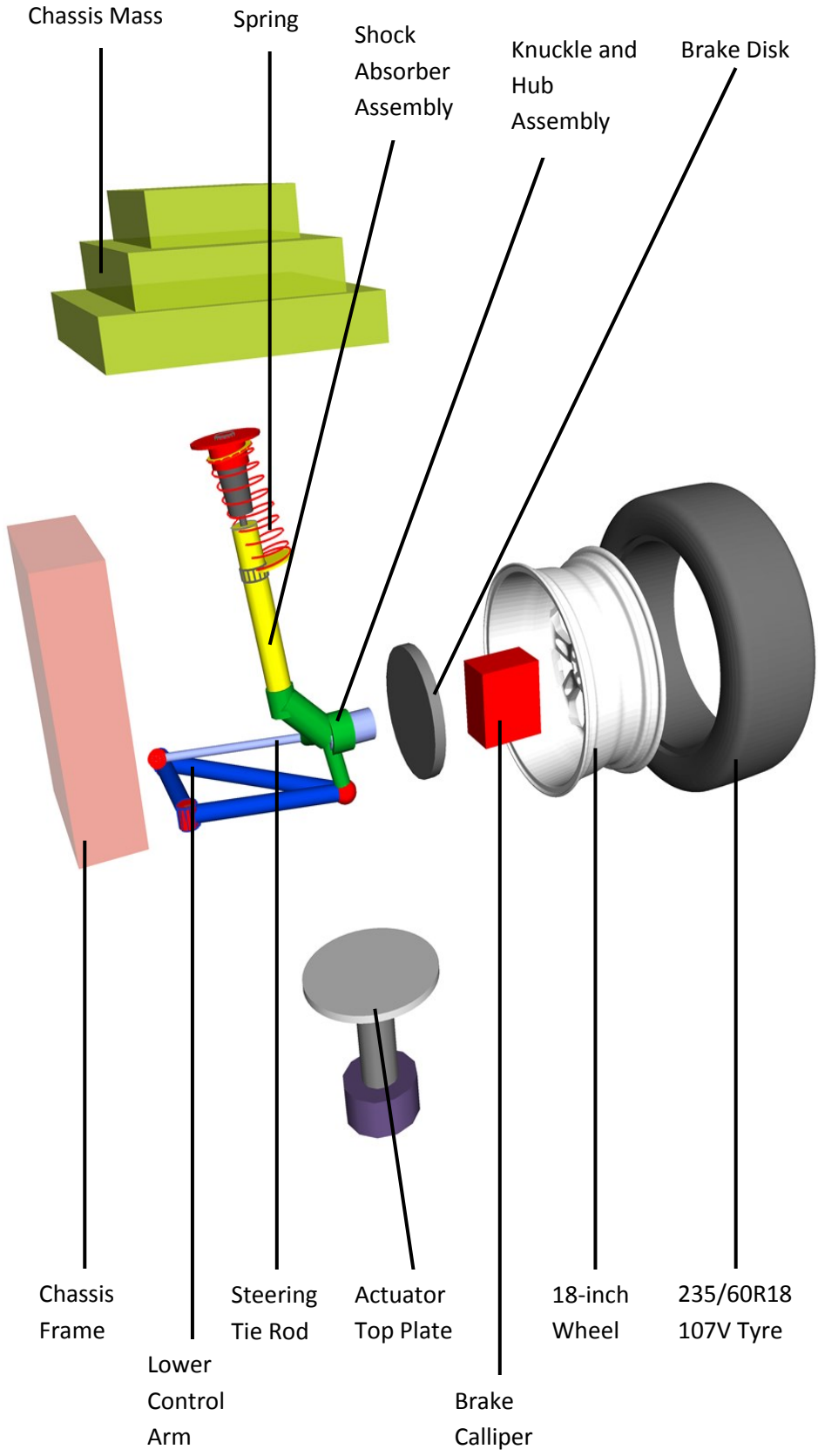

Figure 4.1: Exploded View of Quarter Vehicle Test Rig Model

4.2.1.2 Mass Properties

The mass properties are important characteristics of a component which define its response to an applied force. These properties are the mass of the component, the location of the centre of gravity (CoG) and the mass moment of inertia (MoI). For MBDS modelling, these provide the information for the solution of the equations of motion for the interacting components. Any inaccuracy in the mass properties would ultimately jeopardize the fidelity of the model.

The most evident method of obtaining the mass properties is via direct measurement in the case of the mass and calculations in the case of the location of the CoG and the MoI. The availability of Computer Aided Design (CAD) software has made possible the accurate development of three-dimensional designs of automotive parts and also the possibility of accurate computation of the CoG and MoI [33]. The CAD software is also able to accurately calculate the mass of component provided the density information is available. Various researchers have been successful in the accurate determination of mass properties from CAD data [20, 38, 59].

With the availability of CAD data, the CoG and MoI properties were obtained from the CAD design of the individual components. The mass of each component was obtained from direct measurement using a digital weighing scale. The table 4.1 below contains the mass and inertia of the components of the test rig.

Table 4.1: Mass and Inertia Properties of Quarter Vehicle Test Rig

Component	Mass (kg)	Inertia (kgm^2)		
		X-axis	Y-axis	Z-axis
18-inch wheel	12.65	0.40	0.59	0.40
235/60R18 107V tyre	14.40	0.73	1.34	0.73
Brake Disk	8.56	0.07	0.12	0.07
Brake Calliper	6.50	0.03	0.03	0.03
Knuckle and Hub Assembly	6.36	0.19	0.21	0.15
Shock Absorber	8.08	0.08	0.09	8.75e-4
Spring	3.42	2.33e-8	2.48e-8	4.47e-8
Steering Tie Rod	0.75	8.44e-5	0.01	0.01
Lower Control Arm	7.00	0.16	0.11	0.27
Chassis Frame	56.50	2.43	2.80	1.35
Chassis Mass	450	8.28	11.65	19.32

4.2.1.3 Force Element Characteristics

The force elements are the components in the model which carry load and allow forces to be applied in the model via different force laws. A variety of these exist in a vehicle such as the spring, tyre, shock absorber, anti-roll bar, bushing, bump stop etc. All these components are in place to ensure the comfort of the passengers in the vehicle and optimum performance of the vehicle. The quarter vehicle model was developed with some of these force elements and their characteristics were determined by physical testing carried out at Jaguar Land Rover (for the Spring, Shock Absorber Damping and Bump Stop) and the University of Birmingham (for the Simple Tyre). These force elements were selected because they were the only ones present in the physical quarter vehicle test rig being modelled.

In this current research, the following components' force elements were characterised:

a) Spring
b) Bump Stop
c) Shock Absorber
d) Tyre

4.2.1.3.1 Spring

The spring is characterised by a stiffness constant obtained from the constant velocity compression of the spring while the spring compression displacement and force are recorded. The relationship between the force and displacement is linear

and the factor of the proportionality is the spring stiffness constant as defined by Hooke's law in Equation 4.1.

$$F_s = Kd \tag{4.1}$$

Where F_s = Spring Force

K = spring stiffness constant

d = spring compression displacement

The stiffness, K, was determined as 29kN/m and was entered directly into SIMPACK to model the spring stiffness.

4.2.1.3.2 Bump Stop

The bump stop characterisation is similar to that of the spring in that the relationship between the force and the bump stop displacement is determined by collecting the compression displacement and applied force on the bump stop and plotting the resulting data. The bump stop is usually non-linear and has a higher stiffness as the compression displacement increases. The relationship between the force and displacement of the bump stop is shown in figure 4.2.

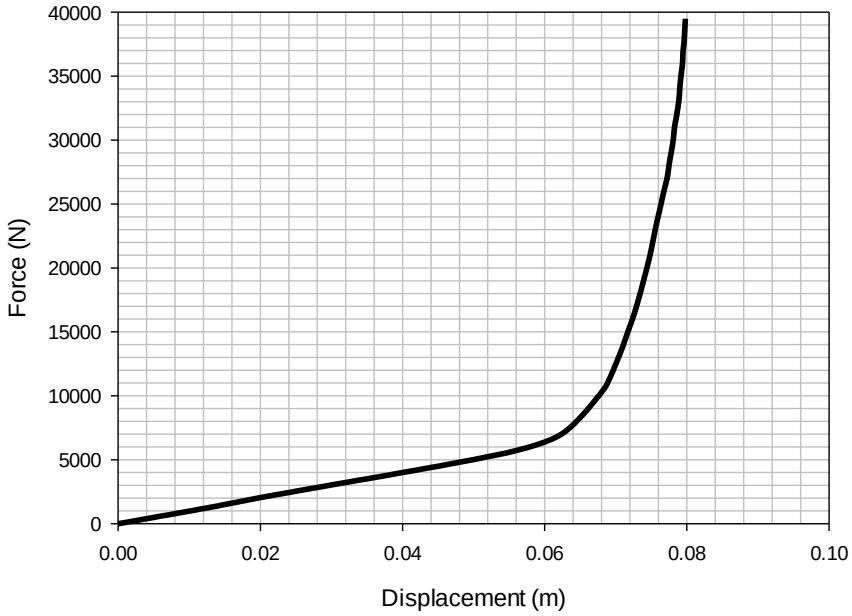

Figure 4.2: Bump Stop Characteristic Courtesy of Jaguar Land Rover

4.2.1.3.3 Shock Absorber

The characterisation of the shock absorber damping was obtained by stroking the damper at a constant amplitude and through different frequencies. The results of the peak damping force and peak velocity at the different frequencies are plotted to describe the damping characteristics. The relationship is not linear like the spring but differs in the direction of the compression and rebound as indicated in figure 4.3.

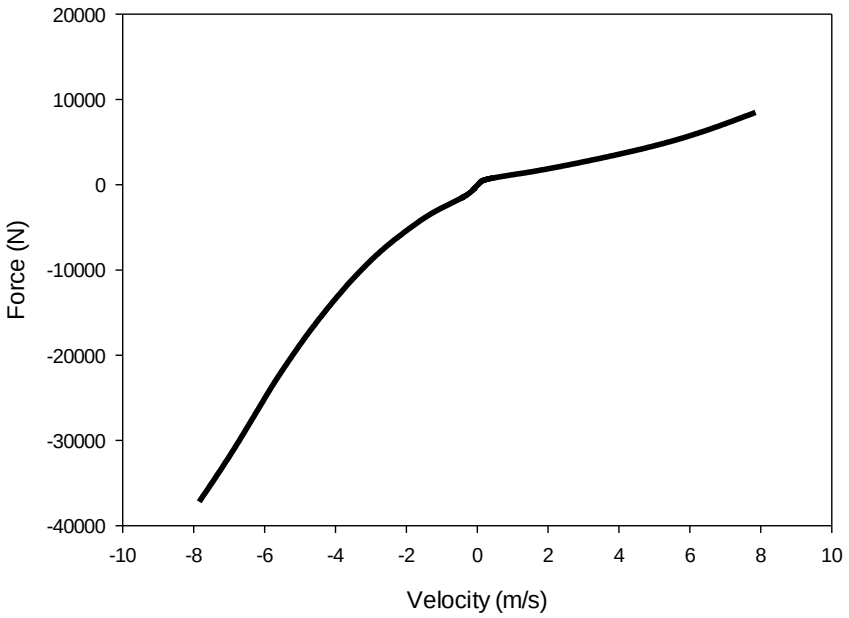

Figure 4.3: Shock Absorber Damping Characteristic Courtesy of Jaguar Land Rover

4.2.1.3.4 Tyre

The tyre is indeed very important in road load analysis because it functions as the intermediary between the road surface and vehicle. Various tyre models highlighted in the literature survey present a plethora of options for modelling.

SIMPACK has in-built functions that allow the use of various tyre models such as those highlighted in the literature survey section of this thesis. FTire and a simple tyre were chosen for comparison in order to determine the best performing tyre model for this current research. The FTire model was developed by an industry affiliate and provided for this study while the stiffness and damping of the simple tyre model were determined by modal analysis on the Tri-axial tyre rig. The idea of the simple tyre was to simplify the tyre characteristic parameters while ensuring that the simulation was time efficient.

4.3 SIMPLE TYRE MODEL DEVELOPMENT

This section focuses on the development of the simple tyre model as described by Olatunbosun [91]. The simple tyre comprises a spring element and a damper element connected in parallel. The simple tyre model was chosen because the tyre parameters could be determined with the available equipment at the University of Birmingham. Though the model consists of linear force components, these elements were assumed to sufficiently describe the tyre's behaviour in the tyre vertical axis in the frequency range of the road input of 0 to 50Hz and hence, sufficient for the purpose of this research. The validity of the assumption was tested and is presented in the model validation section of this thesis.

The tyre is set up as shown in figure 4.4 with a pre-load of 4kN in the tyre vertical axis direction. A swept sine wave signal is sent to the actuator in the tyre vertical axis direction to produce an excitation with a displacement amplitude of 2mm for the frequency range 1 – 20Hz and a step size of 0.1Hz. The amplitude of 2mm was chosen based on the limitation of the tyre test rig as the servo valves of the rig cannot maintain amplitudes larger than 2mm as the test frequency increases. While the sine wave was generated on the test rig, the acceleration and the load at the wheel hub were recorded and used for the analysis of the magnitude and phase of the response of the tyre assembly and hence, the stiffness and damping properties.

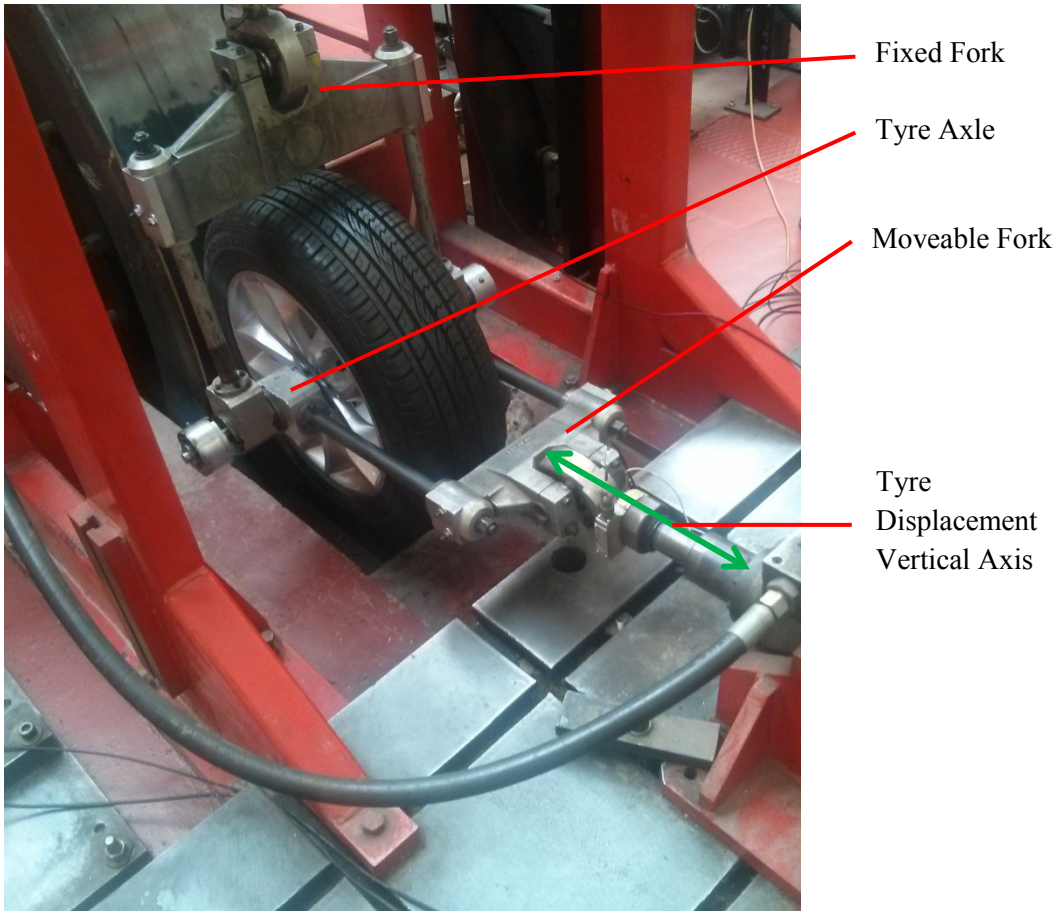

Figure 4.4: Tyre Modal Test Setup on Tri-axial Test Rig

The test setup can be represented as a one-degree of freedom system as in the figure 4.5 with the rigid surface representing the drum.

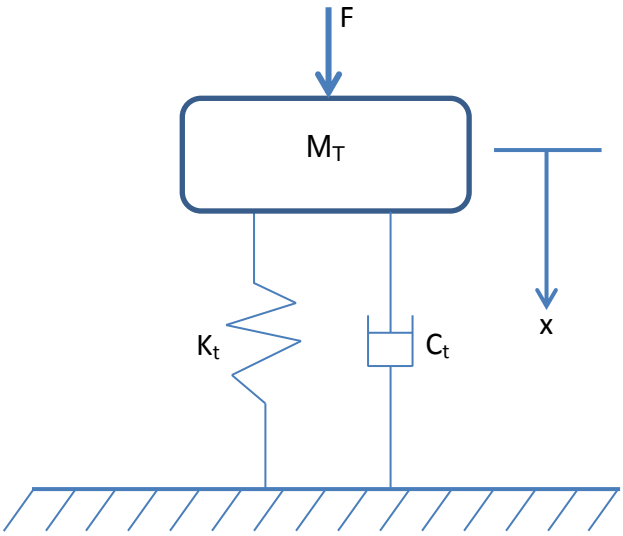

Figure 4.5: Schematic of Test Setup

Where M_T is the total moving mass of the wheel-tyre assembly, the axle and the moveable fork

$$M_T = M_w + M_a + M_f \tag{4.2}$$

M_w = Mass of wheel-tyre assembly

M_a = Mass of axle

M_f = Mass of moveable fork

K_t = Stiffness of Tyre

C_t = Damping of Tyre

F = Tyre Vertical Force

x = Tyre Vertical displacement

The equation of motion of the system shown in figure 4.5 is given in Eq 4.3 below

$$M_T\ddot{x} + C_t\dot{x} + K_t x = F \tag{4.3}$$

For a harmonic force, F is defined as

$$F = F_0 e^{i\omega t} \tag{4.4}$$

Where

F_0 = amplitude of force

ω = angular frequency of excitation

t = time

i = complex number operator

The displacement, x is defined as

$$x = Xe^{i\omega t} \tag{4.5}$$

Where

X = amplitude of displacement

Hence, the velocity is defined as

$$\dot{x} = i\omega X e^{i\omega t} = i\omega x \tag{4.6}$$

And the acceleration is defined as

$$\ddot{x} = i^2\omega^2 X e^{i\omega t} = i\omega\dot{x} \tag{4.7}$$

Hence, substituting Eq 4.4 – Eq 4.7 into Eq 4.3 gives

$$M_T i\omega\dot{x} + C_t\dot{x} + K_t\dot{x}/i\omega = F \tag{4.8}$$

The input mobility of the test setup is derived from Eq 4.8 and represented in Eq 4.9

$$\frac{\dot{x}}{F} = \frac{i\omega}{(K_t - M_T\omega^2) + i\omega C_t} \tag{4.9}$$

Rationalising the Denominator of Eq 4.9 gives Eq 4.10

$$\frac{\dot{x}}{F} = \frac{\omega^2 C_t + i\omega(K_t - M_T\omega^2)}{(K_t - M_T\omega^2)^2 + (\omega C_t)^2} \tag{4.10}$$

The modulus of the mobility is obtained from Eq 4.10

$$\left|\frac{\dot{x}}{F}\right| = \frac{\omega}{\sqrt{(K_t - M_T\omega^2)^2 + (\omega C_t)^2}} \tag{4.11}$$

The peak of a bode magnitude plot of the mobility is the point of resonance where the derivative of the mobility with respect to the angular frequency is equal to zero.

Therefore,

$$\frac{d}{d\omega}\left|\frac{\dot{x}}{F}\right| = 0 \tag{4.12}$$

Hence, the following is obtained at the peak:

$$K_t{}^2 - (M_T\omega^2)^2 = 0 \tag{4.13}$$

And since the stiffness constant K_t is not a negative value, Eq 4.13 is true when

$$K_t = M_T\omega^2 \tag{4.14}$$

The plot of the magnitude of the mobility and frequency from the experimental test on the tyre as shown in figure 4.6 below indicates a resonant frequency of $f_0 = 11.4Hz$.

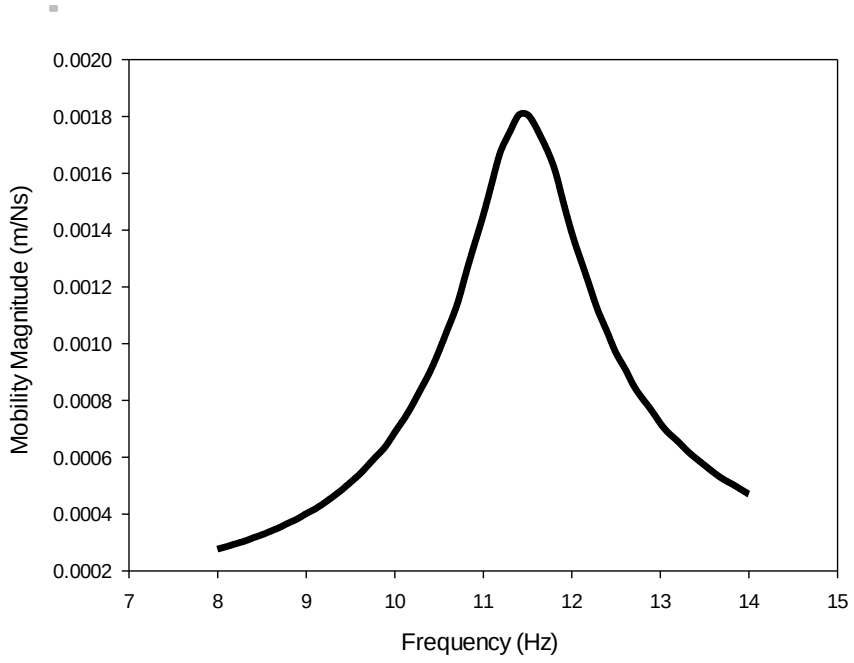

Figure 4.6: Mobility Bode Plot

At the resonant frequency, the damping coefficient can also be calculated by substituting Eq 4.14 into Eq 4.11. This gives Eq 4.15 which shows that the damping coefficient is the inverse of the mobility at the resonant frequency.

$$\left|\frac{\dot{x}}{F}\right| = \frac{1}{C_t} \tag{4.15}$$

The total moving mass M_T is computed from the impedance of the moving mass defined by the inverse of the mobility. The force F acting on the total moving mass when it is not in contact with the rigid drum surface is defined as:

$$F = M_T \ddot{x} \tag{4.16}$$

Replacing the acceleration term with velocity from Eq 4.7 gives the impedance as:

$$\frac{F}{\dot{x}} = i\omega M_T \tag{4.17}$$

The gradient of the bode plot of the Impedance in the figure 4.7 gives the total moving mass M_T as 75.15kg.

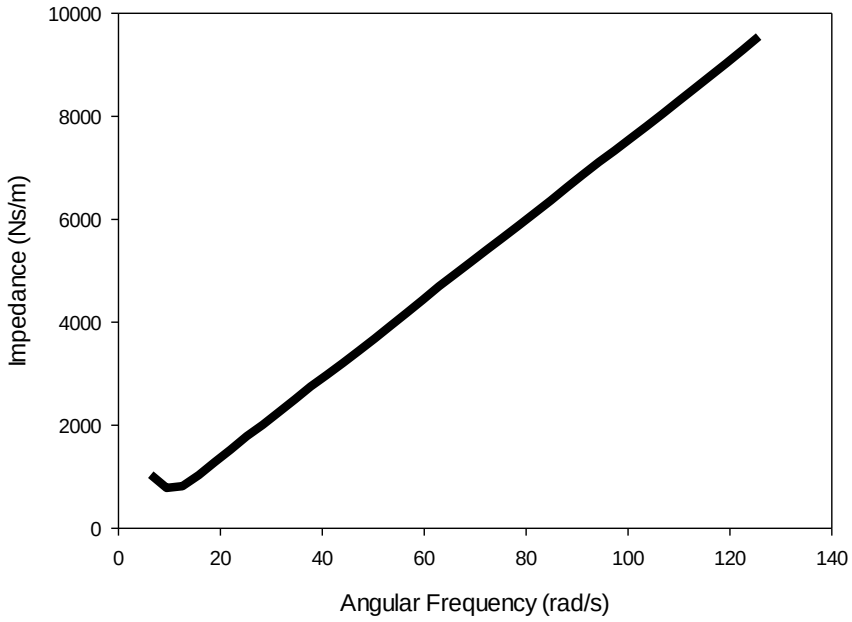

Figure 4.7: Impedance Bode Plot

With all the values for M_T and f_0 determined as 75.15kg and 11.4Hz respectively, the values of K_t and C_t were calculated by substituting M_T and f_0 into equations 4.14 and 4.15. Hence, K_t and C_t were computed as 385.57kN/m and 552.50Ns/m respectively.

4.4 QUARTER VEHICLE MODEL VALIDATION

The final test rig model is assembled by defining the mass and inertia properties of the components, the geometry of each part, the characteristics of the force element and finally, the joints which connect them together. The final assembly of the model is shown in figure 4.8.

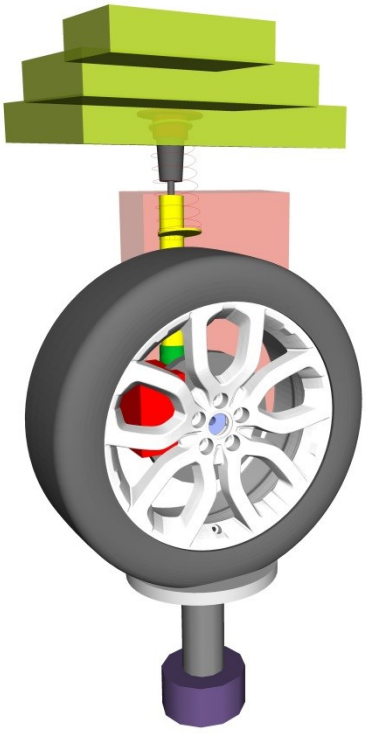

Figure 4.8: Quarter Vehicle Test Rig Model

The next phase of the model development is the validation of the model in SIMPACK. It is important that the data generated from the Quarter Vehicle Test rig model correlates with that from the physical test rig and is also reliable. Hence, the data from the model is correlated with data from the test rig. The correlation of the data is done for both the frequency and amplitude responses of the model and test rig.

In carrying out this validation, both the physical Quarter vehicle test rig (figure 3.1) and SIMPACK model (figure 4.8) were excited with the same drive signal of fixed displacement amplitude. The drive signals chosen to drive the test rig and SIMPACK model were the square wave, sine wave and triangle wave. These drive signal types were chosen because they were available as in-built functions in the digital controller. Each validation test involved setting a signal amplitude and frequency and driving the test rig and model with the selected drive signal then comparing the responses of the test rig with that from the model. The amplitudes for the drive signals were chosen in line with the health and safety consideration of running the test rig with the chosen signals and the severity of the input drive signals. Hence, the square and triangle wave, which have a greater shock impact than the sine wave on the test rig, had amplitudes of 10mm while the sine wave had an amplitude of 15mm. Likewise, the frequencies of the drive signals were chosen based on the safe frequencies for the chosen amplitudes of running the test rig. Though the actual deflection of the tyre contact patch on the Quarter vehicle test rig was not measured, based on the setup of the quarter vehicle test rig (moving contact patch), the tyre's additional deflections from the validation drive signals are in the range of the 2mm amplitude used for the characterisation of the simple tyre as

the entire test rig is moved vertically upwards and downwards from the contact patch.

4.4.1 Validation 1

The first validation was carried out using a square wave road input at the tyre contact patch. The signal had the following specification:

- Amplitude: 10mm
- Frequency: 0.5Hz

The feedback of the displacement from the test rig is used as the drive signal in the model in order to ensure the consistency of the drive signal in both cases as the feedback from the test rig is usually not the same as the drive command signal which in this case is the square wave. The results from the excitation are shown in figures 4.9 - 4.11.

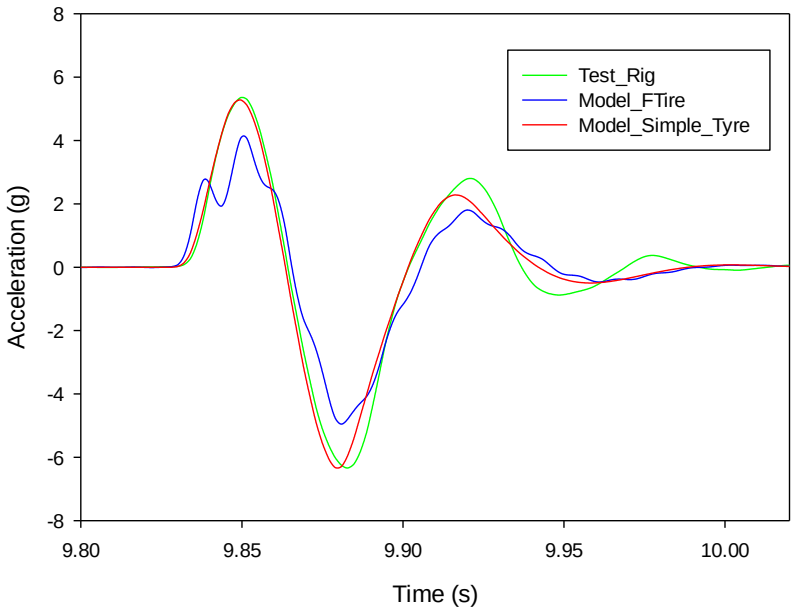

Figure 4.9: Square Wave Input Acceleration Response - Up Stroke

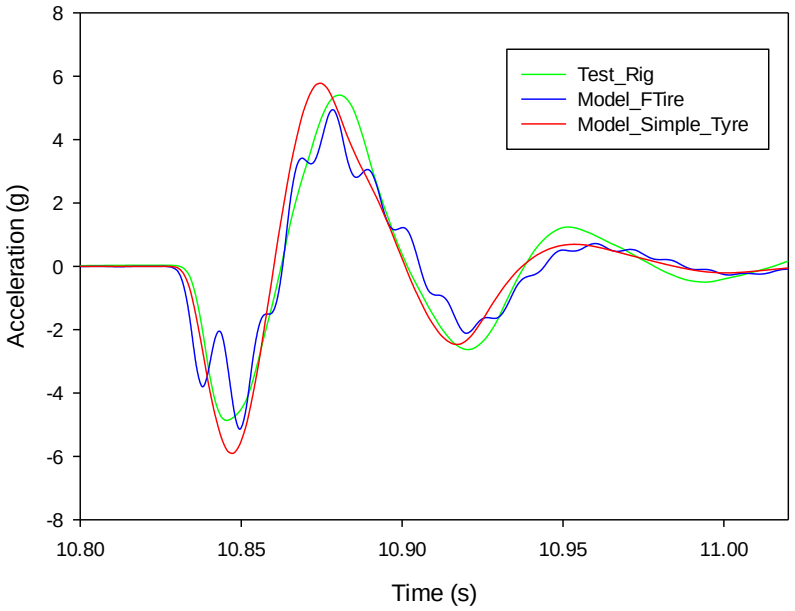

Figure 4.10: Square Wave Input Acceleration Response – Down Stroke

The wheel hub acceleration response as displayed in figures 4.9 and 4.10 indicate a good correlation between the test and simulation model based on a visual inspection. The quality of the correlation is examined by the root mean square error

(RMSE) computed for both the simple tyre and FTire models. The error value is also computed as a percentage of the peak test rig acceleration response.

The root mean square error is computed as:

$$RMSE = \sqrt{\frac{\sum\left(e(s)\right)^2}{n_s}} \qquad (1.1)$$

Where

e(s) = error in the signal

n_s = number of samples in signal

The RMSE for the simple tyre and FTire models was computed as 0.15g (2.77% of peak value) and 0.25g (4.62% of peak value) respectively. This implies that the response from the FTire model doesn't perform as well as that from the simple tyre model.

The next step in this validation was the comparison of the frequency response of the test rig and simulation model. The result of the power spectral density (PSD) analysis of the square wave wheel acceleration response in figures 4.9 and 4.10 is shown in figure 4.11.

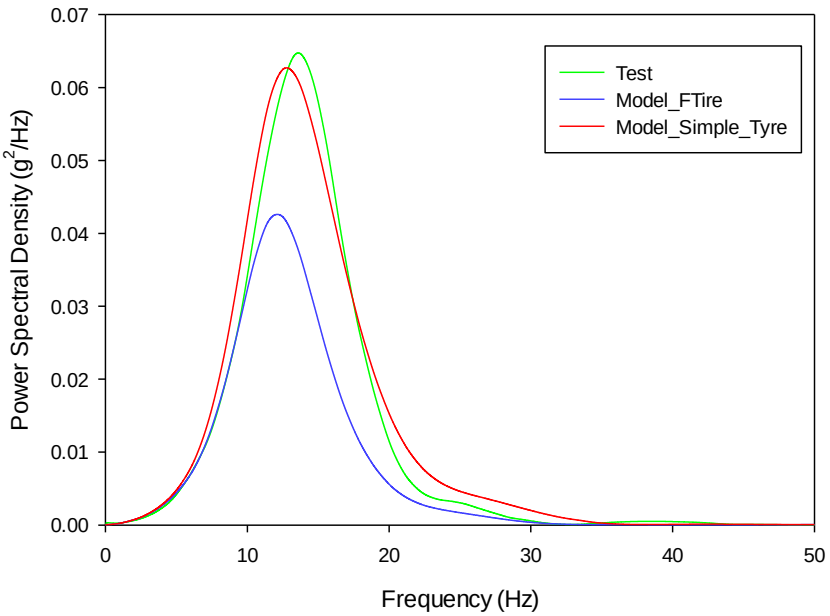

Figure 4.11: Power Spectral Density of Wheel Hub Acceleration

The frequency response result shows the peaks for the test, FTire model and simple tyre model as 13.5Hz, 12.2Hz and 12.8Hz respective. This again shows that the simple tyre model's behaviour in the quarter vehicle model is better than that from the FTire model. The difference in the FTire behaviour can be attributed to the fact that the model was developed for a rolling tyre while the simple tyre properties were obtained from a non-rolling tyre test. For this reason, the use of the FTire model is not considered any further in this current research; all simulations are carried out using the simple tyre model.

The peak frequency of 13.5Hz observed in figure 4.11 for the wheel hub acceleration response of the entire quarter vehicle is somewhat close to the resonant frequency of 11.4Hz for the tyre-wheel assembly alone as shown in figure 4.6. The variation in the frequency is due to the inclusion of the various suspension

elements, such as the spring and damper, as well as the sprung mass in the quarter vehicle test rig (figure 3.1); these suspension components were not present in the tyre-wheel assembly as seen in figure 4.4 The effects of these suspension components and sprung mass on the resonance frequencies are investigated in chapter 5 of this thesis.

4.4.2 Validation 2

The second validation is carried out using a sine wave input drive signal with the following specification:

- Amplitude: 15mm
- Frequency: 1Hz

The comparison of the wheel acceleration response from the test and simulation model is shown in the figure 4.12. The result again shows a good correlation between the test rig response and model.

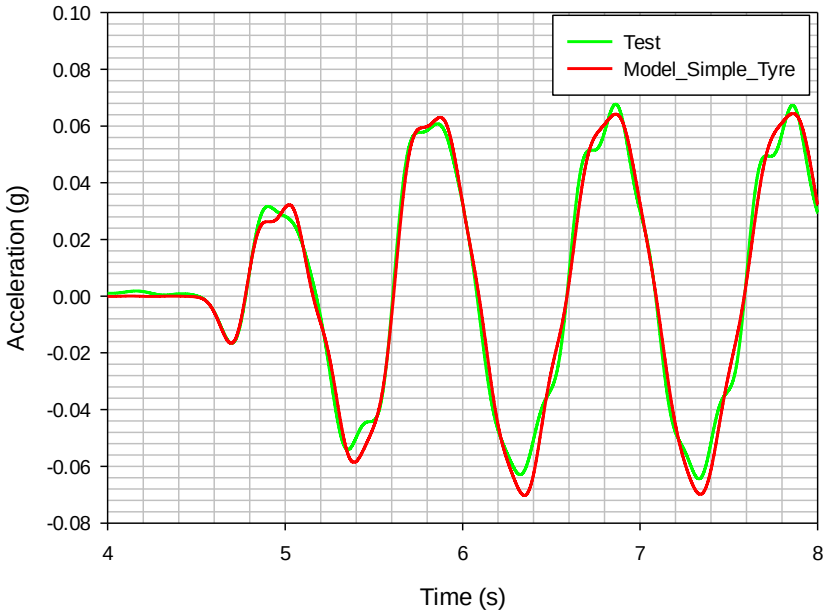

Figure 4.12: Sine Drive Input Acceleration Response

4.4.3 Validation 3

The final validation is carried out using a triangle wave input drive signal with the following specification:

- Amplitude: 10mm
- Frequency: 1Hz

The comparison of the wheel acceleration response from the test and simulation model is shown in the figure 4.13. The result, once again, shows a good correlation for the peaks and troughs in the test rig and model response.

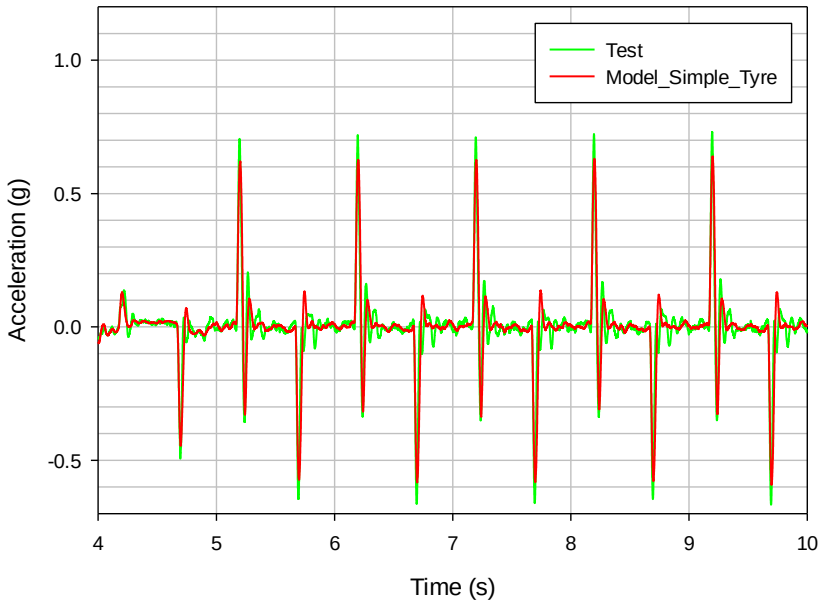

Figure 4.13: Triangle Wave Drive Input Acceleration Response

The results of the model validation indicate the accuracy and fidelity of the CAE model. Hence, the model was classed as fit for generating reliable data for use in the latter sections of this thesis.

4.5 FULL VEHICLE MODELLING

The full vehicle model is an approximate model of the commercial SUV from which the Quarter vehicle test rig was developed. The model has a total of 17 degrees of freedom in all the vehicle axis directions as shown in figure 4.14 except the vehicle's longitudinal direction (translation on the horizontal axis) and the yaw direction (rotation about the vertical axis). This model comprises the left hand front (LHF), left hand rear (LHR), right hand front (RHF) and right hand rear (RHR) suspension units, the wheels and tyres, the chassis and anti-roll bars.

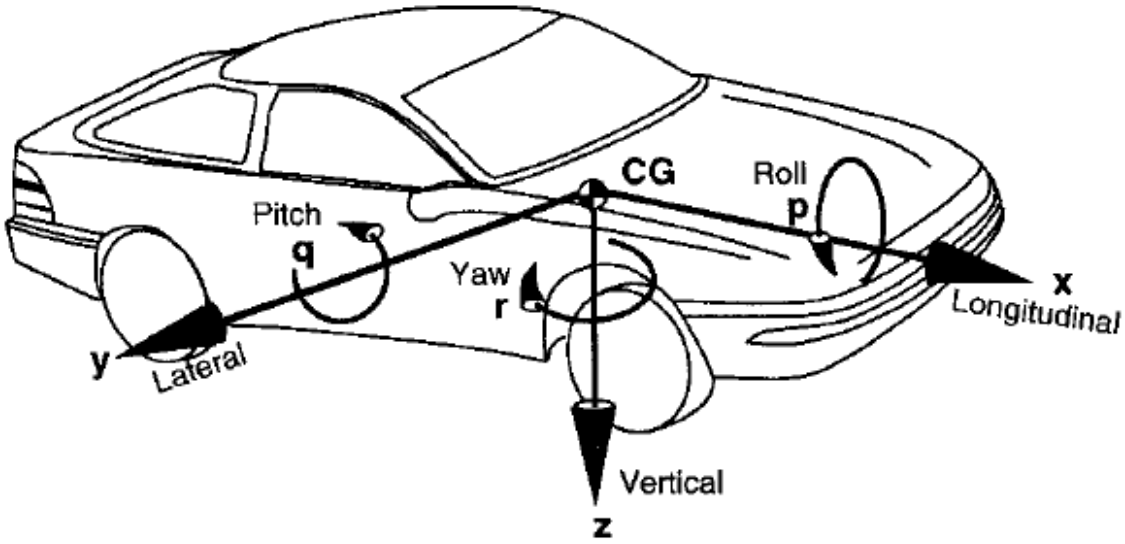

Figure 4.14: SAE Vehicle Axis System [92]

The chassis, vehicle body and other mass elements were represented as simple geometrical shapes with the MoI and CoG calculated from the available CAD data. The tyre, spring, bump stop and shock absorber characteristics are the same as used in the quarter vehicle model setup as highlighted in the preceding section. In addition to the components identified for the quarter vehicle model, front and rear anti-roll bars were included in the full vehicle model. The force properties of these anti-roll bars were supplied by the vehicle manufacturer of the SUV. The full vehicle model assembly is shown in figure 4.15.

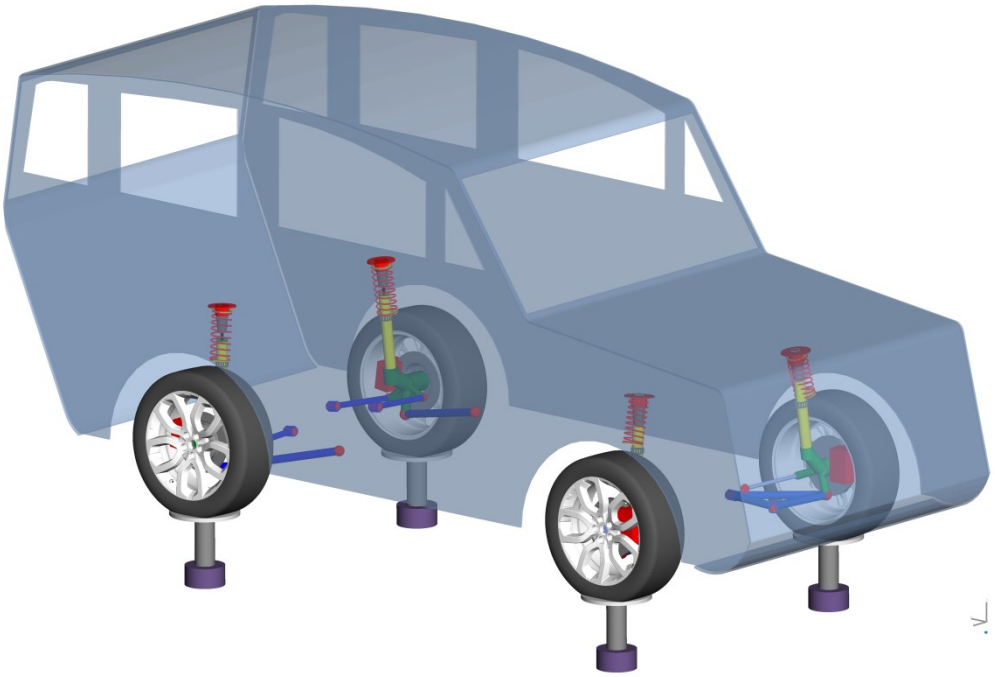

Figure 4.15: Full Vehicle Model

4.6 FULL VEHICLE MODEL VALIDATION

In the absence of any usable road input drive for the validation of the full vehicle mode, a drive file for a kerb drive over event collected from a proving ground data acquisition exercise is generated from this model using QanTiM. The aim of this was to observe how well this model could reproduce the acquired data, hence indicating a level of similarity to the original vehicle. The results from the developed drive file produced the results in figures 4.16 – 4.19.

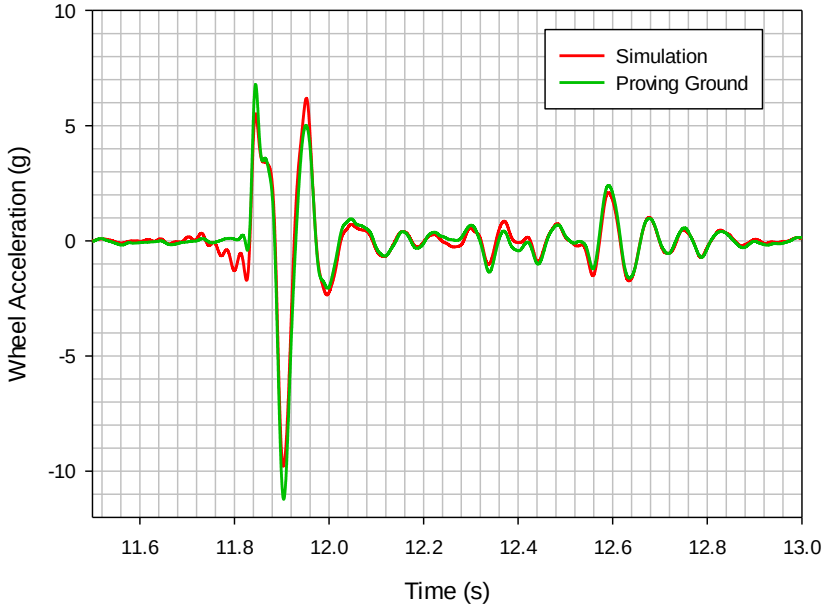

Figure 4.16: LHF Wheel Acceleration Response

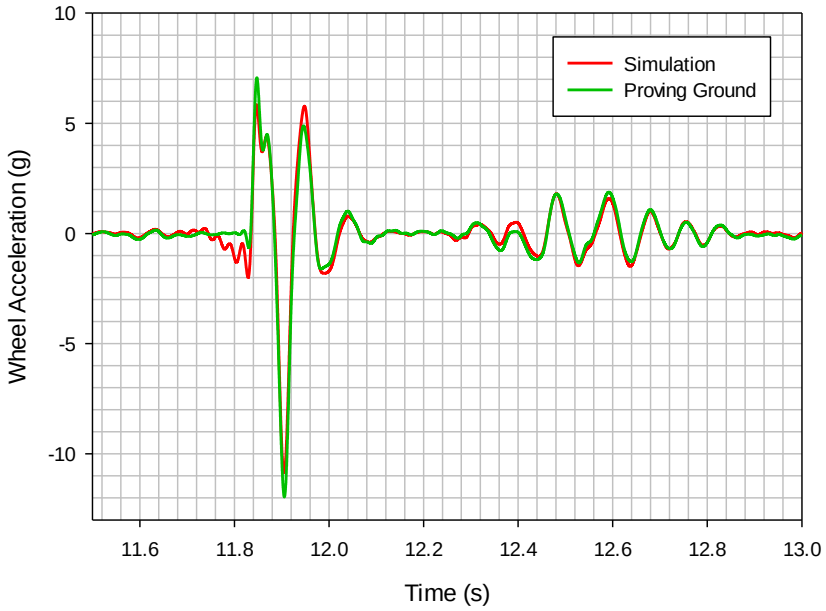

Figure 4.17: RHF Wheel Acceleration Response

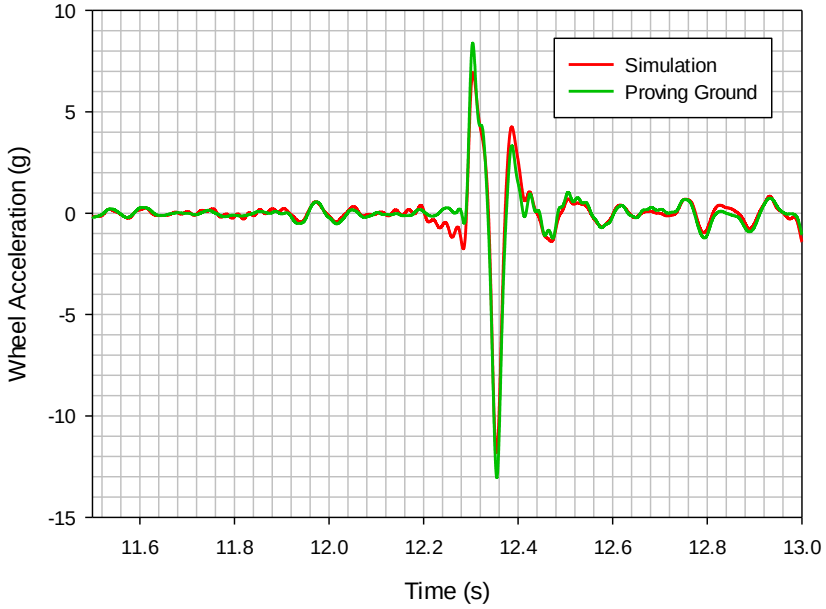

Figure 4.18: LHR Wheel Acceleration Response

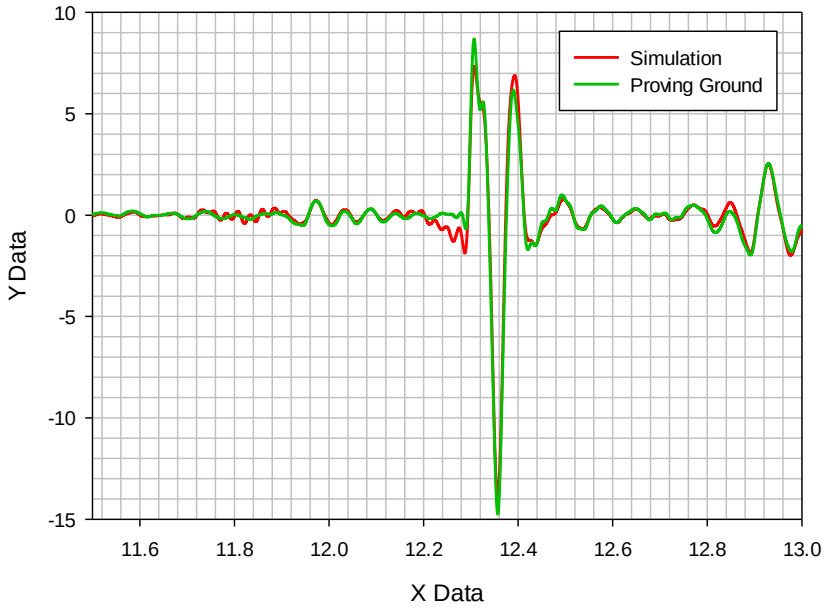

Figure 4.19: RHR Wheel Acceleration Response

These results show the acceleration response of the wheel to the iterated road input drive file and it can be observed that there's a good visual correlation between the data collected from the proving ground data acquisition and that from the simulation.

4.7 CONCLUSION

The validation of the developed MBD simulation models of both the quarter vehicle and the full vehicle show reliable results. With the fidelity of the results in place, these models would be used for the generation of road load data for use in the latter section of this thesis and would also provide a platform to test the accuracy of the artificial neural network method adopted in this research.

4.8 SUMMARY

CAE models of the quarter vehicle test rig and a full vehicle were developed in SIMPACK with the physical characteristics of the various suspension system components obtained from testing and the manufacturer of the SUV. A simple tyre model was developed for the CAE model using a one degree of freedom system. The developed model of the quarter vehicle test rig was thereafter validated using a square wave, sine wave and triangle wave input drive signals to drive both the test rig and model. The presented results of the comparison of the response from both the test rig and model indicated a good correlation. Similarly, the full vehicle model was validated by iterating the drive file for a kerb run-over road event and comparing the response of the model with that collected from the proving ground data acquisition with the results showing a good model performance. Hence, the Quarter

Vehicle model and Full Vehicle model were proven as fit for the generation of data for use in the latter section of this thesis.

CHAPTER FIVE: CHARACTERISATION OF THE EFFECTS OF VEHICLE PARAMETER VARIATION

5.1 INTRODUCTION

Having completed the development of the MBS model of the quarter vehicle (QV) test rig and full vehicle (FV) models in the last chapter, this chapter investigates the effects of the changes in vehicle parameters on the vehicle's response as it traverses the road surface. The aim of this chapter is to represent the effects of the variation of the vehicle configuration parameters on the road load data as a way to understand the trends in the road load data. The effects of the changes in the vehicle configuration parameter on the effective road input signal is also investigated. The effective road input signal can in future works be used for durability testing as done by Backer et al.[26]

The chapter is divided into two sections; the first is the characterisation of the road load data from the variation of the vehicle parameters in the QV and FV models and the second is the characterisation of the effective road input signal with the variation of the vehicle parameters in both the QV and FV models.

5.2 ROAD LOAD VARIATION IN VEHICLE VARIANTS

Vehicle variants were discussed in the literature survey section where the advantage of the transfer of knowledge from the development of a predecessor model to newer model was highlighted. Various vehicle parameters could be altered in response to meeting design or durability performance targets for a production vehicle. Some of such parameters that are changed in a vehicle configuration include spring stiffness, shock absorber damping characteristics, bump stop

damping characteristics, wheel base, kerb weight, number of chassis frame to body mount points etc. The implementation of these parameter variations in the vehicle would induce a change in the behaviour and response of the vehicle. These are changes that need to be captured so that the design engineer can optimise the performance of the new vehicle configuration.

In order to understand how the vehicle parameter changes affect the response of the vehicle, the road load data from the various vehicle configurations are investigated and presented as statistical trends to characterise the peak values, range and the frequency content of the vehicle responses [14, 93].

5.3 QUARTER VEHICLE ROAD LOAD DATA CHARACTERISATION

The characterisation of the road load data for the variants of the quarter vehicle was considered first because of its simplicity. The quarter vehicle is the simplest system that captures the behaviour of the vehicle while excluding the effects of vehicle roll and pitch.

In order to drive the quarter vehicle with a realistic road input, a proving ground (PG) road load data of the commercial SUV from which the quarter vehicle test rig was designed is back calculated via QanTiM to provide a corresponding displacement time history drive file to the PG road load data. The event from the PG is a "*3-inch kerb drive-over*" event at a vehicle speed of 10 km/h. The assumption in this analysis is that the effective road input signal for all the vehicle variants is constant. The PG road load data for which a back-calculated drive file was generated is the left hand front (LHF) wheel hub vertical acceleration response to the kerb drive-over

event. The section corresponding to the wheel hub's impact with the kerb is as shown in figure 5.1.

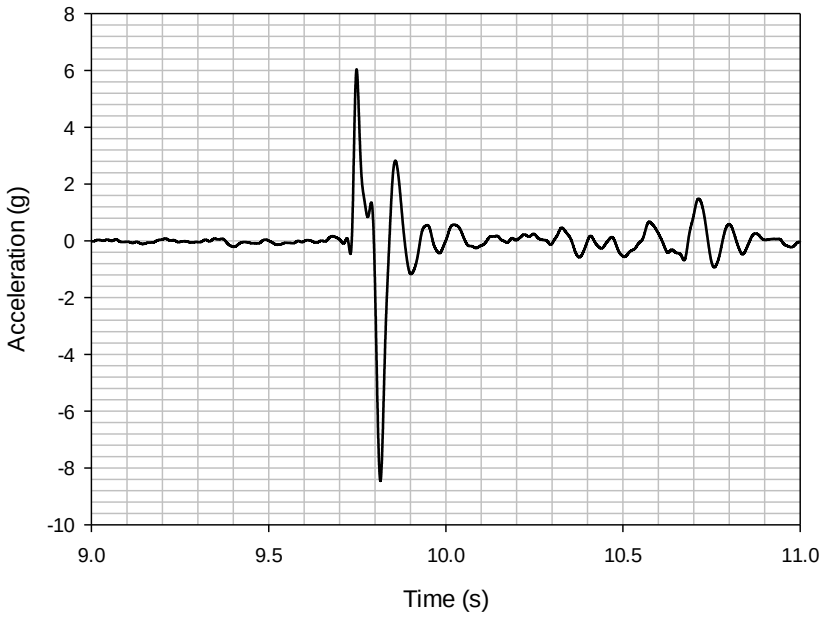

Figure 5.1: LHF Wheel Hub Vertical Acceleration for the 3-Inch Kerb Drive Over Event

The back-calculated drive file is generated from the original quarter vehicle configuration with the following details:

Total Quarter Vehicle Mass: 520kg

Spring Stiffness: 29kN/m

Damping Characteristic Factor: 1

The damping characteristic factor is the numerical factor by which the original shock absorber damping characteristic, as indicated in Figure 4.3, is multiplied in order to scale up or down the values of the damping characteristic curve.

The generated input drive file is shown in figure 5.2.

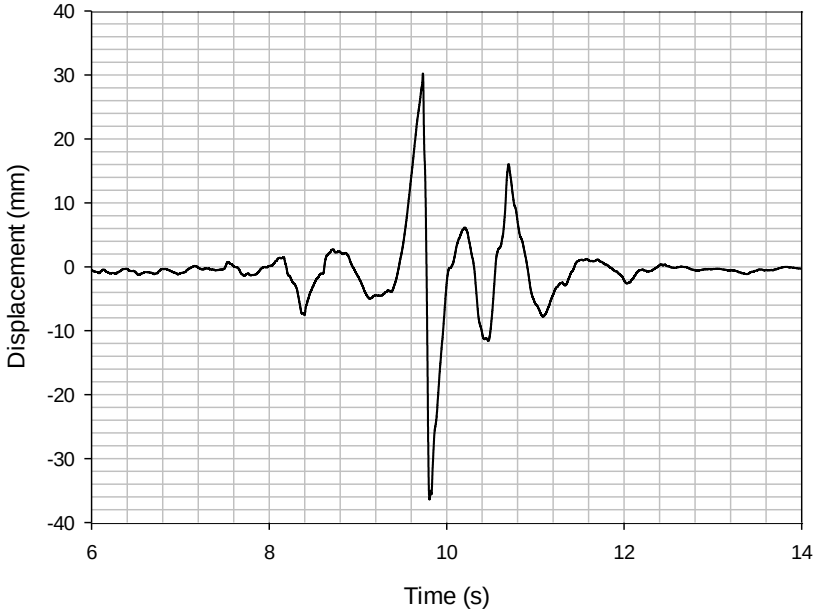

Figure 5.2: LHF Drive File Generated from PG Event

The investigation of the effects of the variation of the quarter vehicle parameters was carried out in 3 categories based on the variant parameter while other parameters were kept constant. The varying parameter categories are as follows:

QV1. Damping Characteristic factor

QV2. Spring Stiffness

QV3. Quarter Vehicle Weight

The table 5.1 summarises the simulation scenarios based on the 3 categories.

Table 5.1: Quarter Vehicle (QV) RLD Characterisation Simulation Scenarios

Simulation Scenario #	Damping Characteristic Factor	Spring Stiffness (kN/m)	Quarter Vehicle Weight (kg)
1	0.75	29	520
2	1.00	29	520
3	1.50	29	520
4	1.25	29	520
5	1.00	25	520
6	1.00	29	520
7	1.00	35	520
8	1.00	40	520
9	1.00	29	520
10	1.00	29	650
11	1.00	29	780

The results from the simulation of scenarios presented in table 1 are displayed in charts to show the variation in the road load data. These results are categorised using the peak values and the range of the hub acceleration response for each simulation scenarios in table 5.1. The peak values are the maximum acceleration values while the range values are the difference between the maximum and minimum acceleration values. The range and peak values are as shown in figure 5.3.

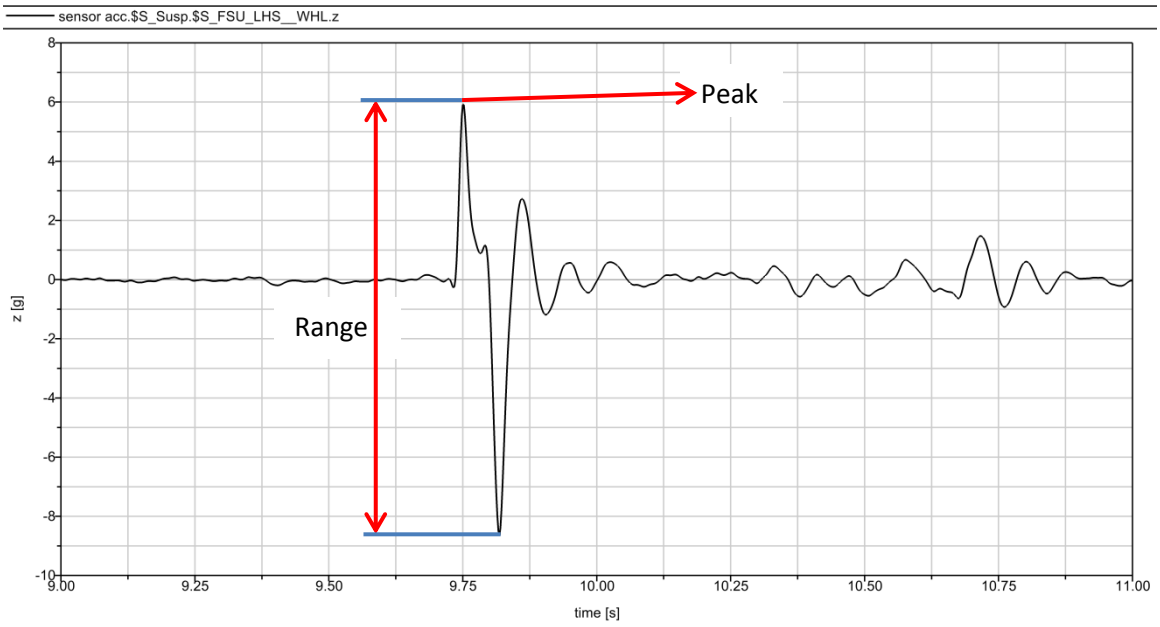

Figure 5.3: Sample Hub Acceleration Response

5.3.1 QV 1 (Variable Damping Characteristic factor) Results

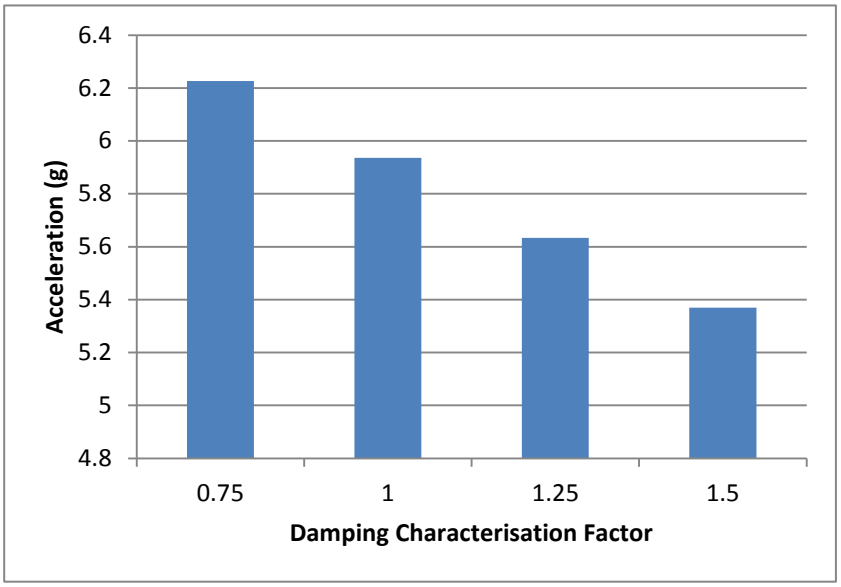

Figure 5.4: QV 1 Unsprung Mass Acceleration (Peak)

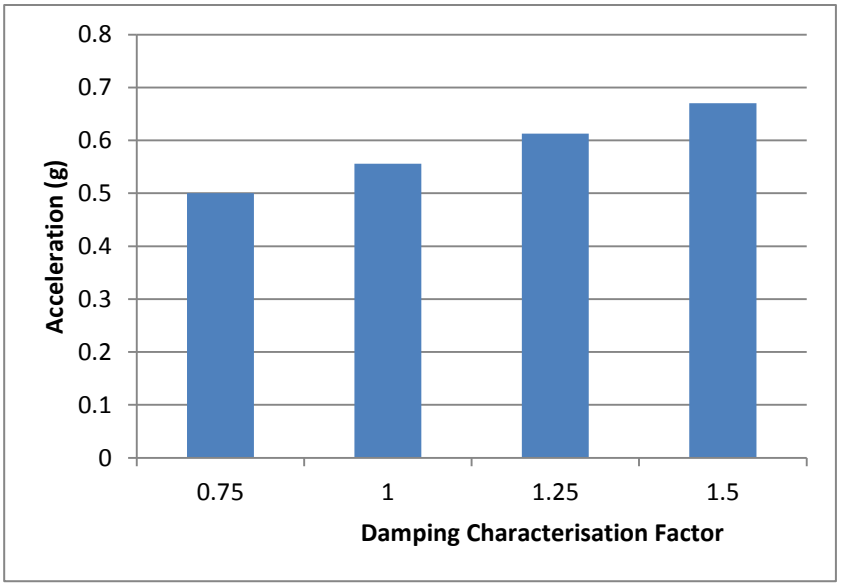

Figure 5.5: QV 1 Sprung Mass Acceleration (Peak)

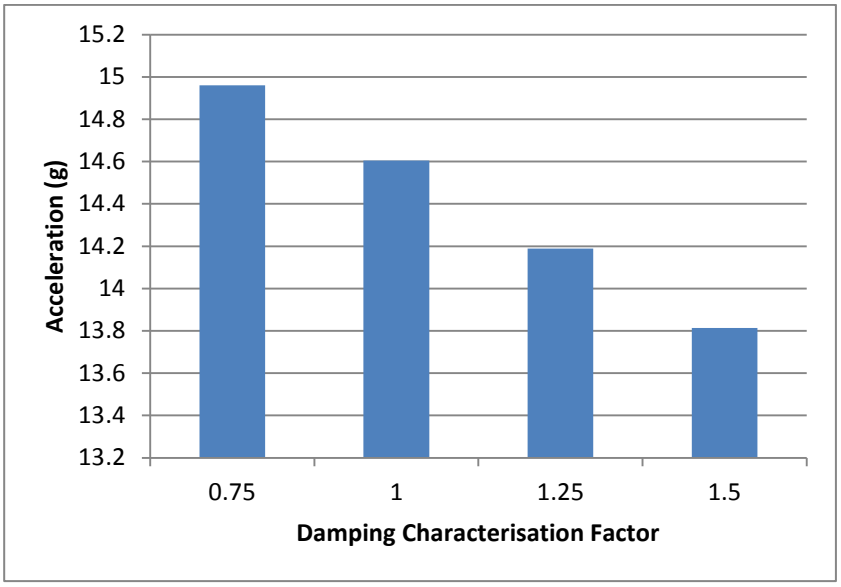

Figure 5.6: QV 1 Unsprung Mass Acceleration (Range)

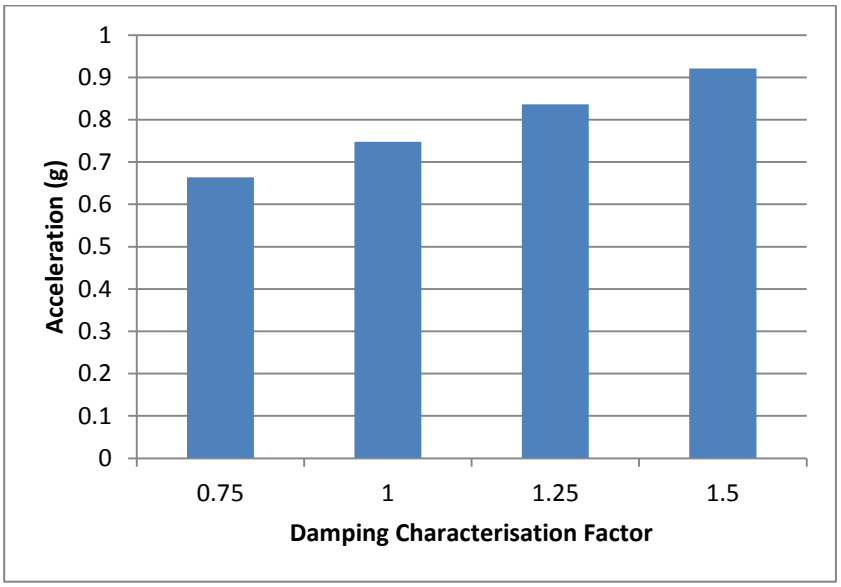

Figure 5.7: QV 1 Sprung Mass Acceleration (Range)

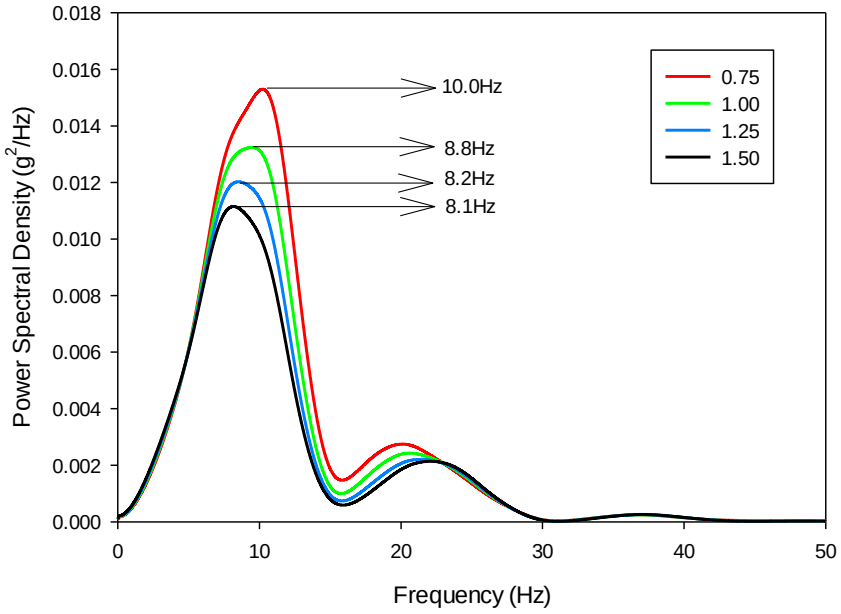

Figure 5.8: QV 1 Frequency Response Variation of Unsprung Mass Acceleration with Damping Characteristic Factor

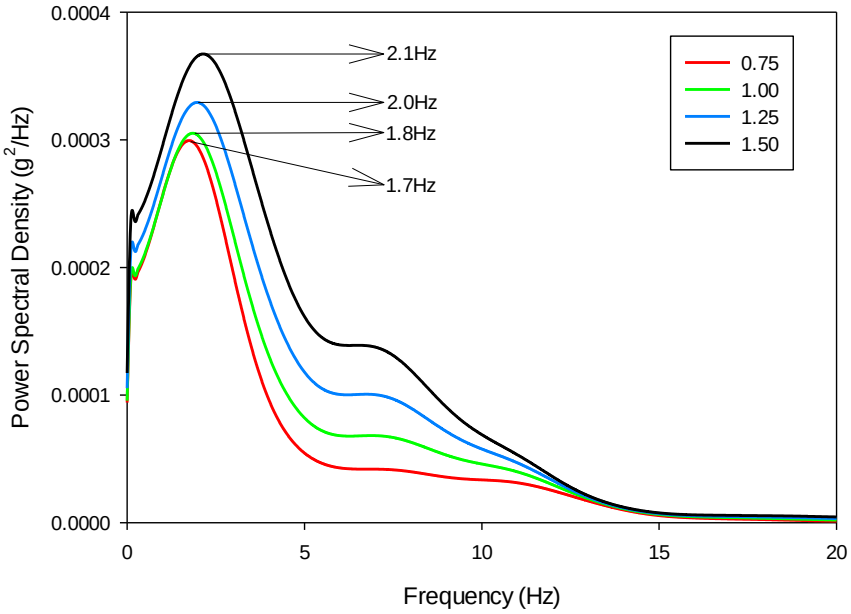

Figure 5.9: QV 1 Frequency Response Variation of Sprung Mass Acceleration with Damping Characteristic Factor

The results from category 1 simulation scenarios in figures 5.4 – 5.7 indicate a decreasing trend in the unsprung mass acceleration and an increasing trend in the sprung mass acceleration as the damping characteristic factor increases. This is an expected trend because the damping force increases with the damping characteristic factor thereby limiting the oscillation of the unsprung mass and increasing the peak acceleration of the sprung mass.

The frequency response plot for the unsprung mass acceleration in figure 5.8 shows a negative shift in the first resonance frequency of unsprung mass as well a positive shift of the second resonance frequency of the unsprung mass though the second resonance frequency seems to be a harmonic of the first frequency. The frequency response for the sprung mass acceleration in figure 5.9 indicates a positive shift in the resonance frequency and is similar to the trend of the second resonance frequency of the unsprung mass acceleration in figure 5.8.

5.3.2 QV 2 (Variable Spring Stiffness) Results

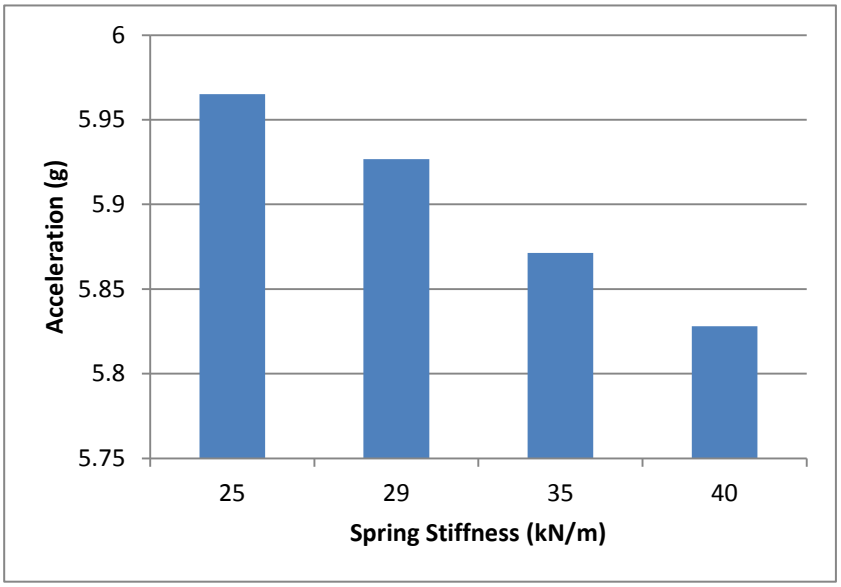

Figure 5.10: QV 2 Unsprung Mass Acceleration (Peak)

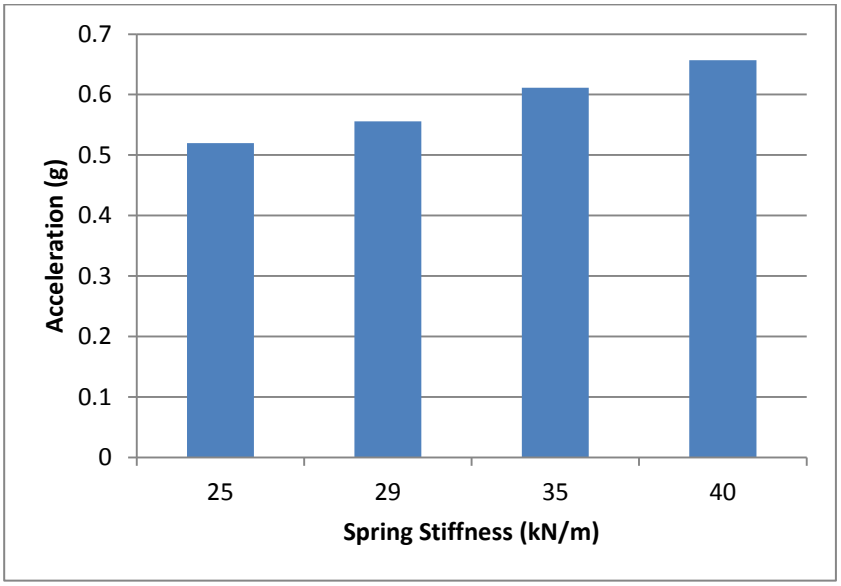

Figure 5.11: QV 2 Sprung Mass Acceleration (Peak)

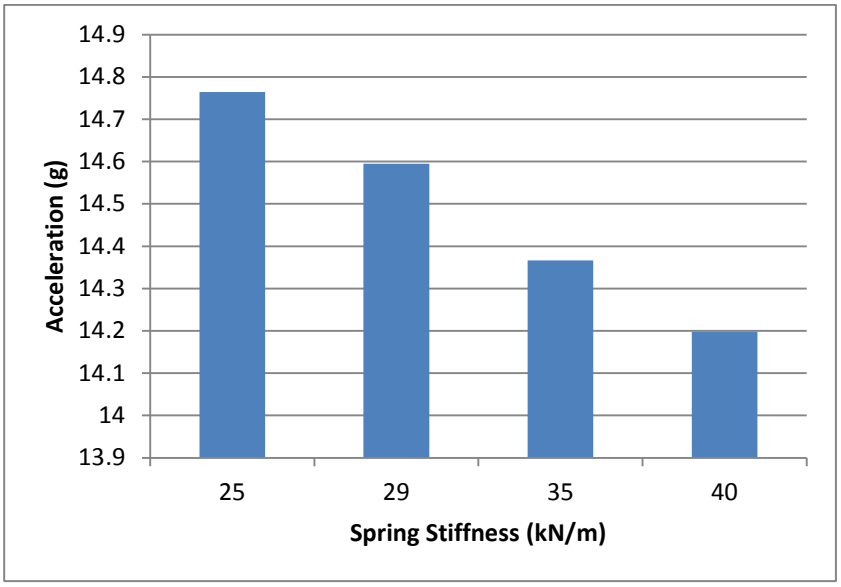

Figure 5.12: QV 2 Unsprung Mass Acceleration (Range)

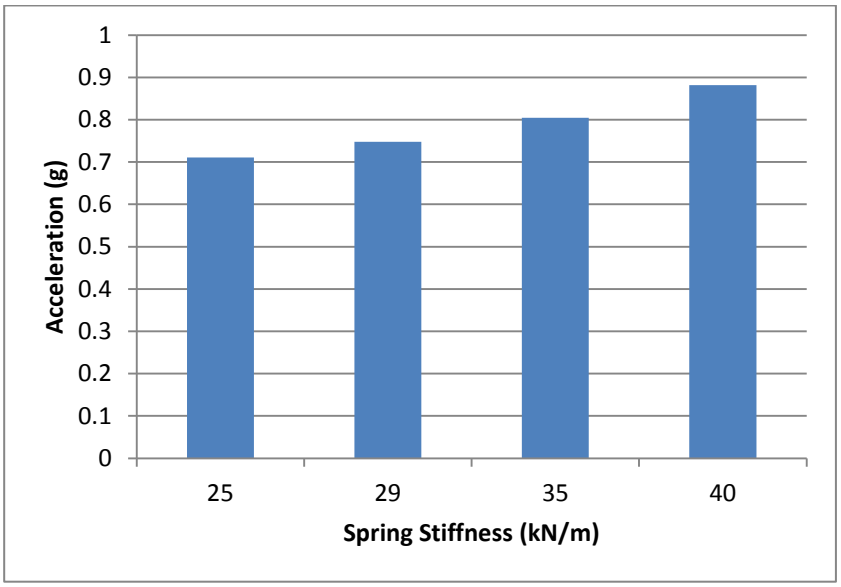

Figure 5.13: QV 2 Sprung Mass Acceleration (Range)

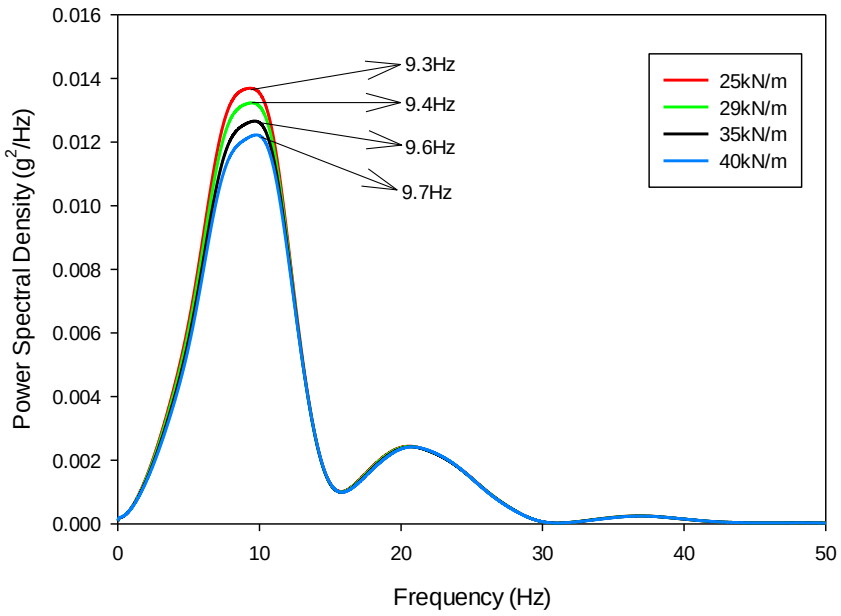

Figure 5.14: QV 2 Frequency Response of Unsprung Mass Acceleration to Spring Stiffness Variation

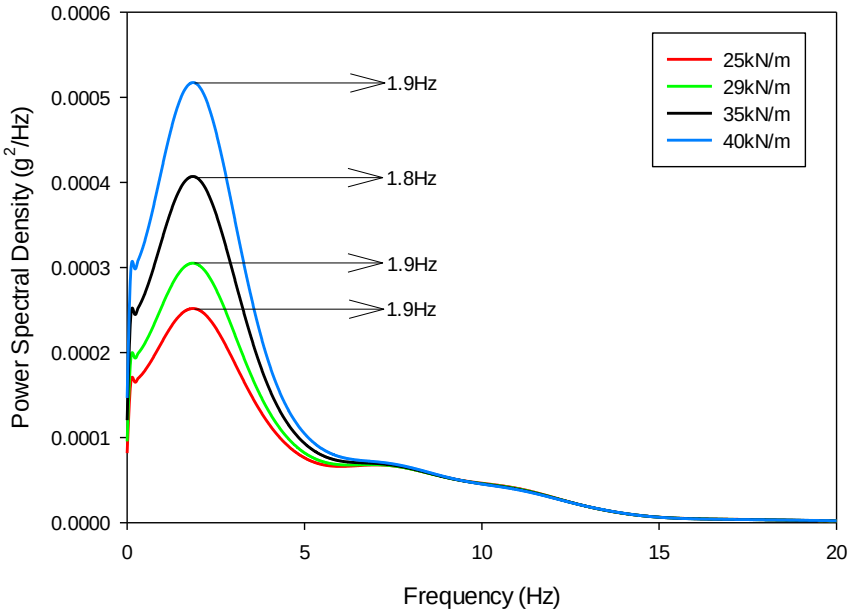

Figure 5.15: QV 2 Frequency Response of Sprung Mass Acceleration to Spring Stiffness Variation

The effect of the increasing spring stiffness has a noticeable negative trend on the unsprung mass acceleration and a positive trend on the sprung mass acceleration as observed in figures 5.10 – 5.13. This implies a decrease in the vibrational response of the unsprung mass and an increase in the vibration of the sprung mass as the spring stiffness increases. The frequency response plots shown in figure 5.14 and 5.15 also confirm this as the power spectral density of the unsprung mass acceleration decreases at the resonance frequency as the spring stiffness increases while that of the sprung mass acceleration increases at the resonance frequency as the spring stiffness increases.

5.3.3 QV 3 (Variable Quarter Vehicle Weight) Results

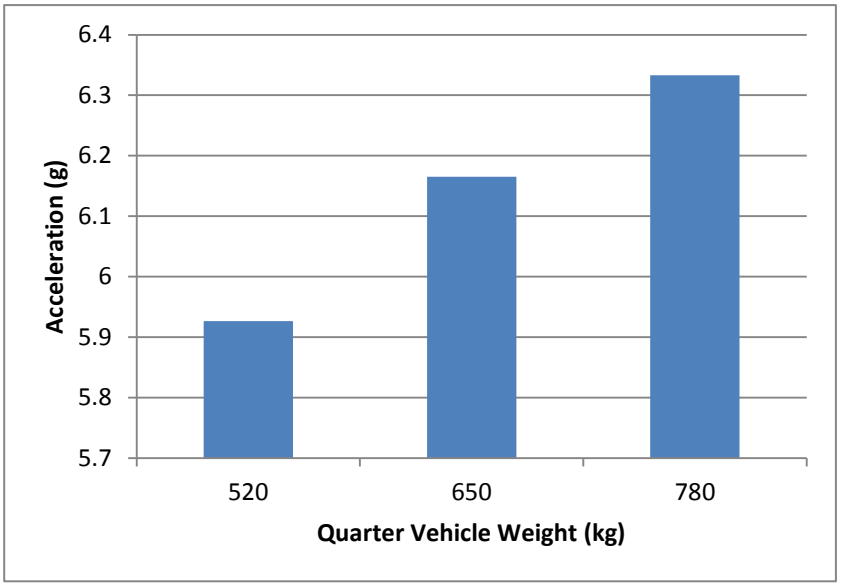

Figure 5.16: QV 3 Unsprung Mass Acceleration (Peak)

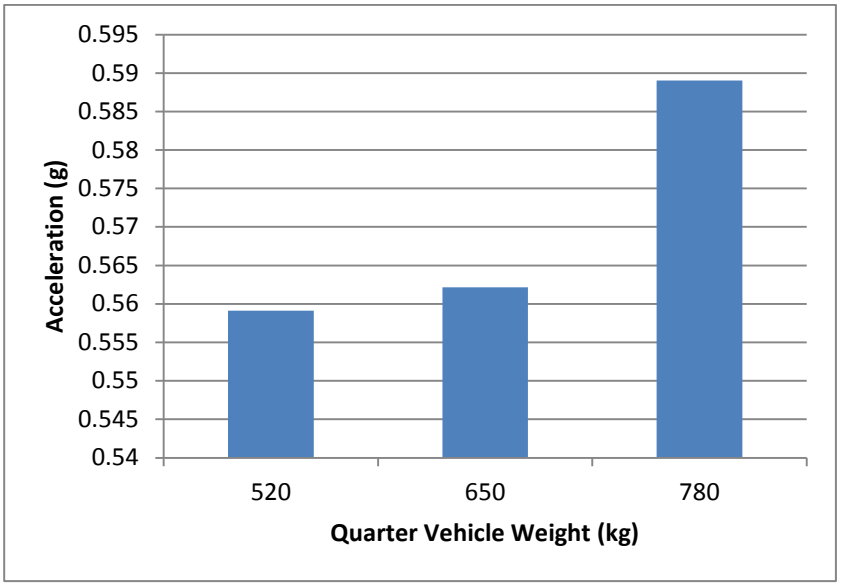

Figure 5.17: QV 3 Sprung Mass Acceleration (Peak)

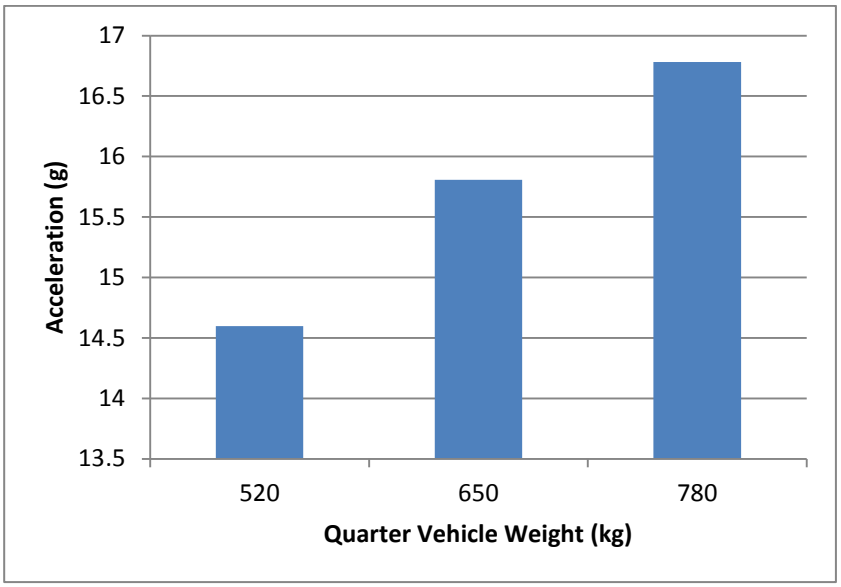

Figure 5.18: QV 3 Unsprung Mass Acceleration (Range)

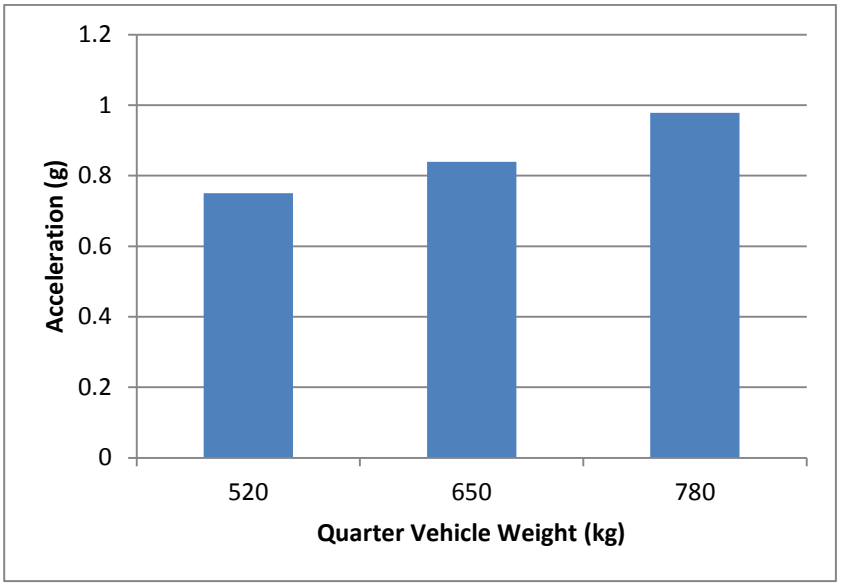

Figure 5.19: QV 3 Sprung Mass Acceleration (Range)

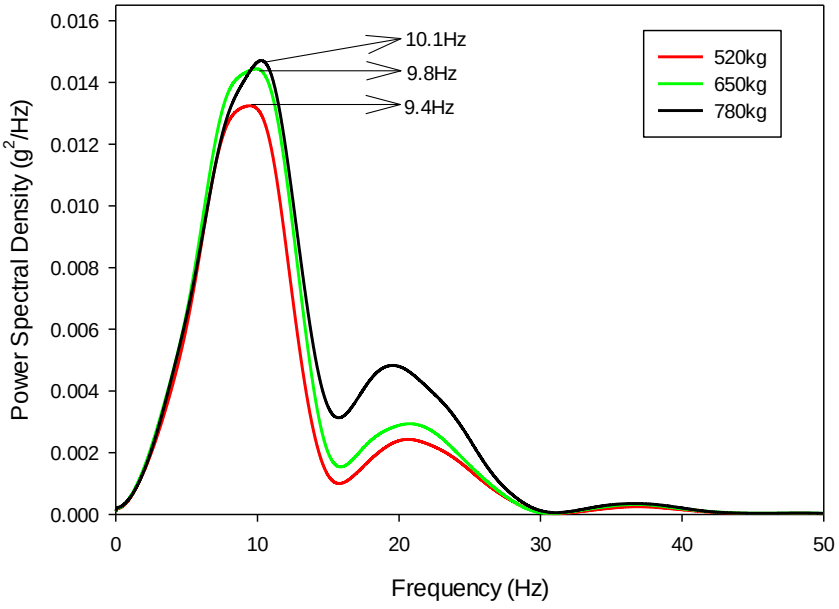

Figure 5.20: QV 3 Frequency Response of Unsprung Mass acceleration to Quarter Vehicle Weight Variation

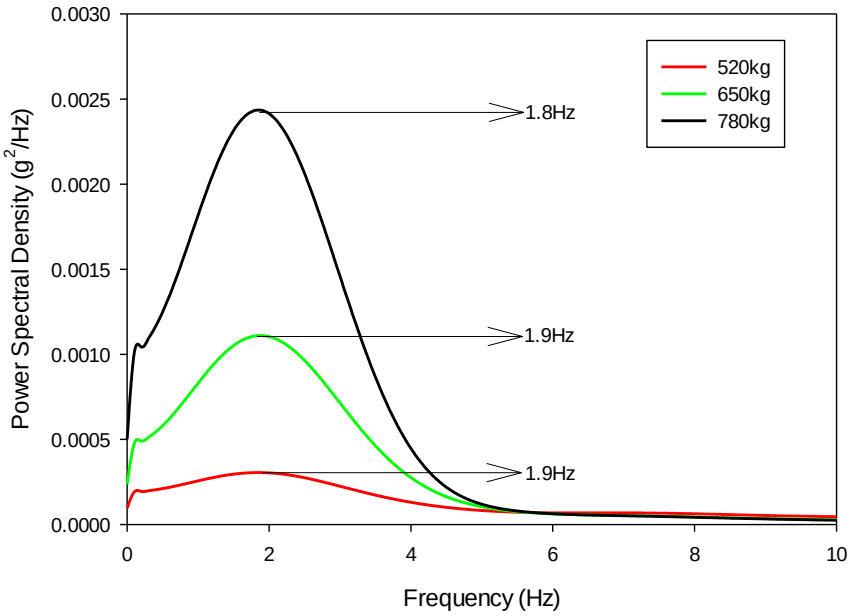

Figure 5.21: QV 3 Frequency Response of Sprung Mass acceleration to Quarter Vehicle Weight Variation

The visible trend in the sprung mass and unsprung mass acceleration as shown in figures 5.16 – 5.19 are positive upward trends for the increasing quarter vehicle weight. It can be clearly observed that the relationship between the quarter vehicle weight and the unsprung mass acceleration is fairly linear while that of the sprung mass acceleration is non-linear. The frequency response plot in figure 5.20 shows that there is a positive shift in the first resonance frequency of the unsprung mass as the quarter vehicle mass increases. The frequency plot, however, shows a negative shift in the second resonance frequency as the vehicle weight is increased. The frequency plot in figure 5.21, for the sprung mass acceleration, shows a consistent and positive trend at the resonance frequency as the quarter vehicle weight increases. The trends observed particularly in the frequency plot of the unsprung mass acceleration are as a result of the non-linear bump stop being engaged as the

quarter vehicle weight increases. The results for QV3 without the bump stop are presented as follows to observe the effects of the bump stop:

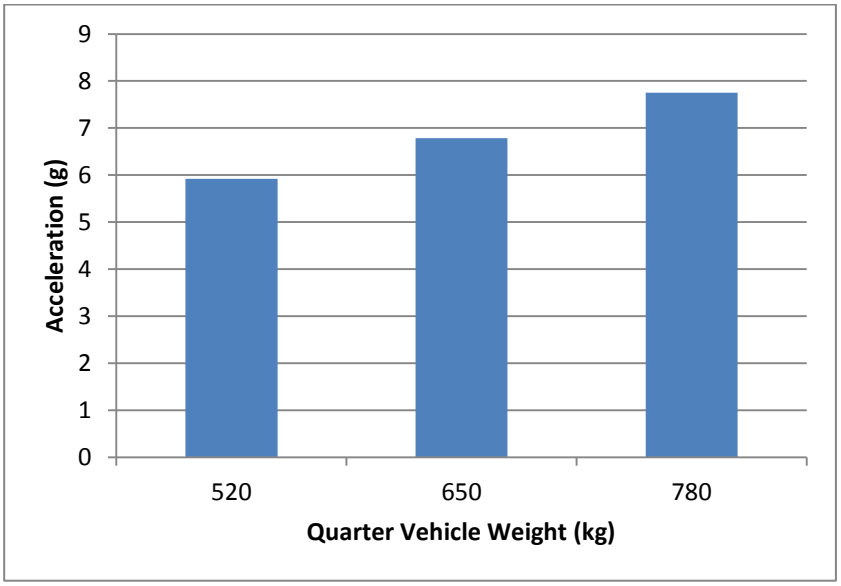

Figure 5.22: QV 3 Unsprung Mass Acceleration without Bump Stop (Peak)

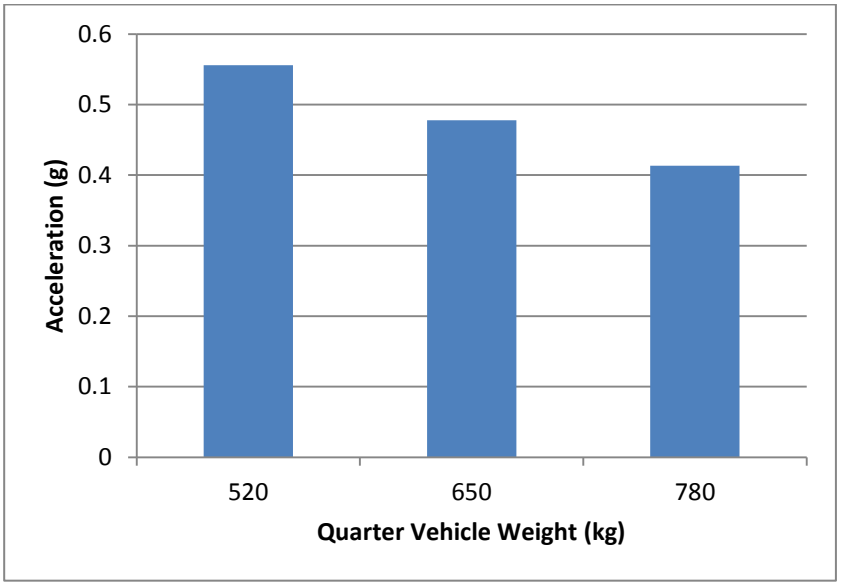

Figure 5.23: QV 3 Sprung Mass Acceleration without Bump Stop (Peak)

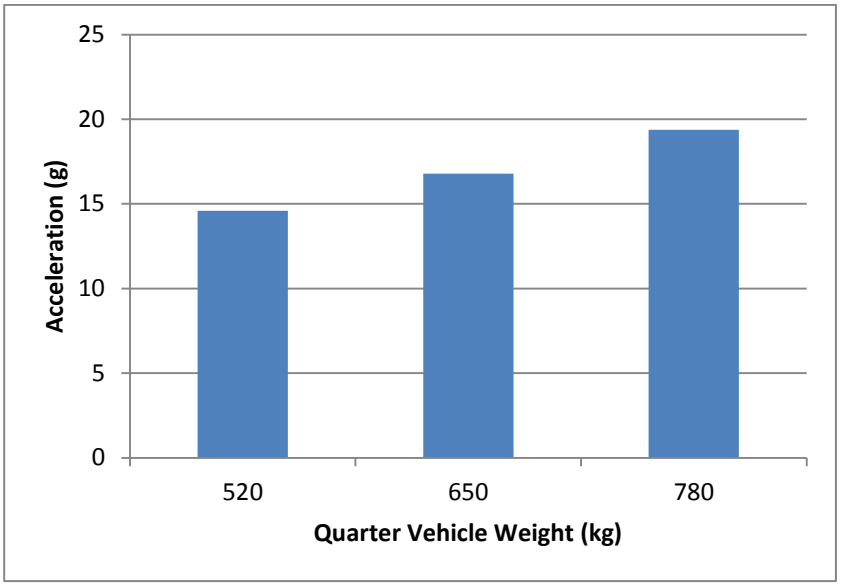

Figure 5.24: QV 3 Unsprung Mass Acceleration without Bump Stop (Range)

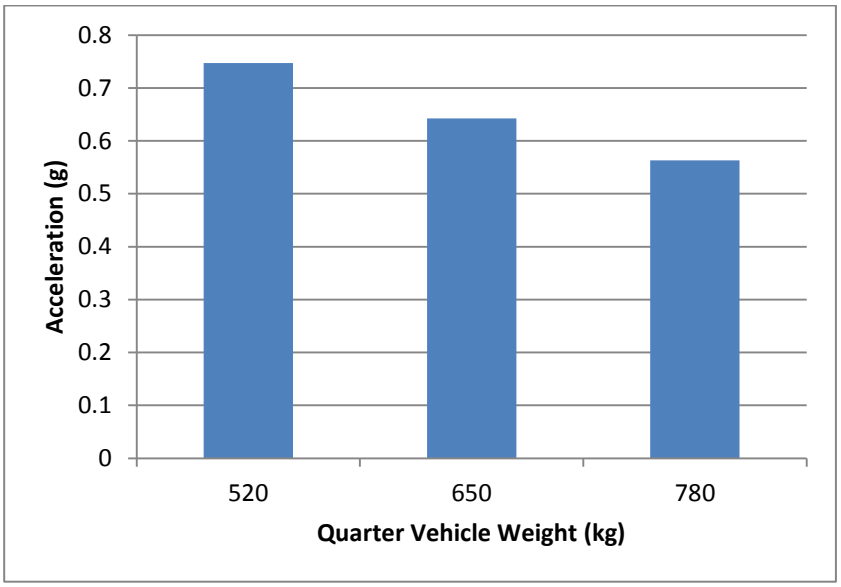

Figure 5.25: QV 3 Sprung Mass Acceleration without Bump Stop (Range)

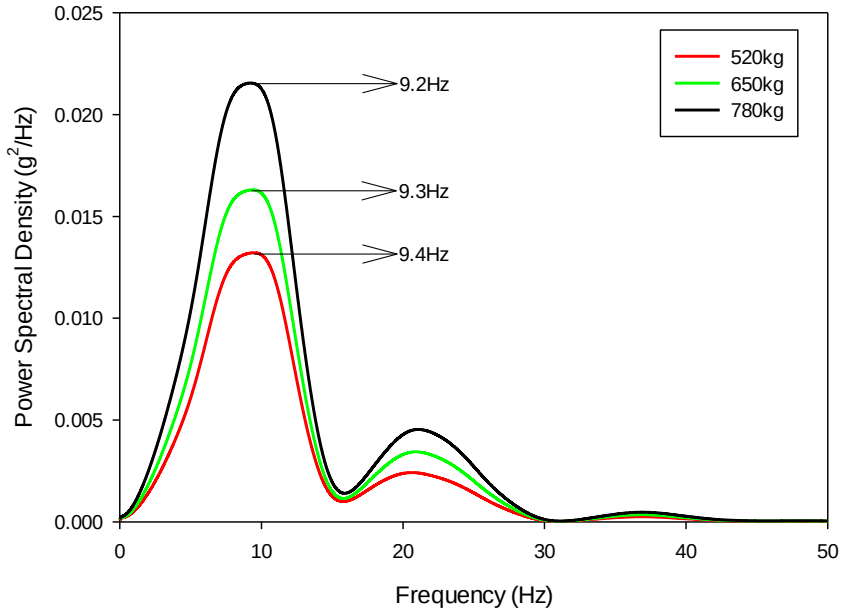

Figure 5.26: QV 3 Frequency Response of Unsprung Mass acceleration to Quarter Vehicle Weight Variation without Bump Stop

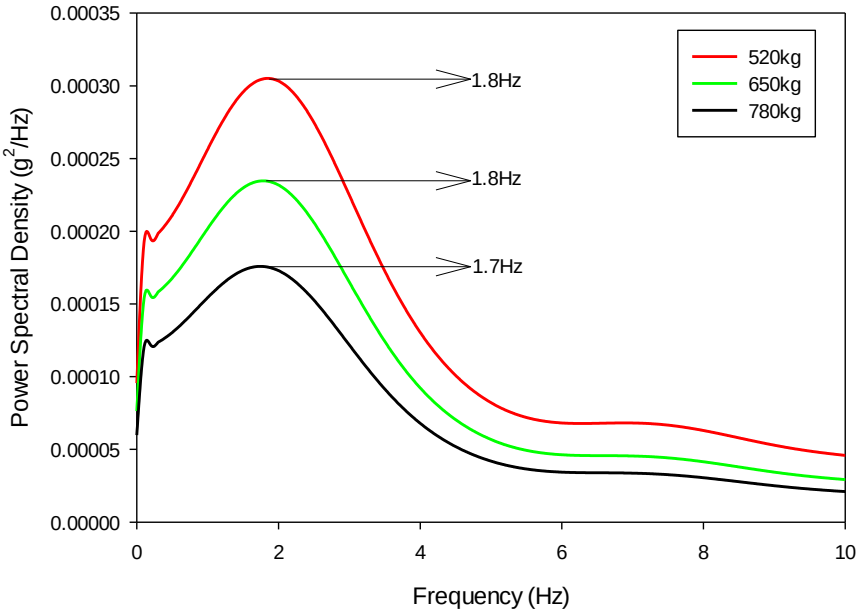

Figure 5.27: QV 3 Frequency Response of Sprung Mass acceleration to Quarter Vehicle Weight Variation without Bump Stop

The results in figures 5.22 – 5.25 indicate an increasing trend for the unsprung mass acceleration and a decreasing trend for the sprung mass acceleration. This is considerably different from those in figures 5.16 – 5.19 where the sprung mass acceleration had an increasing trend as the quarter vehicle weight increased. This clearly indicates the effect of the bump stop being engaged for the higher quarter vehicle weights. With the bump stop engaged, an additional stiffness is introduced to the suspension and this generates higher acceleration responses in the sprung mass compared with if it were not present. Likewise, a comparison of the plots of the frequency content of the sprung and unsprung mass acceleration without the bump stop in figures 5.26 and 5.27 with those in figures 5.20 and 5.21 show similar results for the sprung mass acceleration while the unsprung mass acceleration from the QV without the bump stop indicates a negative shift in the first resonance frequency as the quarter vehicle weight increases. This negative shift is what would be expected in a system with increasing vehicle weight without any limits on the suspension travel or increase in the suspension stiffness.

5.4 FULL VEHICLE ROAD LOAD DATA CHARACTERISATION

A follow up to the completed characterisation of the road load data collected from the quarter vehicle model which excluded the effect of roll and pitch is the full vehicle road load data characterisation. This is carried out using the same method applied for the quarter vehicle model. The vehicle parameters considered for the full vehicle variants are categorised as follows:

FV1. Overall Vehicle Weight

FV2. Front Spring Stiffness

FV3. Rear Spring Stiffness

FV4. Front Damping Characteristic Factor

FV5. Rear Damping Characteristic Factor

Carrying out a full factorial Design of Experiment characterisation on all the vehicle configuration parameters chosen would require a large number of simulation runs, hence a few design cases for the characterisation are carried out as highlighted in table 5.2. The drive signal for the full vehicle road load characterisation is the drive file generated from the “3-inch kerb drive-over” PG event. The file was back-calculated from the acceleration response of all the wheels (LHF, RHF, LHR, RHR) using QanTiM. These drive file signals are shown in figure 5.28.

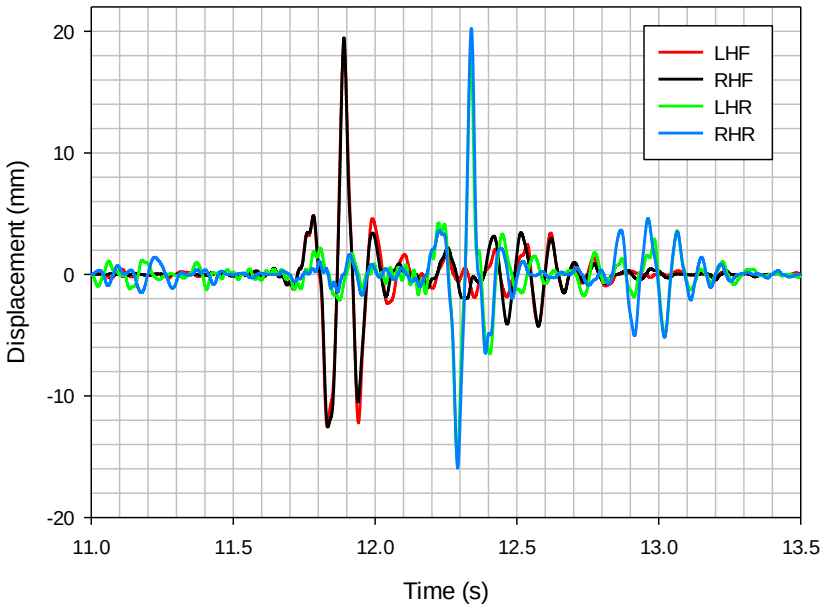

Figure 5.28: Full Vehicle Drive File from PG Event

The chosen values of each of the vehicle parameters considered for the variants as previously listed are summarised in tables 5.2 and 5.3 as simulation scenarios.

Table 5.2: Full Vehicle RLD Characterisation Simulation Scenarios – 1

Simulation Scenario #	Overall Vehicle Weight (kg)	Front Spring Stiffness (kN/m)	Rear Spring Stiffness (kN/m)	Front Damping Characteris-tic Factor	Rear Damping Characteris-tic Factor
1	1500	29	31	1	1
2	1900	29	31	1	1
3	2300	29	31	1	1
4	1900	25	31	1	1
5	1900	35	31	1	1
6	1900	40	31	1	1
7	1900	29	26	1	1
8	1900	29	36	1	1
9	1900	29	41	1	1

Table 5.3: Full Vehicle RLD Characterisation Simulation Scenarios – 2

Simulation Scenario #	Overall Vehicle Weight (kg)	Front Spring Stiffness (kN/m)	Rear Spring Stiffness (kN/m)	Front Damping Characteris-tic Factor	Rear Damping Characteris-tic Factor
10	1900	29	31	0.75	1
11	1900	29	31	1.50	1
12	1900	29	31	1.25	1
13	1900	29	31	1	0.75
14	1900	29	31	1	1.50
15	1900	29	31	1	1.25

The results of the simulation scenarios identified in tables 5.2 and 5.3 are put into column charts for easy visualisation of the variation in the road load data for the vehicle variants.

5.4.1 FV 1 (Vehicle Weight Variation) Results

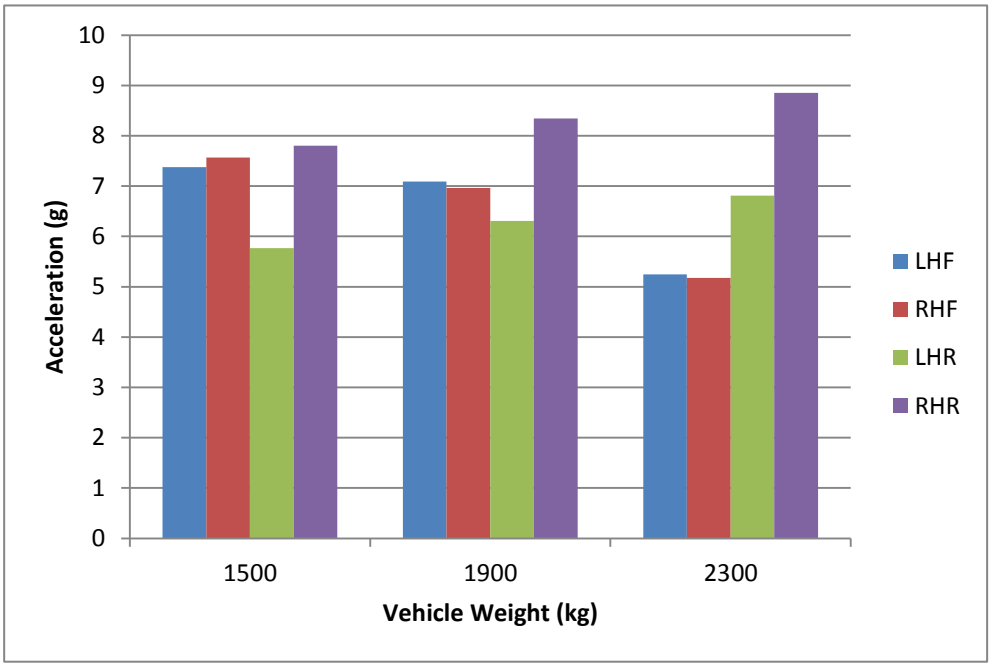

Figure 5.29: FV 1 Peak Unsprung Mass Acceleration vs Vehicle Weight

The results in figure 5.29 indicate that the acceleration of the rear wheels (unsprung mass) increases as the vehicle weight increases while that of the front wheels decrease. This can be attributed to the location of the centre of gravity of the vehicle which in this case is closer to the front wheels of the vehicle than the rear.

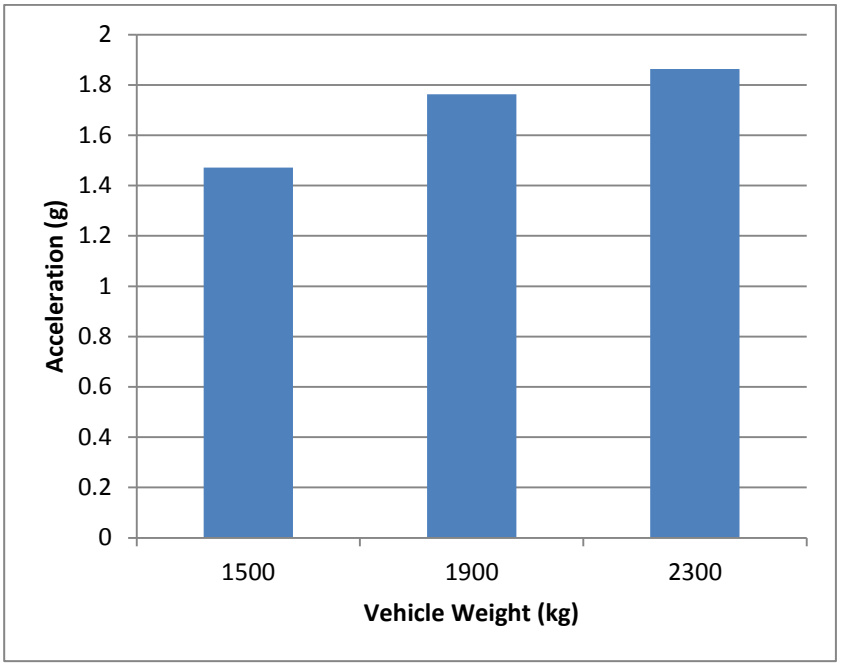

Figure 5.30: FV 1 Peak Sprung Mass Acceleration vs Vehicle Weight

Figure 5.30 indicates a positive incremental trend in the sprung mass acceleration as the vehicle weight increases. This is similar to what was observed in the case of the quarter vehicle characterisation.

5.4.2 FV 2 (Front Spring Stiffness Variation) Results

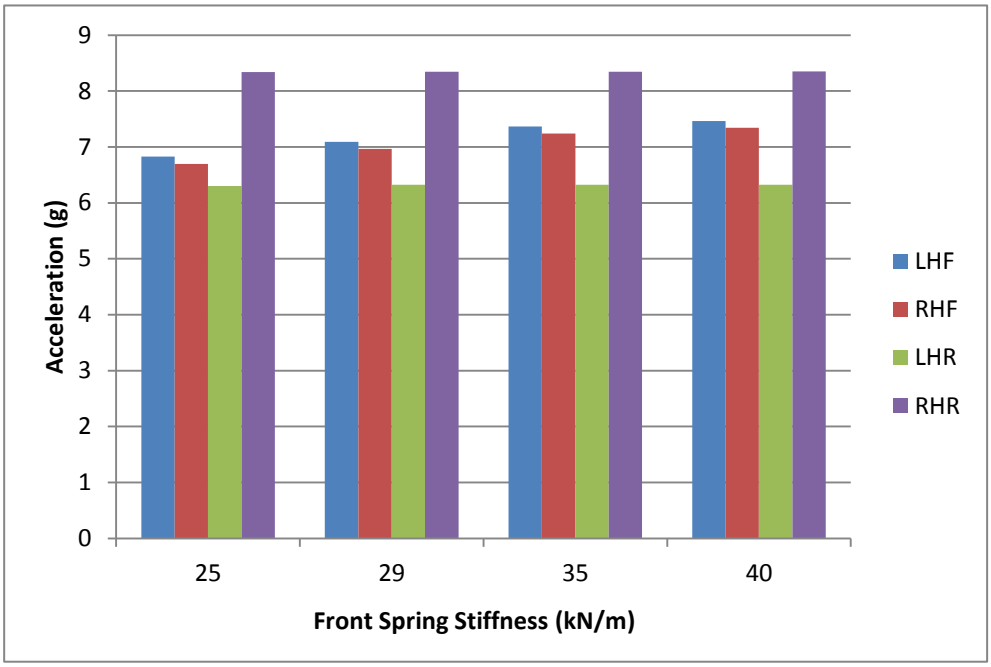

Figure 5.31: FV 2 Peak Unsprung Mass Acceleration vs Front Spring Stiffness

The results of increasing the front spring stiffness values on the unsprung mass acceleration of the front and rear wheels are shown in figure 5.31. These indicate a positive trend only on the front wheels while the responses of the rear wheels remain fairly constant. This positive trend is opposite to the trend obtained from the quarter vehicle as shown in figure 5.10 and it can be inferred that the positive trend is an effect of both the vehicle roll and pitch in response to the road input.

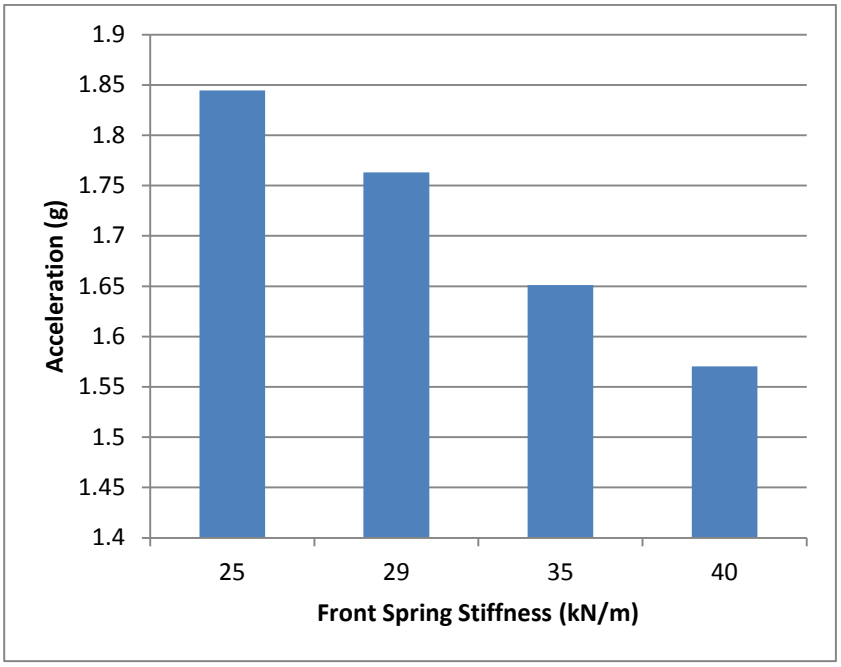

Figure 5.32: FV 2 Peak Sprung Mass Acceleration vs Front Spring Stiffness

Likewise, figure 5.32 shows a negative trend in the sprung mass acceleration response to the changes in the front spring stiffness values which is opposite to the positive trend, in figure 5.11, obtained for the quarter vehicle. The negative trend indicates that less of the input from the road is transmitted to the sprung mass because the spring displacement is decreasing as the stiffness value increases. This is consistent with the power spectral density observed for increasing the spring stiffness in figure 5.14.

5.4.3 FV 3 (Rear Spring Stiffness Variation) Results

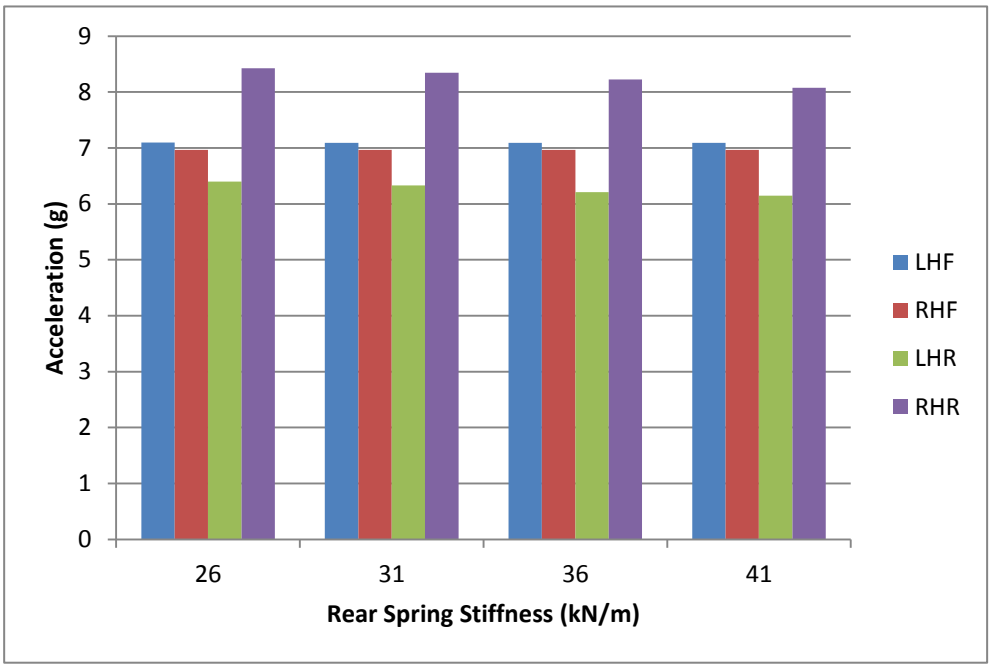

Figure 5.33: FV 3 Peak Unsprung Mass Acceleration vs Rear Spring Stiffness

Figure 5.33 shows the variation in the unsprung mass acceleration to the changes in the rear spring stiffness values. It can be observed from the results that the response from the front wheels are unaffected by the variation in the rear spring stiffness values while the response of the rear wheels indicate a negative trend to the increasing stiffness value. The response of the rear wheels to the variation in the rear spring stiffness is the opposite of the response of the front wheels to the variation in the front spring stiffness.

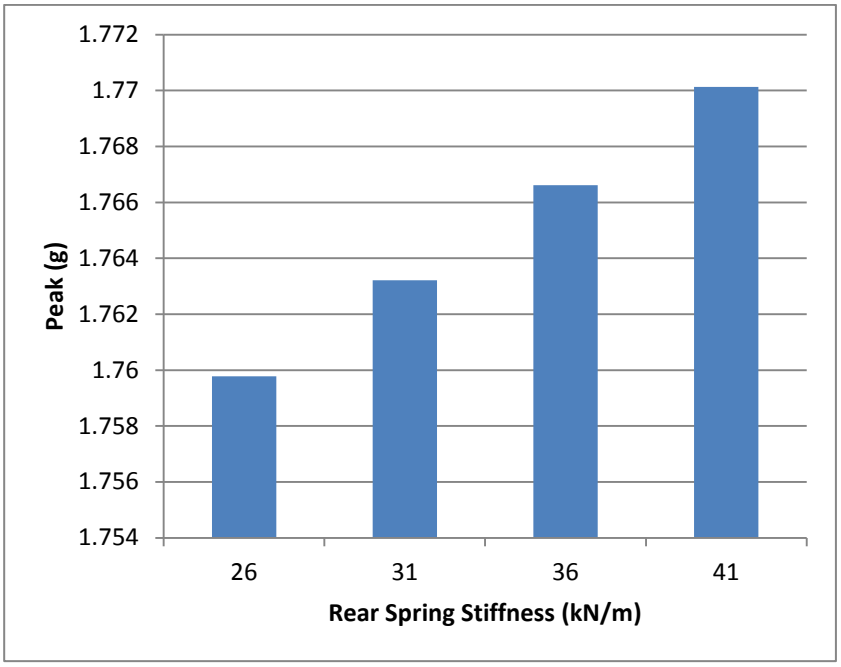

Figure 5.34: FV 3 Peak Sprung Mass Acceleration vs Rear Spring Stiffness

The acceleration response of the sprung mass as shown in figure 5.34 indicates a positive trend as the rear spring stiffness values increase. This is opposite to the trend observed for the front spring stiffness values as shown in figure 5.32.

5.4.4 FV 4 (Front Damping Factor Variation) Results

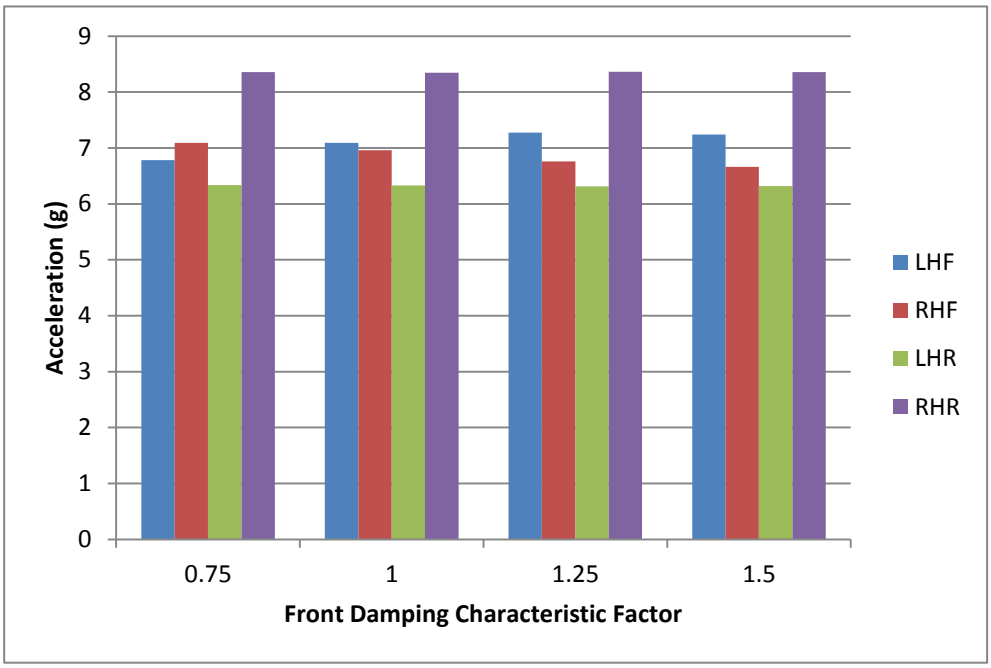

Figure 5.35: FV 4 Peak Unsprung Mass Acceleration vs Front Damping Characteristic Factor

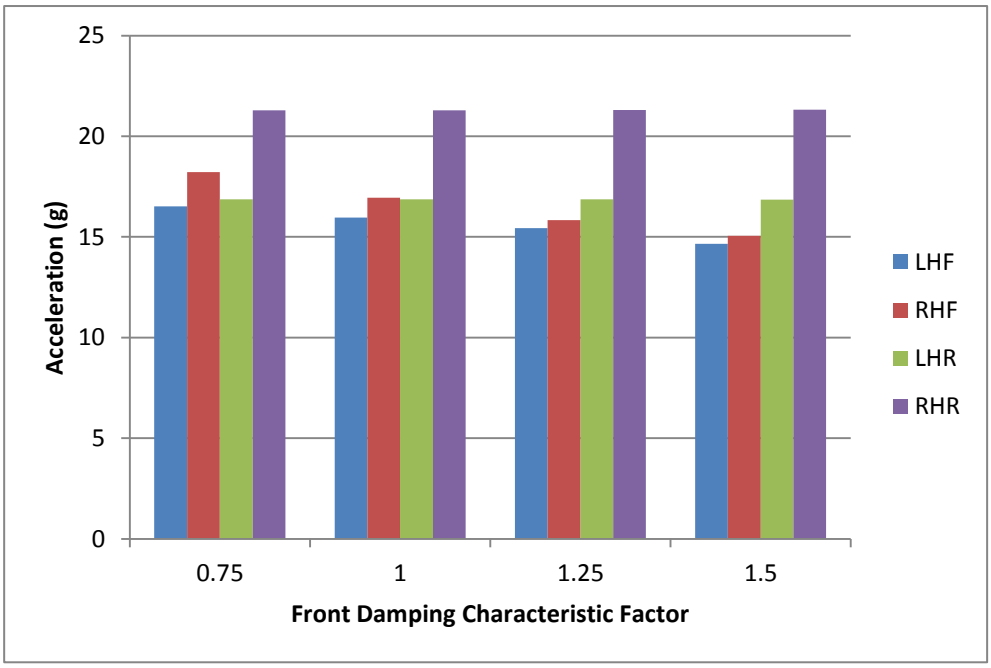

Figure 5.36: FV 4 Range of Unsprung Mass Acceleration vs Front Damping Characteristic Factor

Figures 5.35 and 5.36 show a steady negative trend in the magnitude of the unsprung mass acceleration response of the front wheels while the response of the rear wheels remain constant. The response of the front wheels is consistent with the trend observed from the quarter vehicle in figures 5.4 and 5.6.

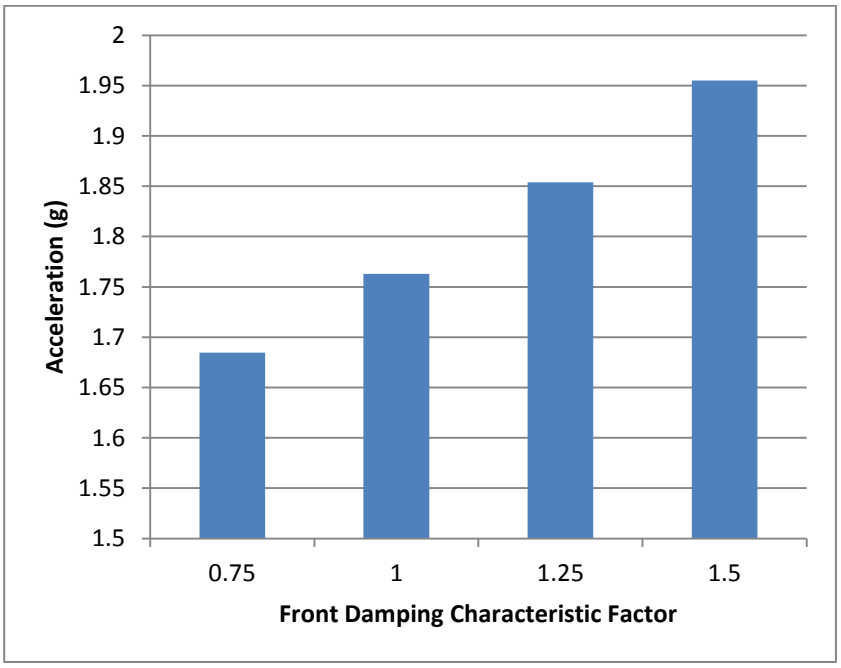

Figure 5.37: Peak Sprung Mass Acceleration vs Front Damping Characteristic Factor

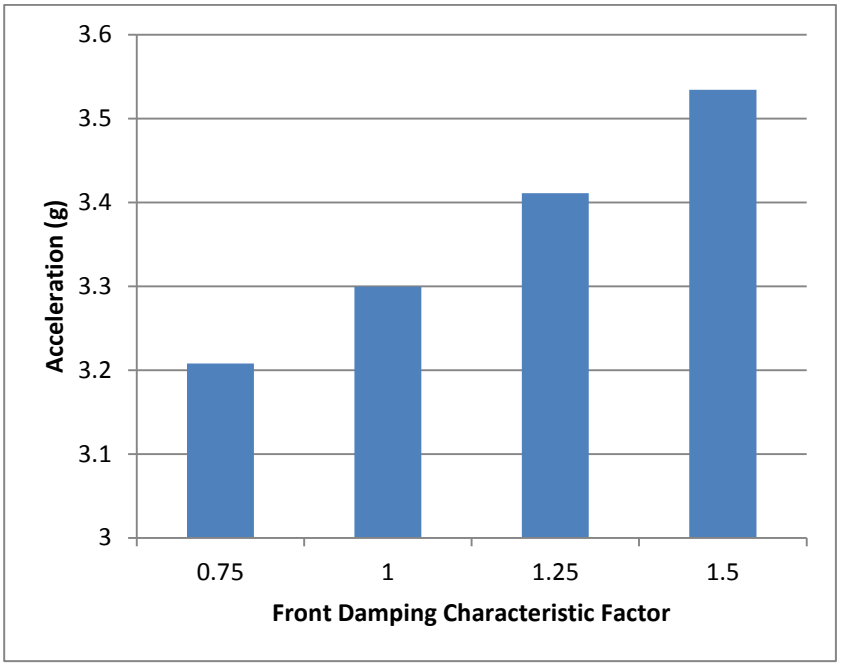

Figure 5.38: Range of Sprung Mass Acceleration vs Front Damping Characteristic Factor

Figures 5.37 and 5.38 show a positive trend in the sprung mass acceleration response to the increasing front damping characteristic factor similar to the trend observed for the quarter vehicle

5.4.5 FV 5 (Rear Damping Factor Variation) Results

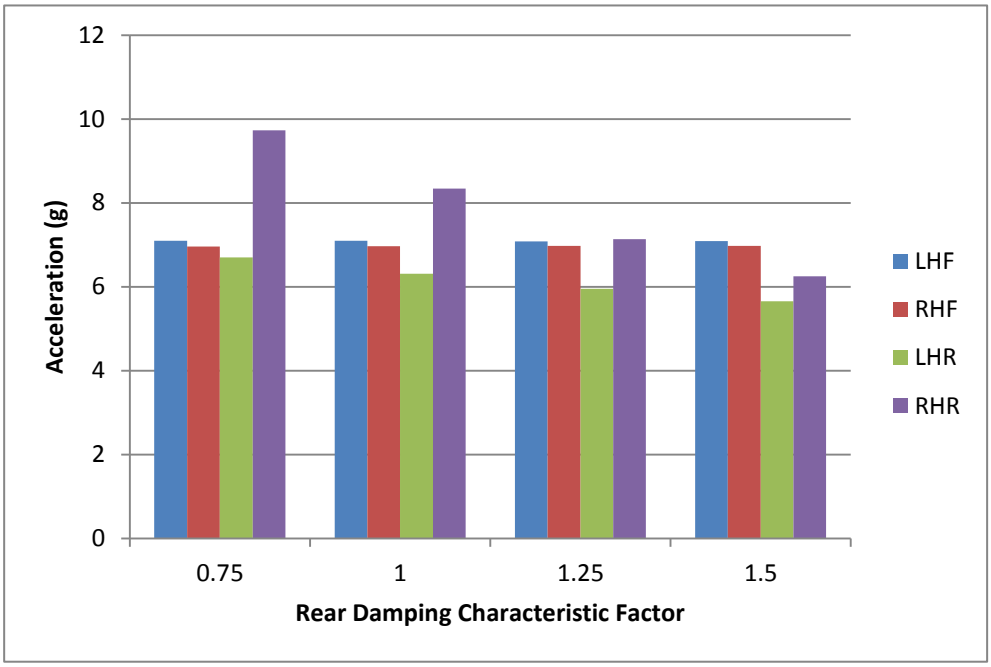

Figure 5.39: FV 5 Peak Unsprung Mass Acceleration vs Rear Damping Characteristic Factor

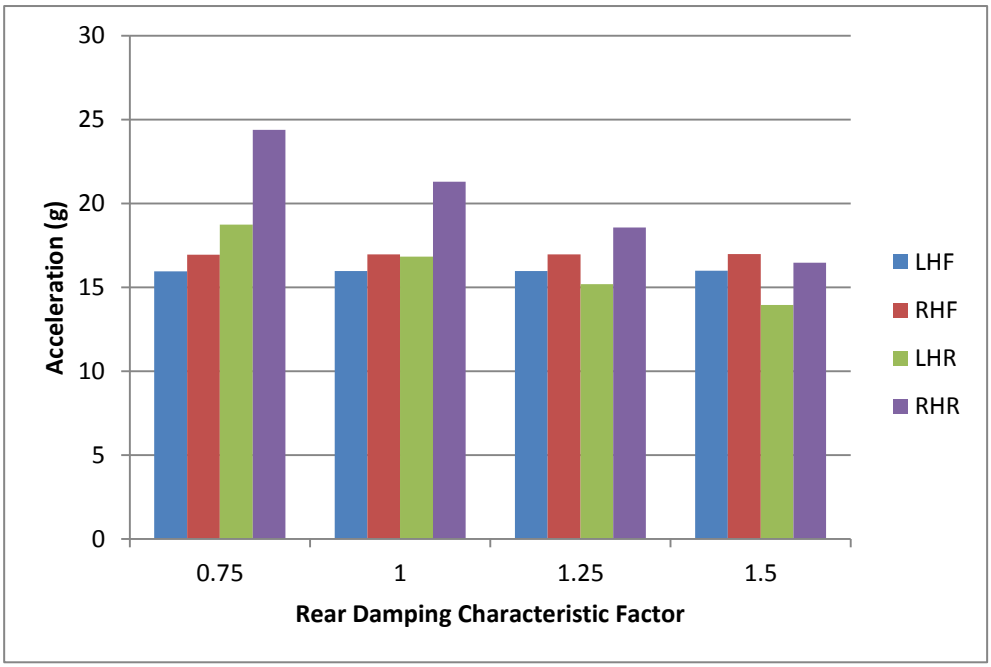

Figure 5.40: FV 5 Range of Unsprung Mass Acceleration vs Rear Damping Characteristic Factor

The result of the increase in the rear damping characterisation factor on the unsprung mass acceleration as shown in figure 5.39 and 5.40 indicate a negative trend in the rear wheels and no change in the response of the front wheels. This trend is similar to that observed in the front wheels to the change in the front damping characteristic factor in figure 5.36.

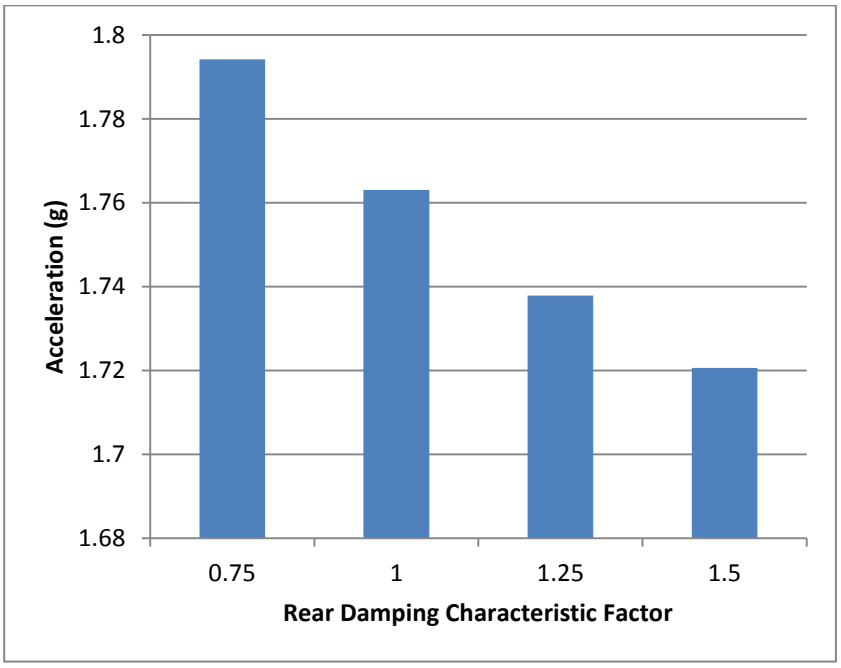

Figure 5.41: FV 4 Peak Sprung Mass Acceleration vs Rear Damping Characteristic Factor

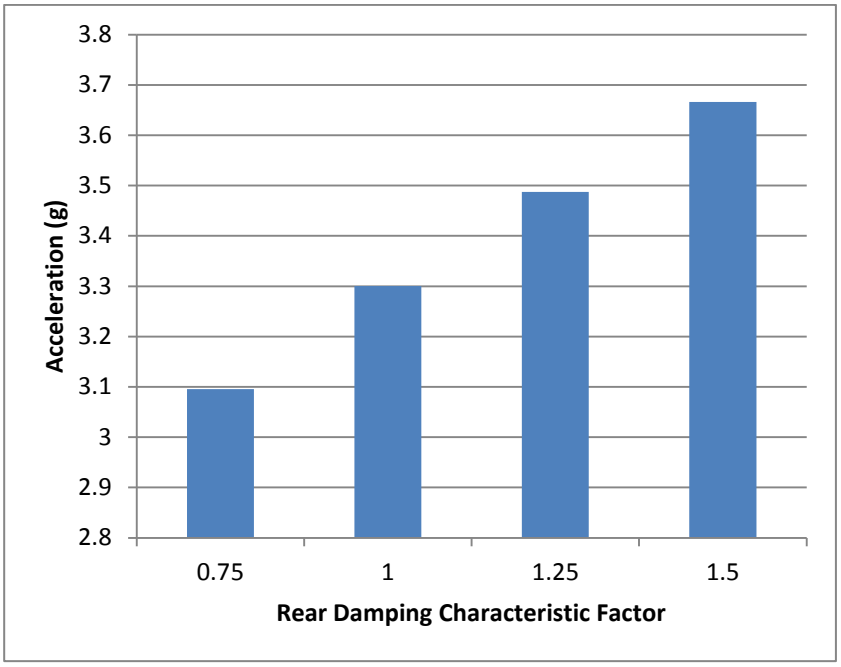

Figure 5.42: FV 4 Range of Sprung Mass Acceleration vs Rear Damping Characteristic Factor

Figure 5.42 indicates a positive trend in the response of the sprung mass acceleration to the increasing rear damping characteristic factor. Though the peak values decrease as the damping factor increases in figure 5.41, the magnitude of the response increases as observed in the range of the response in figure 5.42.

5.5 ROAD LOAD CHARACTERISATION CONCLUSION

The results of the variation in vehicle parameters in relation to road load data presented indicate variability in the road load data as the vehicle parameters change. These variations which include the peak acceleration in the sprung and unsprung masses would extend to other vehicle performance indices such as the fatigue life of various components in the vehicle. A road load data characterisation as such could provide the design engineer with information on the extent to which each vehicle parameter can be tuned without jeopardizing the performance

requirements of the vehicle. Although the information from the characterisation of the road load is useful, it would not suffice as the variability in the effective drive signal was not accounted for. The next section considers the effect of the changes in the vehicle parameters on the effective drive signals in a bid to determine how much variability occurs in them as the vehicle parameters change.

5.6 EFFECTIVE ROAD DRIVE SIGNAL VARIATION

In the preceding section, the effect of vehicle parameter variations on the road load data was examined and characterised using a fixed effective road drive signal. A summary of the results from the three categories of the quarter vehicle simulation scenarios and the five categories of the full vehicle simulation scenarios show the variability in the road load data as the vehicle parameters change. The assumption in those simulation scenarios was that the drive signal was constant for all the vehicle variants which would be the case if the durability event road surfaces could be accurately digitized and deployed for use in driving the vehicle variant models as done by Roy and Villaire [5] and Scime [9]. In the absence of a digitized road, it is hypothesised that the effective drive input signal for each vehicle variant would change as the vehicle parameters are modified. To illustrate this hypothesis, the drive signal for a set of quarter vehicle variants and the full vehicle variants were developed and compared to elucidate the variability in the effective drive input. The variation of the effective drive input was quantified by calculating the root mean square error (RMSE) of the higher vehicle parameter drive signal in comparison to the lower vehicle parameter drive signal and also as a percentage of the peak value of the lower vehicle parameter drive signal. The drive signals for the quarter vehicle

and full vehicle variants are presented in order to compare the drive files as the vehicle parameters change.

The root mean square error is computed as:

$$RMSE = \sqrt{\frac{\sum\left(e(s)\right)^2}{n_s}} \quad (5.1)$$

Where

e(s) = error in the signal

n_s = number of samples in signal

The drive signals are generated in QanTiM while ensuring that the response from the final drive signal for each vehicle variant achieved a RMSE ≤ 0.1g.

5.6.1 Results

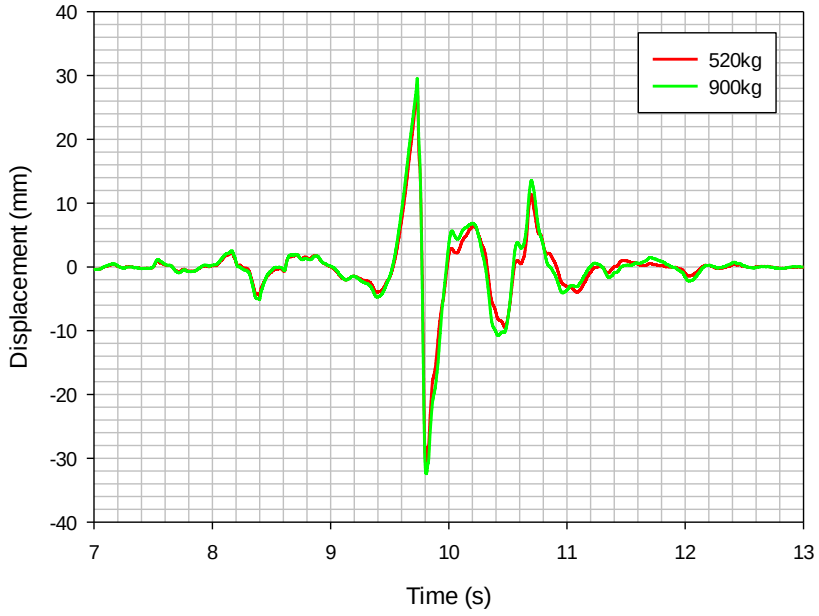

Figure 5.43: Drive Signal Variation with Quarter Vehicle Weight

The result in figure 5.43 above shows a slight variation in the drive signals for the quarter vehicle weight of 900kg in comparison with the weight of 520kg. The variation is particularly noticeable at the peaks and troughs of the drive signal after the 9-second mark. The root mean square error of the 900kg vehicle weight drive signal is computed as 0.614mm (2.14%). This indicates a fairly minimal variation in the drive signal for the 900kg quarter vehicle weight compared with 520 kg.

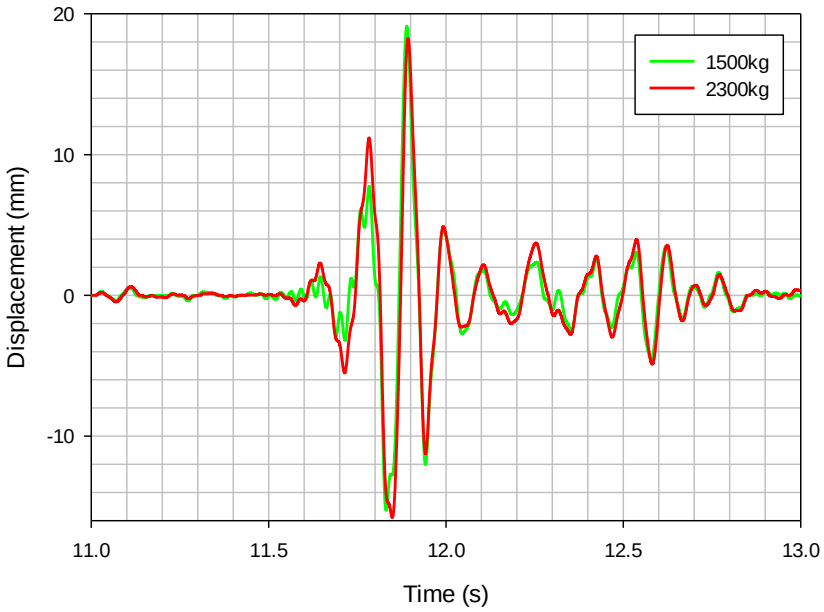

Figure 5.44: LHF Drive Signal Variation with Vehicle Weight

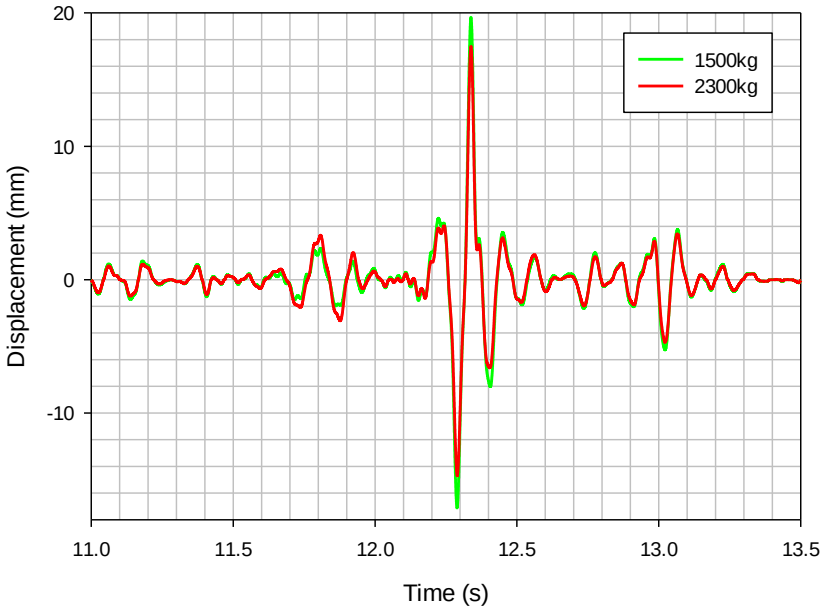

Figure 5.45: LHR Drive Signal Variation with Vehicle Weight

Figures 5.44 and 5.45 are the LHF and LHR drive signal variation for the vehicle weights respectively. The root mean square error for the drive signals are 1.074mm

(5.62%) for the LHF vehicle weight and 0.451mm (2.29%) for the LHR. The error in the drive signal can be observed to be smaller in the rear side signal compared with the front side signal and more visible at the peaks and troughs of the drive signals.

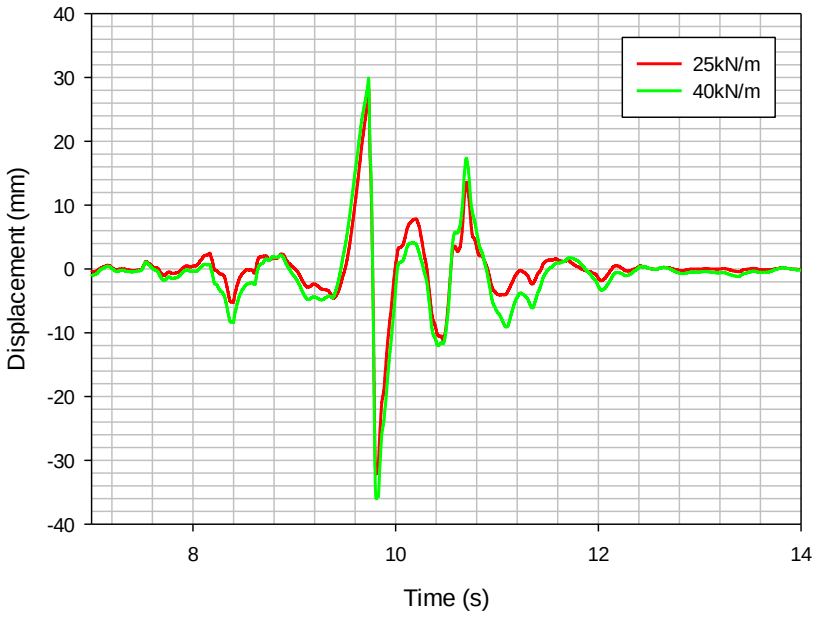

Figure 5.46: Drive Signal Variation with Quarter Vehicle Spring Stiffness

The effect of the spring stiffness variation on the quarter vehicle drive signal is shown in figure 5.46 and the variation in drive signal is also noticeable at the peaks and troughs, similar to that noticed in figure 5.43 for the quarter vehicle weight variation. The root mean square error for the 40kN/m spring is computed as 1.450mm (4.85%). This signifies a larger variation in the drive signal as the spring stiffness value is increased.

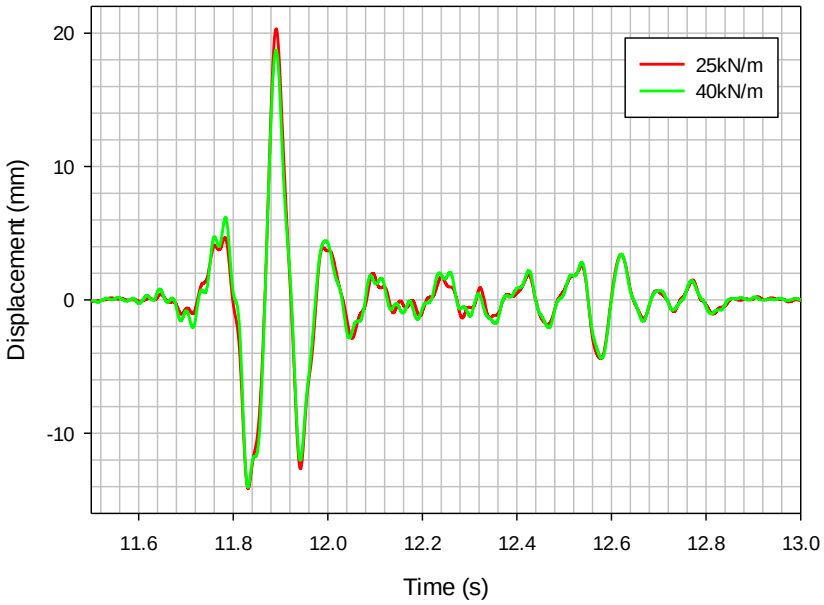

Figure 5.47: LHF Drive Signal Variation with Front Spring Stiffness

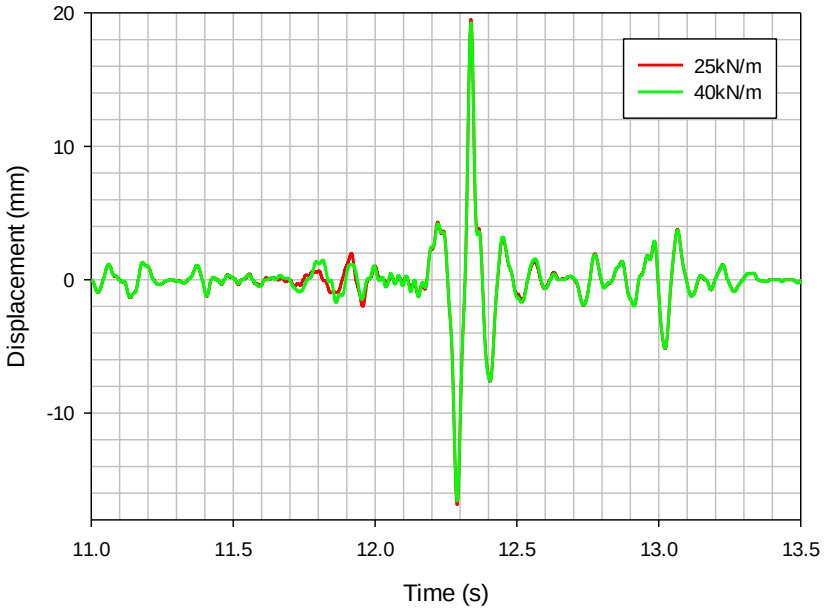

Figure 5.48: LHR Drive Signal Variation with Front Spring Stiffness

The LHF and LHR drive signals are presented in figures 5.47 and 5.48 with root mean square errors of 0.415mm (2.04%) and 0.258mm (1.32%) respectively. The error values indicate that the variation in the drive signal for a change in the spring stiffness is minimal for the full vehicle compared with the quarter vehicle where the error was as large as 1.450mm.

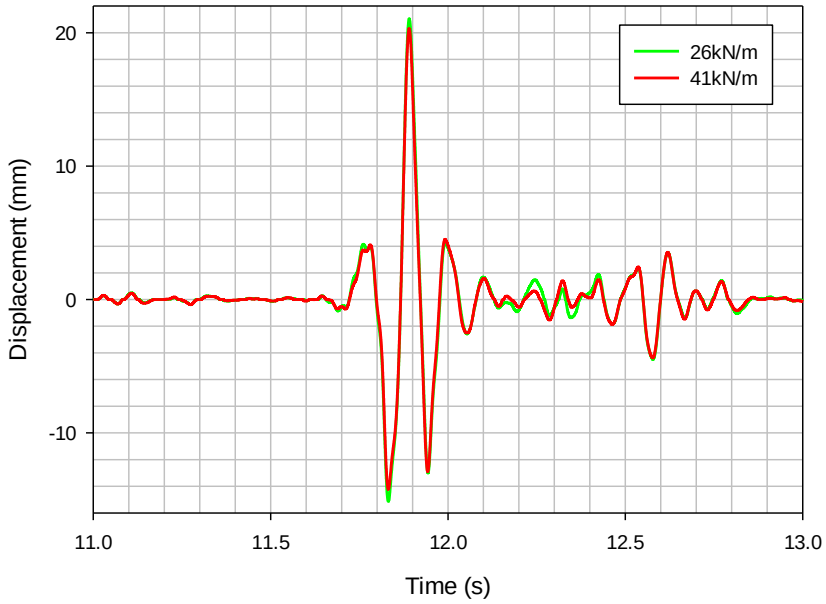

Figure 5.49: LHF Drive Signal Variation with Rear Spring Stiffness

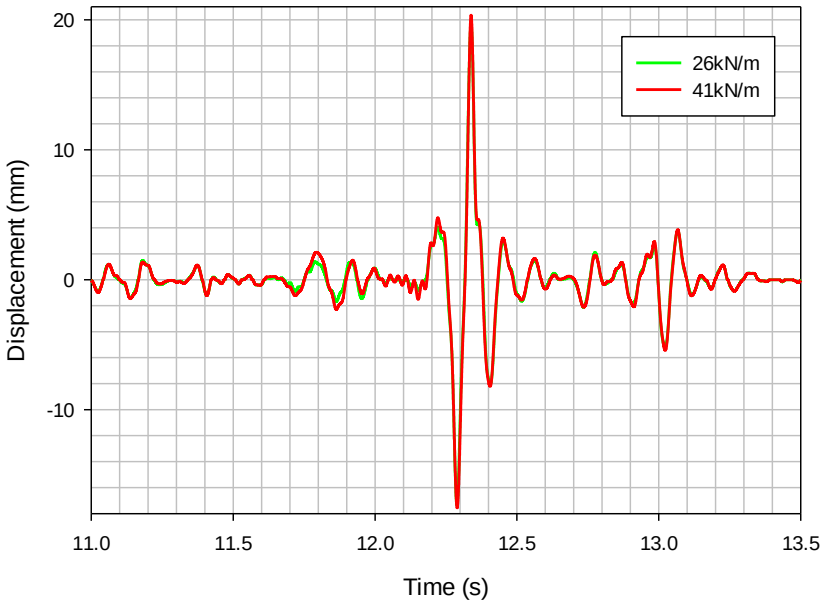

Figure 5.50: LHR Drive Signal Variation with Rear Spring Stiffness

The variation in drive signals for the changes in the rear spring stiffness values are presented in figures 5.49 and 5.50 with root mean square errors of 0.300 (1.43%) and 0.272 (1.38%) for the LHF and LHR respectively. The results are similarly low like those obtained for the front spring stiffness values.

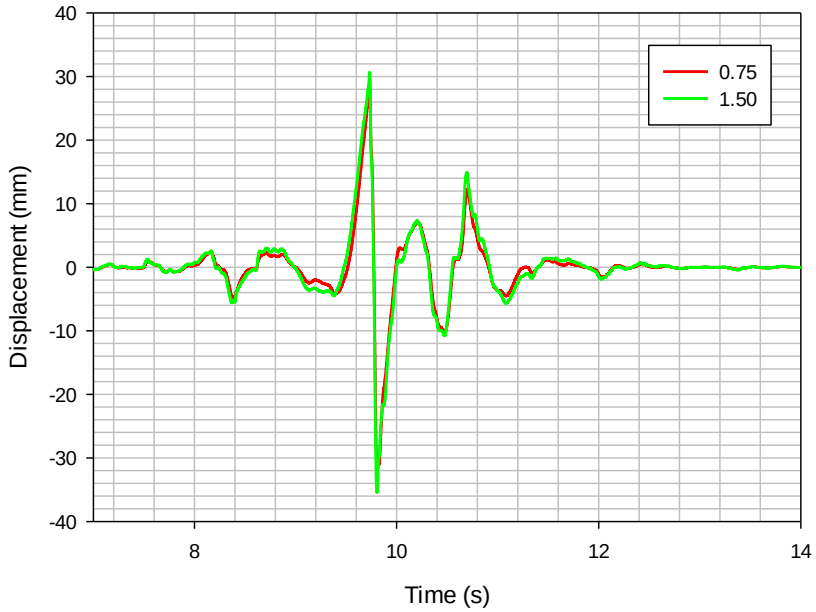

Figure 5.51: Drive Signal Variation with Quarter Vehicle Damping Characteristic Factor

Figure 5.51 shows the variation of the quarter vehicle drive signal to changes in the shock absorber damping characteristics. The mean square error for the damping factor of 1.50 is 0.655 (2.2%). This indicates a larger variation in the drive signal as the damping characteristic changes compared with that observed from changing the quarter vehicle weight.

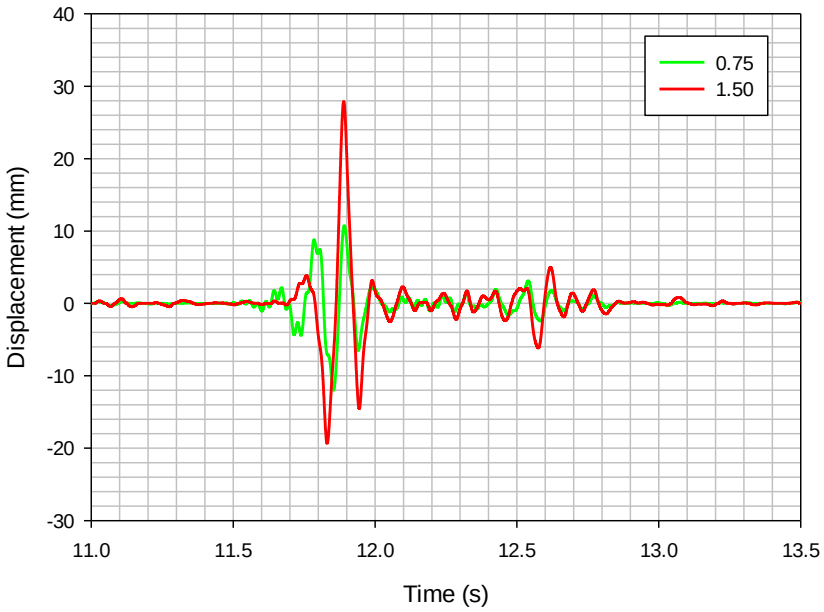

Figure 5.52: LHF Drive Signal Variation with Front Damping Characteristic Factor

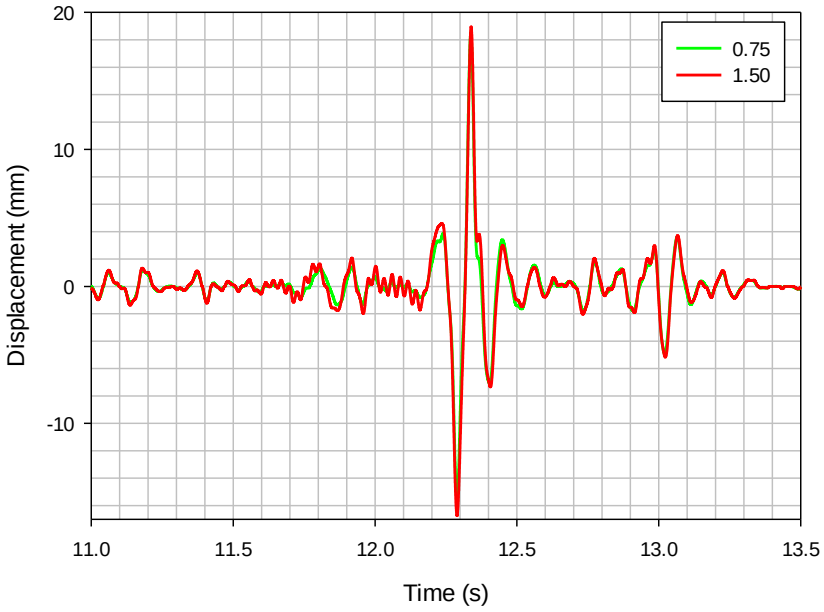

Figure 5.53: LHR Drive Signal Variation with Front Damping Characteristic Factor

Similar to figure 5.51, figures 5.52 and 5.53 show the drive signal variation for the full vehicle with the front damping characteristic factor. The root mean square error for the front drive signal is 3.286mm (30.66%) while that for the rear is 0.481mm (2.60%). A visual inspection of the drive signals in both figures 5.51 and 5.52 also show that the change in the front damping has larger effect on the front drive signal than it does on the rear drive signal.

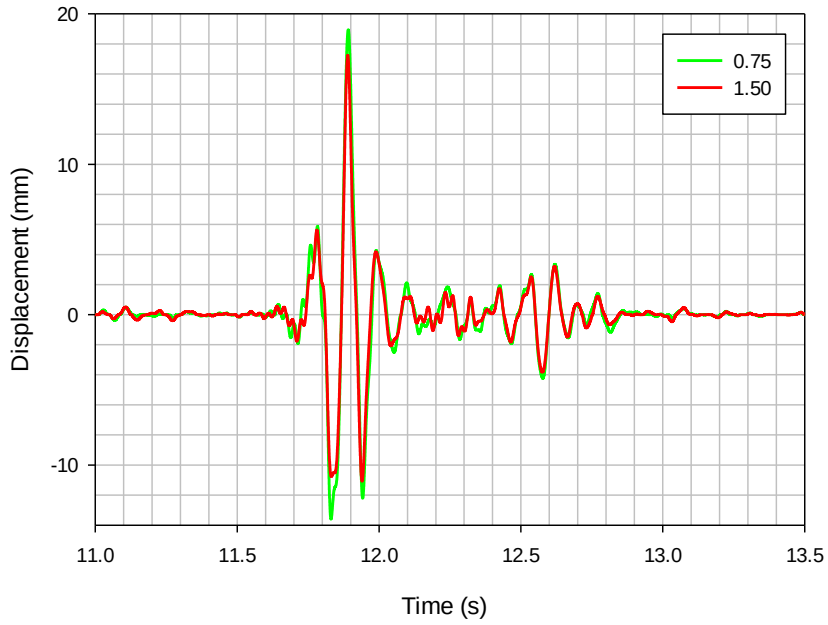

Figure 5.54: LHF Drive Signal Variation with Rear Damping Characteristic Factor

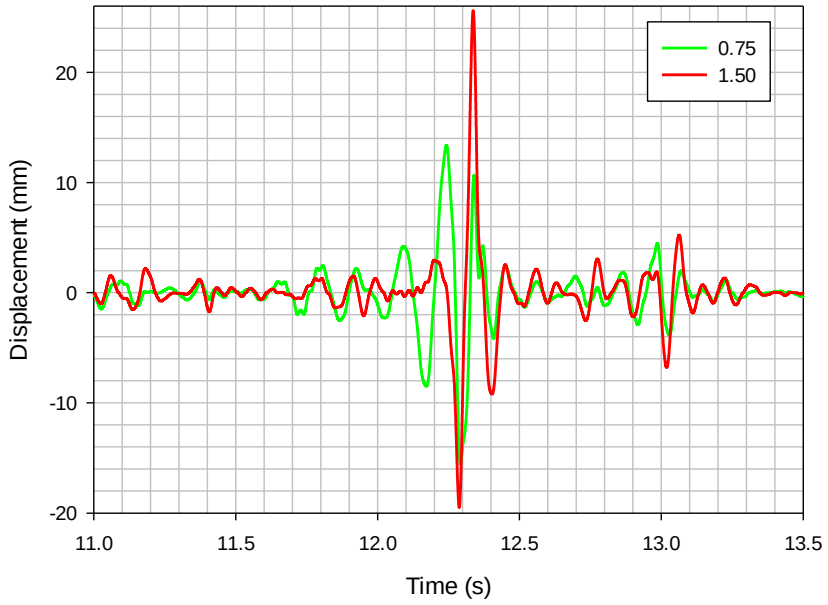

Figure 5.55: LHR Drive Signal Variation with Rear Damping Characteristic Factor

Finally, Figures 5.54 and 5.55 present the LHF and LHR drive signal variation respectively for the changes in rear damping characteristic factor. The root mean square errors in the LHF and LHR drive signals are 0.636mm (3.36%) and 3.621mm (27.04%) respectively. Similar to the case of the change in the front damping characteristic factor, the larger error is noticeable in the LHR drive signal where the damping characteristic factor was increased to 1.50.

The results presented thus far in this chapter have demonstrated the variability in the road load data acquired from the vehicle as the parameters are modified. This variability is in alignment with the hypothesis of this current research.

5.7 CONCLUSION

The method of describing the road load data as vehicle parameters are altered, as explained in this chapter, provide a graphical representation for the easy understanding of how the road load varies with the vehicle's configuration parameters. Though this would prove useful to the vehicle design engineer, the variation in the road input as the vehicle's parameters change would affect its accuracy. The variation in the road input signal as the configuration parameters of the vehicle changes as observed in the preceding section is most prominent for the variation in the shock absorber damping characteristic than the spring stiffness and the vehicle weight. Having shown how the road input varies as the vehicle's configuration parameters change, the use of an artificial intelligence system which is capable of accurately predicting the road input signal as the vehicle's parameters change is proposed and implemented in the subsequent chapter of this thesis.

5.8 SUMMARY

A method of characterising the road load collected from both the quarter vehicle model and full vehicle model using a realistic road input signal was presented to study how the variations in the vehicles' parameters affect the road load data. The characterisation of the variability in the effective road drive signal for changes in some vehicle parameters (vehicle weight, spring stiffness and damping characterisation) was carried out and the results of the characterisation of the indicated variability in the drive signals for changes in the vehicle parameters were most prominent for changes in the damping characterisation. The results of the characterisation of the input drive signal confirmed the hypothesis that the drive signals vary as the vehicle parameters are changed.

CHAPTER SIX: ARTIFICIAL ROAD INPUT TOOL (ARIT) DEVELOPMENT

6.1 INTRODUCTION

The effects of the variation of vehicle parameter configuration on the effective road drive signal were highlighted in the preceding chapter where the variability in the drive signal was observed. A method of artificial neural networks is described in this chapter to demonstrate and investigate the use of an artificial intelligence method in accurately predicting the effective road input for variants of the target vehicle. The details of the selection of the artificial neural network architecture and its optimisation for use in the quarter vehicle and full vehicle models are presented in this chapter. This optimised artificial neural network is named the artificial road input tool (ARIT).

6.2 ARIT DEVELOPMENT PROCEDURE

The following steps were taken in the development of the ARIT's artificial neural network for both the quarter vehicle and full vehicle:

1. Collation and Pre-processing of Network Training Data
2. Selection of Artificial Neural Network Design Architecture
3. Optimisation of the Artificial Neural Network
4. Deployment and Testing of the Artificial Road Input Tool

6.3 QUARTER VEHICLE ARIT DEVELOPMENT

6.3.1 Collation and Pre-processing of Network Data

The data collection process involves gathering of the data that could be used for the training, testing and validation of the neural network. This process of data collection usually takes place outside the neural network design software. In this current research, the data for the artificial neural network comprised the input and the corresponding target data. Some of the vehicle suspension parameters in addition to the wheel vertical acceleration were selected as the input data to the artificial neural network while the effective road drive signal was selected as the output from the network. The data was further divided into three subsets at the outset of the neural network training; training data, validation data, testing data.

The inputs to the neural network are the following:

a. Wheel Vertical Acceleration
b. Quarter Vehicle Weight
c. Damping Characteristic Factor
d. Spring Stiffness

The wheel vertical acceleration is the time history of the response of the quarter vehicle to the effective drive signal generated from the kerb drive-over proving ground event while the output from the neural network is the time domain effective drive signal. This output is the input signal intended to be used to drive the MBDS model of the vehicle in SIMPACK.

The inputs to the neural network were combined in a full factorial [94] design of experiments to generate various quarter vehicle configurations for MBD simulation in order to collect a variety of data for the training of the neural network. The input parameters chosen are shown in table 6.1.

Table 6.1: Quarter Vehicle MBD Simulation Parameters

Quarter Vehicle Weight (kg)	Spring Stiffness (kN/m)	Damping Characteristic Factor
200 (W1)	25 (S1)	0.5 (D1)
400 (W2)	35 (S2)	2.0 (D2)
600 (W3)	45 (S3)	3.5 (D3)

The design of experiments from the combination of the parameters in table 1 generated 27 sets of quarter vehicle configuration as listed in the table 6.2.

Table 6.2: Quarter Vehicle Variant Configurations

W1,S1, D1	W1,S1, D2	W1,S1, D3	W1,S2, D1	W1,S2, D2	W1,S2, D3	W1,S3, D1	W1,S3, D2	W1,S3, D3
W2,S1, D1	W2,S1, D2	W2,S1, D3	W2,S2, D1	W2,S2, D2	W2,S2, D3	W2,S3, D1	W2,S3, D2	W2,S3, D3
W3,S1, D1	W3,S1, D2	W3,S1, D3	W3,S2, D1	W3,S2, D2	W3,S2, D3	W3,S3, D1	W3,S3, D2	W3,S3, D3

The quarter vehicle configurations identified in table 6.2 were used to generate input drive signals in SIMPACK and QanTiM and the results were exported and saved for the neural network training. The data from the simulation was processed with a 2nd order Butterworth low-pass filter with an upper corner frequency set at 50Hz. That was done to ensure that the signals above 50Hz, which is the upper limit of the spectrum of the measured signal as shown in figure 5.7, were cut off.

The final stage of the pre-processing was the conversion of the non-time domain drive input parameters to time domain signals in order to ensure that all the input parameters had the same data format. The parameters were converted to a time domain signal at a sampling rate of 512Hz, the same as the rate of the wheel vertical acceleration input. After the data conversion, the input parameters were concatenated into MATLAB cells with each cell containing a time-step value of each input data. The input data were arranged in the following order in the cell:

1. Wheel Vertical Acceleration
2. Quarter Vehicle Weight
3. Damping Characteristic Factor
4. Spring Stiffness

It is important to note that the artificial neural network training can only be as accurate as the data presented for its training because the training builds knowledge of the input-output relationship into the neural network. Following the collation and pre-processing of the neural network data, the artificial neural network design architecture is selected.

6.3.2 Selection of Artificial Neural Network Design Architecture

A variety of artificial neural network architectures are available in the MATLAB Neural Network toolbox and each one has a suitable purpose. The first criterion for choosing the neural network architecture is that the neural network training method should be supervised as highlighted in the literature survey chapter; unsupervised training methods are commonly used in pattern recognition, self-organization and classification applications. The second criterion is that the network should be capable of accepting time history input data and also produce a time history output data. With the two aforementioned criteria in place, the following neural network architectures which met the criteria in the Neural Network Toolbox of MATLAB were selected:

1. Nonlinear Autoregressive Network with External Input (NARX)
2. Nonlinear Input-Output Network (NION)
3. Cascade-Forward Back propagation Network (CFBPN)
4. Feed-forward Back propagation Network (FFBPN)
5. Feed-forward distributed time delay Network (FFDTDN)

Each of the neural network architectures was trained with the data previously collected in step 1 of the ARIT development procedure and the performances of the networks were assessed by the Mean Squared Error of the network's prediction. The Mean Squared Error (MSE) is defined as:

$$MSE = \frac{1}{N}\sum_{j=1}^{N}\left(T_j - a_j\right)^2 \qquad (6.1)$$

Where a = network outputs

T = target outputs

N = number of network output & target

j = summation index

The data collated in step 1 above was divided into the three subsets; training data, test data and validation data in the ratio 14:3:3.

The transfer function used in the neural network designs are summarised in table 6.3 below.

Table 6.3: Neural Network Transfer Functions

Transfer Function	Input/Output Relation	MATLAB Function
Linear	$a = n$	purelin
Hyperbolic Tangent Sigmoid	$a = \frac{e^{n} - e^{-n}}{e^{n} + e^{-n}}$	tansig

Where a = output

n = Input

The hyperbolic tangent sigmoid transfer function was chosen for the hidden layer and the linear transfer function was chosen for the output layer of the NARX and NION while CFBPN, FFBPN and FFDTDN used the hyperbolic tangent sigmoid in

the output layer. These were chosen because they are common choices in this type of prediction application [1, 65].

The Levenberg-Marquardt (LM) training algorithm was used for the training of the chosen neural network architecture because of its offering of a good training speed in comparison to other algorithms [77]. Following the completion of the network training, the results of the neural network training are presented in table 6.4. The results presented are the averages of three training trials.

Table 6.4: Neural Network Training Result - Section 1

Network Type	Training Algorithm	MSE	Number of Input delays	Hidden Layer TF	Output Layer TF
NARX	LM	0.000293	10	Tansig	Purelin
NION	LM	8.17	10	Tansig	Purelin
CFBPN	LM	9.0281	0	Tansig	Tansig
FFBPN	LM	9.04	0	Tansig	Tansig
FFDTDN	LM	7.79	10	Tansig	Tansig

The results of the performance testing of the neural networks reveal that the Nonlinear Autoregressive Network with External Input (NARX) produced the best

performance results compared with the other network types. Hence, the NARX is used for further analysis in this current research.

6.3.2.1 Background of the NARX Network

The NARX network is an artificial network architecture which has feedback connection between its component layers. The NARX network is built on the linear autoregressive model. The equation (6.2) defines the NARX network model [77].

$$y(t) = f(y(t-1), y(t-2), y(t-3), \dots, y(t-n_y), u(t-1), u(t-2), u(t-3), \dots, u(t-n_u)) \quad (6.2)$$

Where y(t) = Network Output Time Series

u(t) = Network Input Time Series

The Input u(t) in the case of this current research is multi-dimensional and consists of the wheel vertical acceleration, quarter vehicle weight, damping characteristic factor and the spring stiffness. The output, y(t), is the effective drive signal.

There are basically two different configurations of the NARX network. These are the parallel and the series-parallel configurations. In the parallel setup, the estimate of the output of the network is used as the feedback input. Since the true network outputs are available during training, the actual values can be *fed back* instead of an estimated value; this is called the series-parallel configuration. These different configurations are illustrated in figures 6.1 and 6.2.

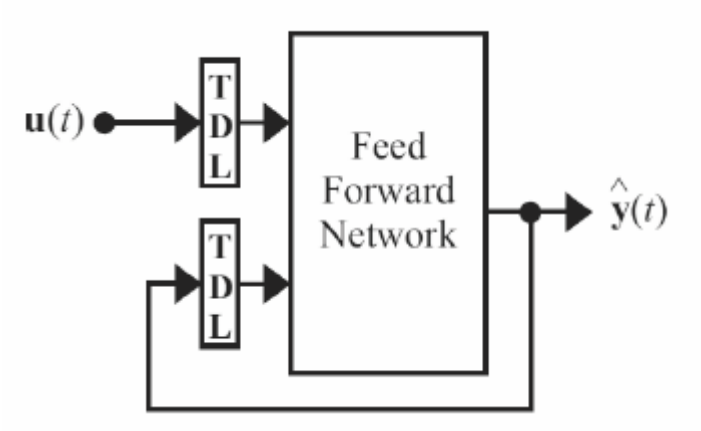

Figure 6.1: Parallel NARX Configuration [77]

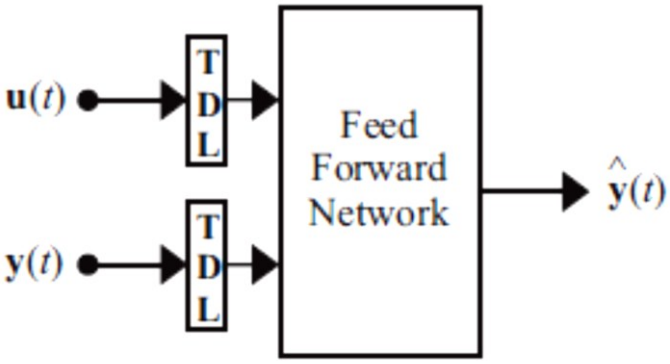

Figure 6.2: Series-Parallel NARX Configuration [77]

Where $\hat{y}(t) = Network\ Output$

$$y(t) = Network\ Output\ used\ as\ Feedback$$

The main advantages of the series-parallel network over the parallel NARX configuration is the ability to train the artificial neural network in a purely feedforward manner like a perceptron network. TDL abbreviates the "*Tapped Delay Line*" which is a group of delay blocks.

6.3.3 Optimisation of the Artificial Neural Network

Having chosen the NARX network in step 2, the next step is the optimisation of the network considering the following properties of the network:

a. The Training Algorithm
b. Number of Input Delays
c. Number of Feedback Delays
d. Size of Hidden layer
e. General Data Processing

The mean squared error in the optimisation of the artificial neural network is computed from the average of three training trials with the exception of the training algorithm selection where the stability of the network over ten training trials was considered.

6.3.3.1 Training Algorithm

The training algorithm is responsible for the readjustment of the biases and the weights of the artificial neurons during the neural network's training. The algorithm readjusts the weights and biases of the neurons in accordance with the performance of the overall network as the training is carried out. A good number of training algorithms have been developed over the years and the performance of each of these algorithms depends on a number of factors such as the type of the artificial neural network, the number of training data, the type of neural network application etc. In order to choose an appropriate training algorithm, seven training algorithms (table 6.5) were tested over ten training trials of the NARX Neural Network.

Table 6.5: Training Algorithm

Neural Network	Training Algorithm	MATLAB Function	Average Training Time (s)
NN 1	Levenberg-Marquardt (LM)	trainlm	1169.2
NN 2	Bayesian Regularization (BR)	trainbr	12808.9
NN 3	BFGS Quasi-Newton (BFGS)	trainbfg	1446.5
NN 4	Resilient Backpropagation (RB)	trainrp	290
NN 5	Scaled Conjugate Gradient (SCG)	trainscg	306.4
NN 6	Conjugate Gradient (CG)	traincgb	314.1
NN 7	Variable Learning Rate Gradient Descent (GDX)	traingdx	38.1

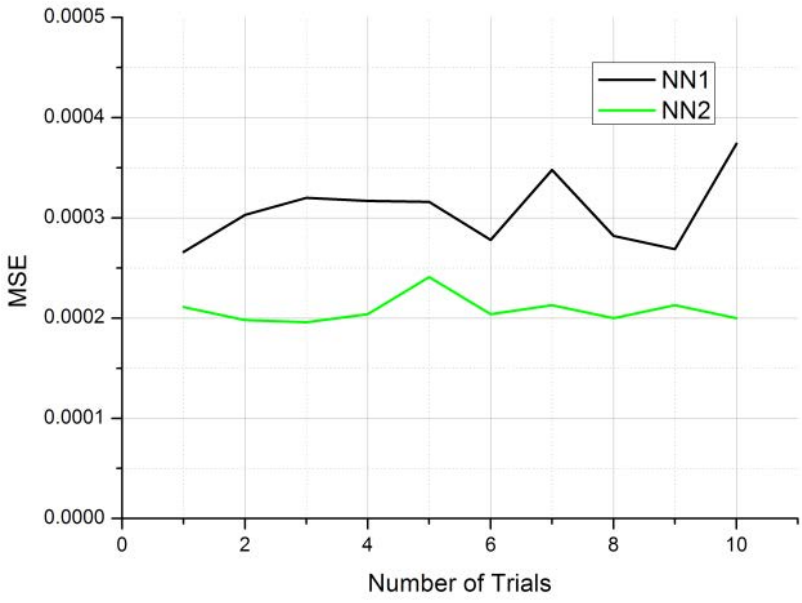

Figure 6.3: Quarter Vehicle Neural Network Performance with Training Algorithm 1

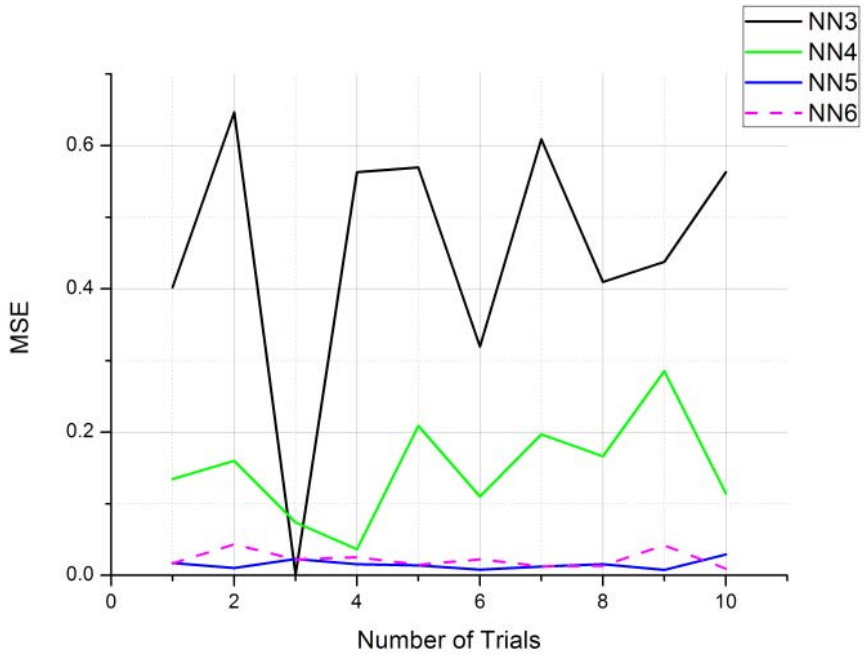

Figure 6.4: Quarter Vehicle Neural Network Performance with Training Algorithm 2

The results of the network training shown in figures 6.3 and 6.4 indicate the variability in the performance of the network with the training algorithms. The worst performing training algorithm was the variable learning rate gradient descent (NN 7) and hence, not included in figures 6.3 and 6.4 for the sake of clarity. The results of this test clearly indicate that the most suitable training algorithms for this purpose are the Levenberg-Marquardt and the Bayesian Regularization. The advantage of the Levenberg-Marquardt algorithm over the Bayesian Regularization is the training speed; the Bayesian Regularization requires up to 1000% more time than the Levenberg-Marquardt algorithm in training. While the Bayesian Regularization requires much more time to train the network, the performance and stability are better than those of the Levenberg-Marquardt as observable in figure 6.3. The

performance of the Bayesian Regularization is consistent with the observation of other researchers [95, 96].

6.3.3.2 Number of Input Delays

Following the choice of the training algorithm is the optimisation of the number of input delays to the NARX network. As earlier stated in the literature survey, the function of the input delay block is to delay the output by a number of time steps. The number of input delays is the number of time steps delays in the data that is presented to the network. In order to optimise this parameter, the effect of the input delay on the performance of the network is examined. The training was carried out using the Levenberg-Marquardt algorithm because of its time efficiency and the effects of the variation in number of input delays is presented in figure 6.5.

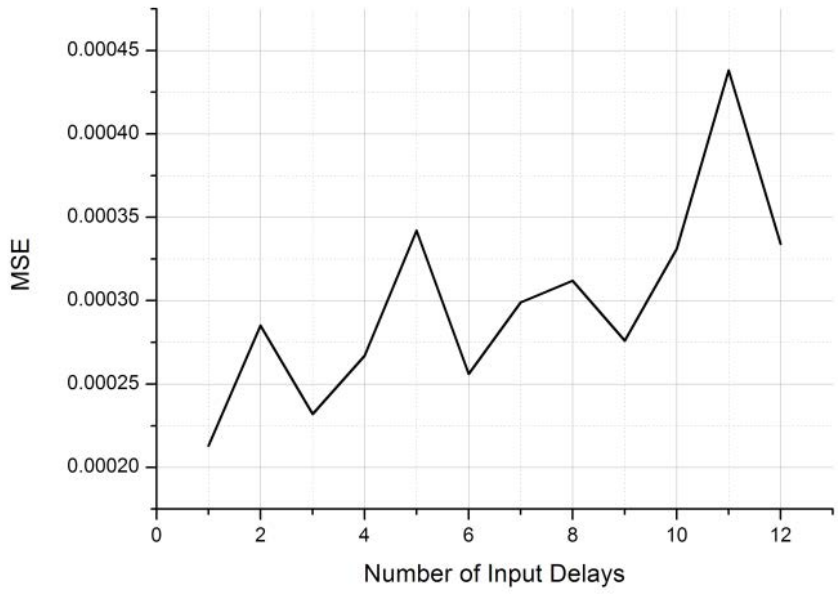

Figure 6.5: Quarter Vehicle NARX Network Performance with Number of Input Delay

The result in figure 6.5 indicates a positive trend in the MSE as the number of input delays increases. The observable conclusion is that the error in the performance of the network increases as the number of input delays increases. Hence, the smallest number of input delays should be considered for use in the NARX network.

6.3.3.3 Number of Feedback Delays

The feedback delay is similar to the input delay in structure and operation but different in the source of the input data to the delay block. The source of the data for feedback delay is the network's output. The optimisation process of the number of feedback delays investigates the effects of the number of delays on the performance of the network. The result of this investigation is shown in figure 6.6.

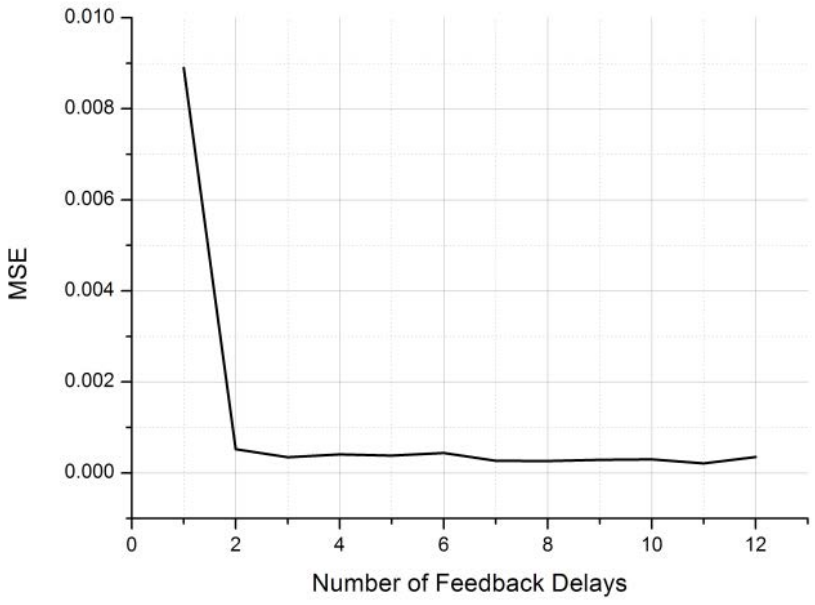

Figure 6.6: Quarter Vehicle NARX Network Performance with Number of Feedback Delays

The figure 6.6 shows a fairly slow decline in the mean squared error performance of the network from the point of two feedback delays upwards. This indicates that the minimum number of feedback delays acceptable for a good network performance is two.

6.3.3.4 Size of Hidden Layer

The size of the hidden layer also requires optimisation in order to ensure a good network performance when it is deployed with new input data sets. A small number of neurons in the hidden layer could lead to the under fitting of the network's performance while too many could lead to over fitting where the network is not able to accurately generalise. The optimum size of the hidden layer was investigated by comparing the network's performance with the size of the hidden layer. The result of the investigation is shown in figure 6.7.

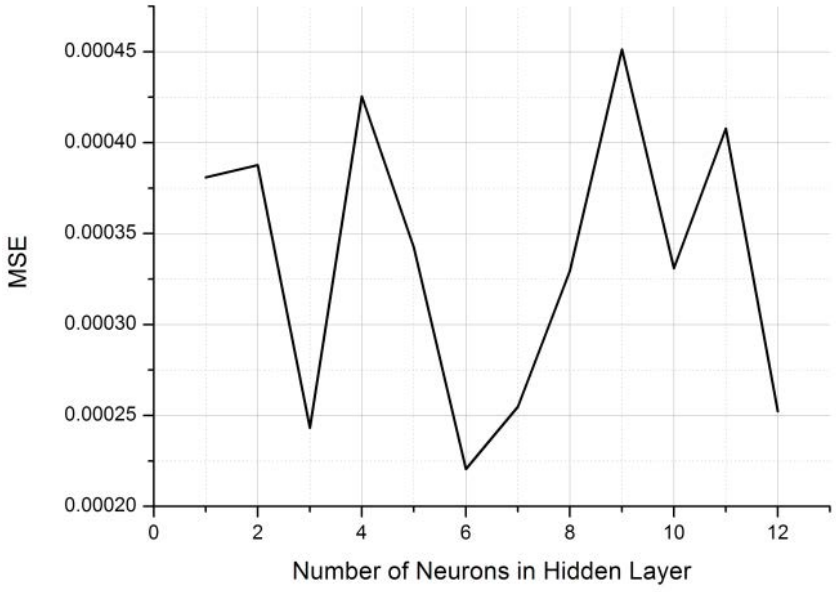

Figure 6.7: Quarter Vehicle NARX Network Performance with Size of Hidden Layer

The result in figure 6.7 doesn't show any observable trend though the network with 6 neurons in the hidden layer performed better than all others.

6.3.3.5 General Data Processing

The survey of literature shows that processing the input data for the training of the neural network produces more efficient training and deployment network performance [1, 77, 97, 98]. The data processing works by pre-processing the input data prior to being fed to the neural network and post-processing the output from the neural network. By default, MATLAB applies a data processing method based on the type of data presented for training the neural network. The data processing procedure is illustrated in figure 6.8. In order to understand how the data processing affects the network's performance, the effects of these processing methods were investigated.

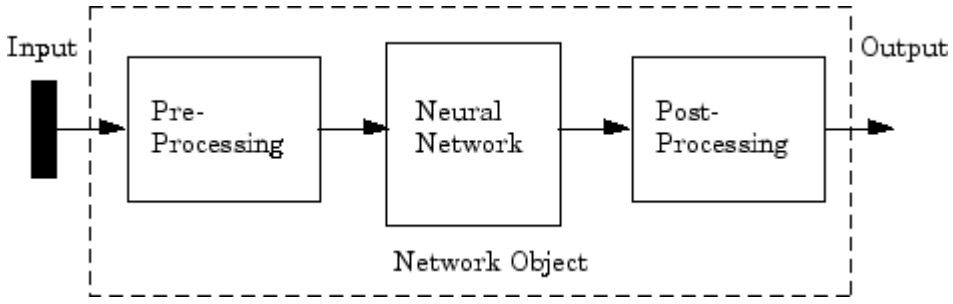

Figure 6.8: Data Processing for Neural Network [77]

The Neural Network Toolbox™ in MATLAB offers a good number of pre-processing and post-processing methods as follows:

a. *Fixunknowns* - Processes data by replacing each row containing unknown values

b. *Mapminmax* - Normalizes the inputs and target values to the range of -1 to 1
c. *Mapstd* - Normalizes the inputs and target to have a mean of zero and variance of one
d. *Processpca* - Processes rows of matrix with the principal component analysis
e. *Removeconstantrows* - Removes matrix rows with constant values
f. *Removerows* - Removes matrix rows with specified indices

All the data processing methods were used except the *fixunknowns* which is applicable only when non numeric data are included in a network's input. The network was trained with the Levenberg-Marquardt algorithm, a hidden layer of 10 neurons, and input and feedback delay size of 10. The results of the investigation are shown in figures 6.9 and 6.10.

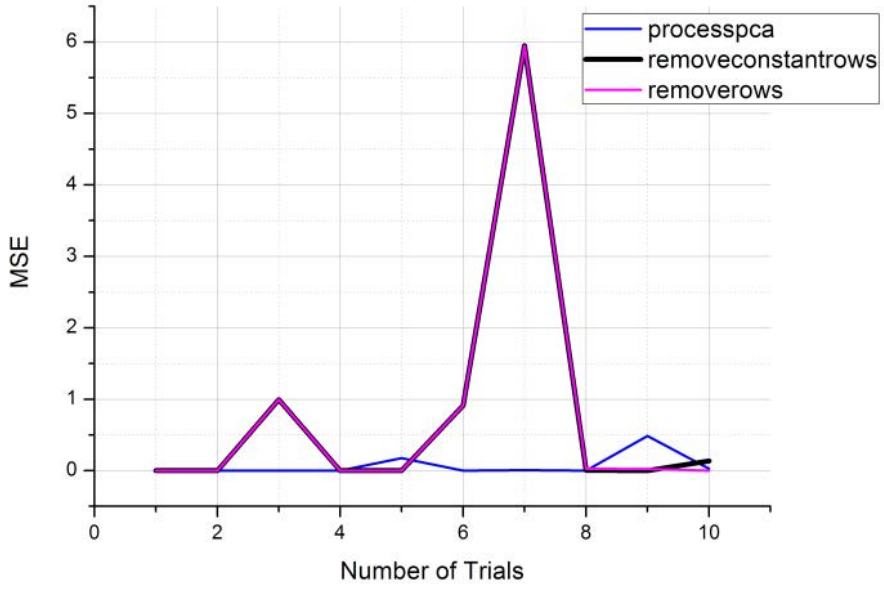

Figure 6.9: Quarter Vehicle NARX Network Performance with Data Processing Methods – 1

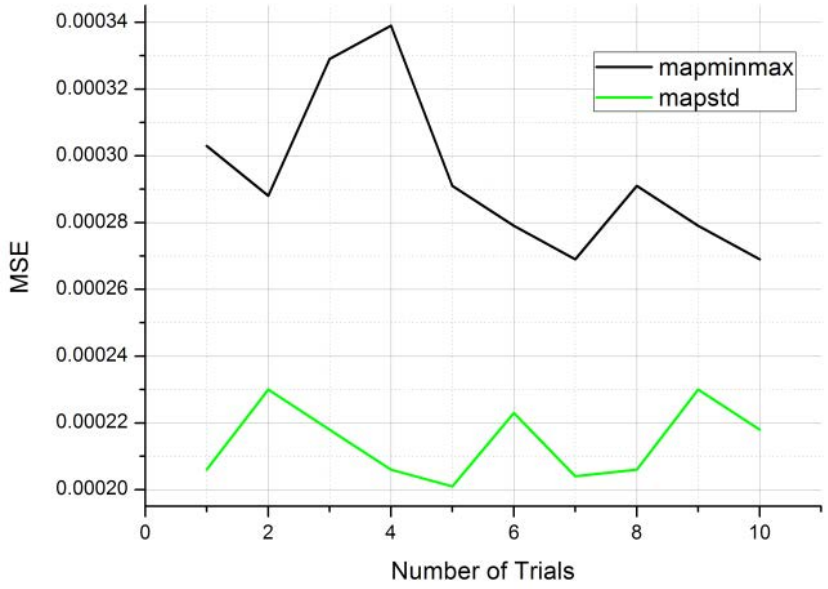

Figure 6.10: Quarter Vehicle NARX Network Performance with Data Processing Methods – 2

Figures 6.9 and 6.10 show that *mapminmax* and *mapstd* produce better network performance than the other methods of data processing for this application. Both methods of data processing indicate a good stability over the 10 trials though *mapstd* has a better network performance than the *mapminmax*.

6.3.4 Deployment and Testing of the Quarter Vehicle Artificial Road Input Tool

With the completion of the artificial neural network optimisation for the various configuration parameters of the NARX network, the network was configured using the recommended settings from the optimisation investigations. The network was trained and the accuracy of the network was tested.

6.3.4.1 Quarter Vehicle Artificial Neural Network Configuration

The NARX network for deployment was trained with the Bayesian Regularisation training algorithm as a result of the performance of this training algorithm as seen in figure 6.3. The Bayesian Regularisation algorithm was chosen over the Levenberg-Marquardt algorithm because of its better performance even though the training time is much slower. Also, the number of input delays was specified as one. The number of feedback delays was chosen as two because it was the smallest number of feedback delays to produce a good network performance. The size of the hidden layer was set at six neurons based on the performance result in figure 6.7. Though there isn't a visible pattern in the network performance with the changes in the number of neurons in the hidden layer, the network with six neurons produced the best results. Both *mapminmax* and *mapstd* were chosen for the data processing based on their good performance and both were implemented in the neural network design. The summary of the NARX network configuration is shown in table 6.6.

Table 6.6: NARX Network Configuration

Configuration Parameter	
Training Algorithm	Bayesian Regularisation
Number of Input Delays	1
Number of Feedback Delays	2
Size of Hidden Layer	6
General Data Processing Method	*mapminmax & mapstd*

6.3.4.2 Quarter Vehicle Artificial Road Input Tool Training and Testing

Once the final network configuration was chosen, a new data set was generated from the MBD simulation and QanTiM drive signal iteration to train the newly created network. The performance results of the training are as follows:

Training Performance (MSE): 3.4286e-4

Test Performance (MSE): 3.375e-4

In order to test the Quarter Vehicle ARIT, new vehicle variant configurations parameters were considered as the input parameters to the neural network. The

drive signal outputs of the neural network were then compared with the iterated drive signal outputs from QanTiM for each of the quarter vehicle variants. The quarter vehicle variants are listed in table 6.7.

Table 6.7: Quarter Vehicle Parameters for ARIT Input

Quarter Vehicle Variant Number	Chassis Mass (kg)	Spring Stiffness(kN/m)	Damping Factor
1	450	29	1.00
2	750	22	1.30
3	620	40	2.00

The quarter vehicle parameters and the vertical wheel acceleration served as the input for the training of the neural network. The output of the neural network was the drive signal for the MBD simulation. The results of the network output were quantified by determining the correlation coefficient of the predicted drive signal and reference signal in each case.

The equation for the correlation coefficient is

$$r = \frac{\sum(g - \bar{g})(m - \bar{m})}{\sqrt{\sum(g - \bar{g})^2 \sum(m - \bar{m})^2}} \qquad (6.3)$$

Where r = correlation coefficient

g = reference signal

m = correlated signal

The results from the calculation of the correlation coefficients indicated that the correlation was very good.

6.3.4.3 Quarter Vehicle Artificial Road Input Tool Testing Results

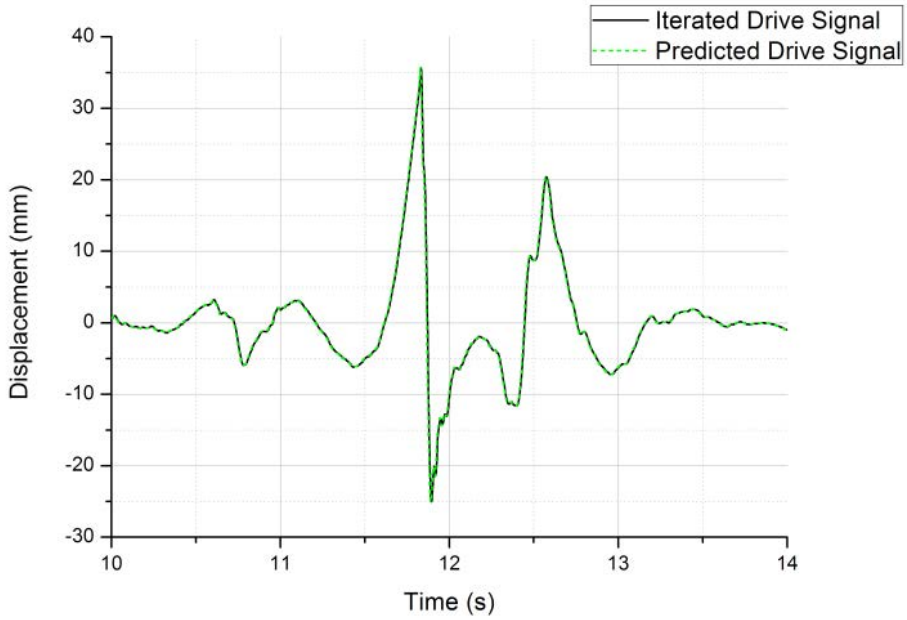

Figure 6.11: Drive Signal for Quarter Vehicle Variant 1

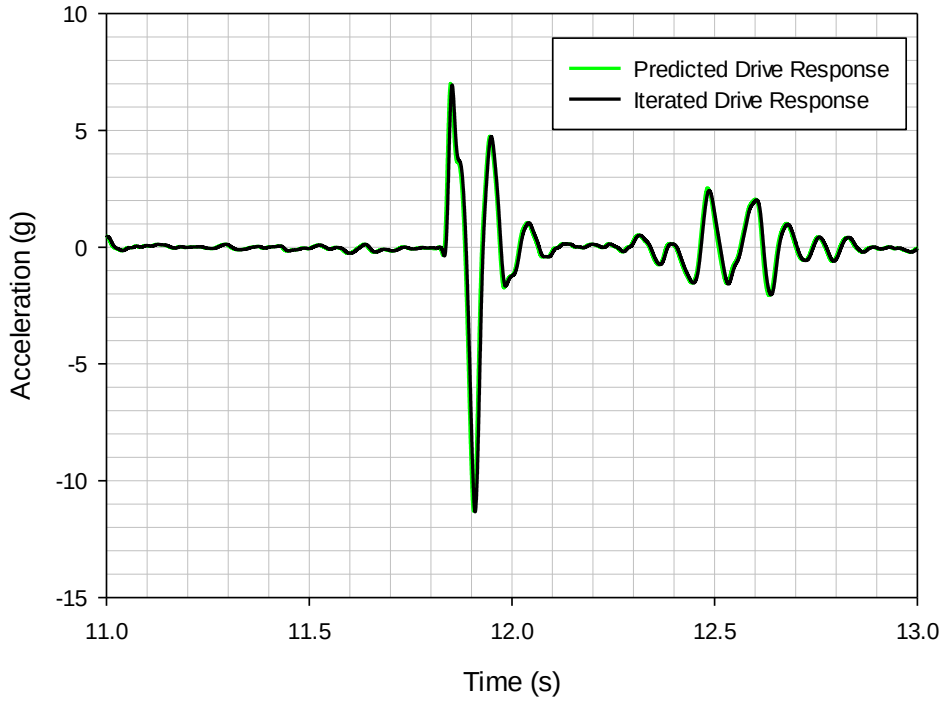

Figure 6.12: Response Signal for Quarter Vehicle Variant 1

The correlation coefficient for the drive signal for variant 1 (figure 6.11) was calculated as 0.99626 while that for the response signal for the same variant (figure 6.12) was computed as 0.956672.

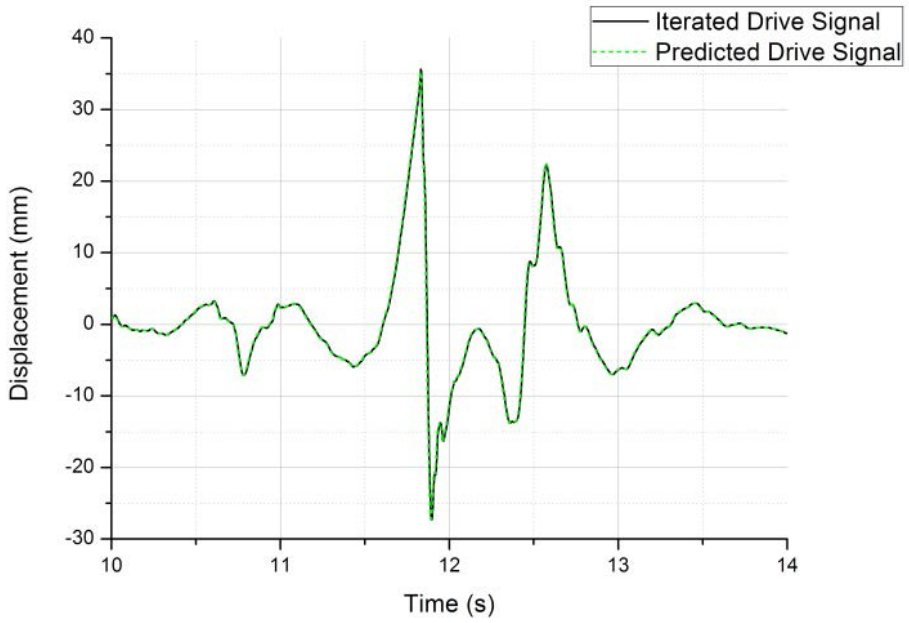

Figure 6.13: Predicted Drive Signal for Quarter Vehicle Variant 2

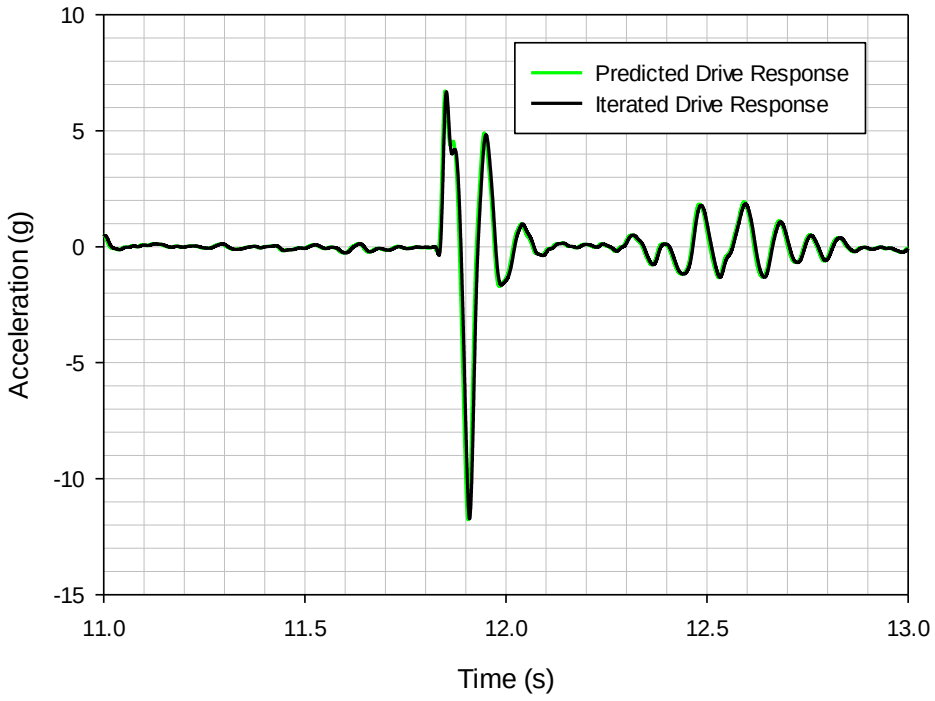

Figure 6.14: Response Signal for Quarter Vehicle Variant 2

The coefficient of correlation for the drive signal for variant 2 (figure 6.13) and the response signal for the same variant (figure 6.14) was calculated as 0.99647 and 0.95608 respectively.

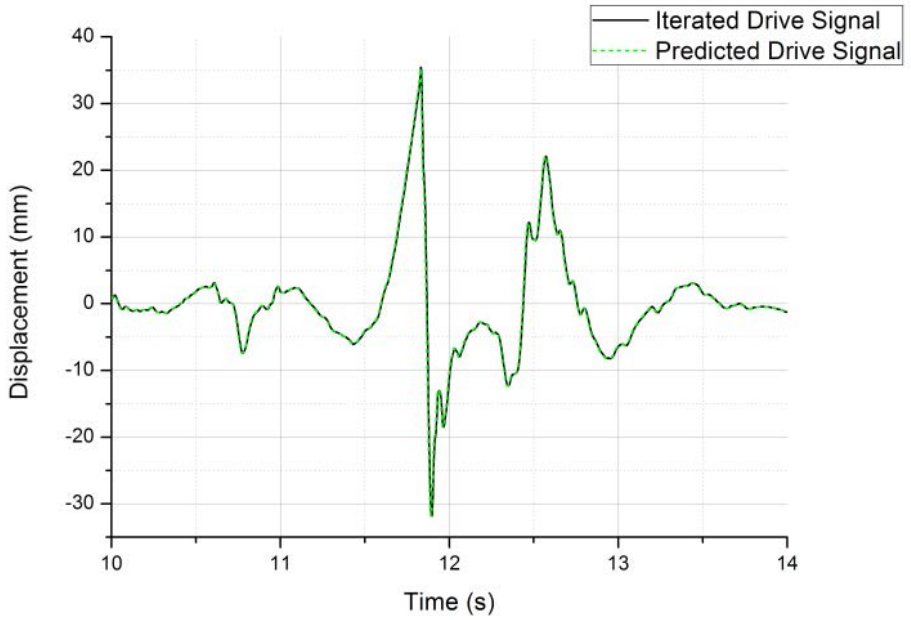

Figure 6.15: Drive Signal for Quarter Vehicle Variant 3

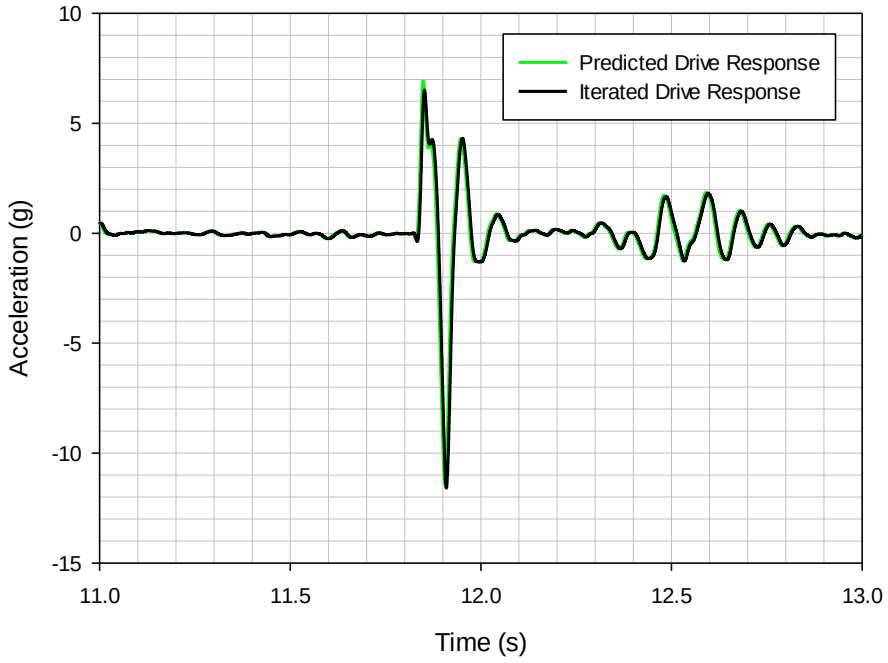

Figure 6.16: Response Signal for Quarter Vehicle Variant 3

Finally, the correlation coefficient for the drive (figure 6.15) and response (figure 6.16) signals for variant 3 were calculated as 0.99593 and 0.95812 respectively.

The results from the testing of the neural network as indicated by the correlation coefficient values indicate a very good correlation between the predicted drive signal and the iterated (expected) drive signal.

The next stage is the application of the same ANN Development procedure to the full vehicle to develop the Full Vehicle ARIT.

6.4 FULL VEHICLE ARIT DEVELOPMENT

6.4.1 Collation and Pre-processing of Network Data

In this stage, the data for the training of the neural network for the full vehicle deployment was gathered and processed for use. The procedure for the collation and processing of the data is similar to that in the quarter vehicle ARIT development, the difference being the larger number of vehicle configuration parameters in the full vehicle case. The vehicle configuration parameters as well as the vertical wheel acceleration of each wheel are used as the network's input.

These inputs to this neural network are as follows:

a. Left-Front Wheel Vertical Acceleration
b. Right-Front Wheel Vertical Acceleration
c. Left-Rear Wheel Vertical Acceleration
d. Right-Rear Wheel Vertical Acceleration
e. Vehicle Weight
f. Front Damping Characteristic Factor
g. Rear Damping Characteristic Factor
h. Front Spring Stiffness
i. Rear Spring Stiffness

These network inputs are arranged in the order they were used in the ANN development for the full vehicle.

The outputs from the neural network are as follows:

a. Left-Front Drive Signal
b. Right-Front Drive Signal
c. Left-Rear Drive Signal
d. Right-Rear Drive Signal

The inputs to the neural network were combined in a 2-level design of experiments to generate various vehicle configuration scenarios for the MBD simulation. The MBD Simulation Parameters considered are shown in the table 6.8.

Table 6.8: Full Vehicle MBD Simulation Parameters

Vehicle Weight (kg)	Front Damping Characteristic Factor	Rear Damping Characteristic Factor	Front Stiffness (kN/m)	Rear Stiffness (kN/m)
1500 (W1)	0.75 (FD1)	0.75 (RD1)	25 (FS1)	26 (RS1)
2300 (W2)	1.5 (FD2)	1.5 (RD2)	40 (FS2)	41 (RS2)

The various combinations of the parameters in table 6.8 produced from the design of experiment is presented in table 6.9.

Table 6.9: Full Vehicle Variant Configurations

W1,FD1,RD1,FS1, RS1	W2,FD1,RD1,FS1, RS1	W1,FD2,RD1,FS1, RS1	W2,FD2,RD1,FS1, RS1
W1,FD1,RD2,FS1, RS1	W2,FD1,RD2,FS1, RS1	W1,FD2,RD2,FS1, RS1	W2,FD2,RD2,FS1, RS1
W1,FD1,RD1,FS2, RS1	W2,FD1,RD1,FS2, RS1	W1,FD2,RD1,FS2, RS1	W2,FD2,RD1,FS2, RS1
W1,FD1,RD2,FS2, RS1	W2,FD1,RD2,FS2, RS1	W1,FD2,RD2,FS2, RS1	W2,FD2,RD2,FS2, RS1
W1,FD1,RD1,FS1, RS2	W2,FD1,RD1,FS1, RS2	W1,FD2,RD1,FS1, RS2	W2,FD2,RD1,FS1, RS2
W1,FD1,RD2,FS1, RS2	W2,FD1,RD2,FS1, RS2	W1,FD2,RD2,FS1, RS2	W2,FD2,RD2,FS1, RS2
W1,FD1,RD1,FS2, RS2	W2,FD1,RD1,FS2, RS2	W1,FD2,RD1,FS2, RS2	W2,FD2,RD1,FS2, RS2
W1,FD1,RD2,FS2, RS2	W2,FD1,RD2,FS2, RS2	W1,FD2,RD2,FS2, RS2	W2,FD2,RD2,FS2, RS2

The full vehicle configurations in table 6.9 were executed in SIMPACK and the drive files iterated in QanTiM in order to generate data for the training of the neural

network. The same method of data processing as used for the quarter vehicle was applied to the case of the full vehicle ANN development. The data was divided into training data set, testing data set and validation data set in the ratio 8:1:1.

6.4.2 Selection of Artificial Neural Network Design Architecture

Based on the investigation carried out in the earlier sections of this chapter on the suitability and performance of various neural network architectures, the Nonlinear Autoregressive Network with External Input (NARX) was selected for the prediction of the drive signal. Similar to the quarter vehicle ANN development, the performance of the network is assessed by the Mean Squared Error (MSE) as defined in Equation 6.1.

6.4.3 Artificial Neural Network Optimisation

A method similar to that used for the optimisation of the quarter vehicle ANN is used for the full vehicle. The following elements of the NARX network are optimised for performance:

1. The Training Algorithm
2. Number of Input Delays
3. Number of Feedback Delays
4. Size of Hidden layer
5. General Data Processing

As with the quarter vehicle ANN, the mean squared error in the optimisation of the full vehicle artificial neural network is computed from the average of three training

trials with the exception of the training algorithm selection where the stability of the network over five training trials was considered.

6.4.3.1 Training Algorithm

The results from the choice of the training algorithm for the quarter vehicle ANN optimisation in figures 6.3 and 6.4 indicated that the Bayesian Regularization produced the best result among other training algorithms. To confirm this result was applicable to the case of the full vehicle ANN, five training trials were carried out on all seven algorithms highlighted in table 5 and the results of the best performing networks are shown in the figure 6.17.

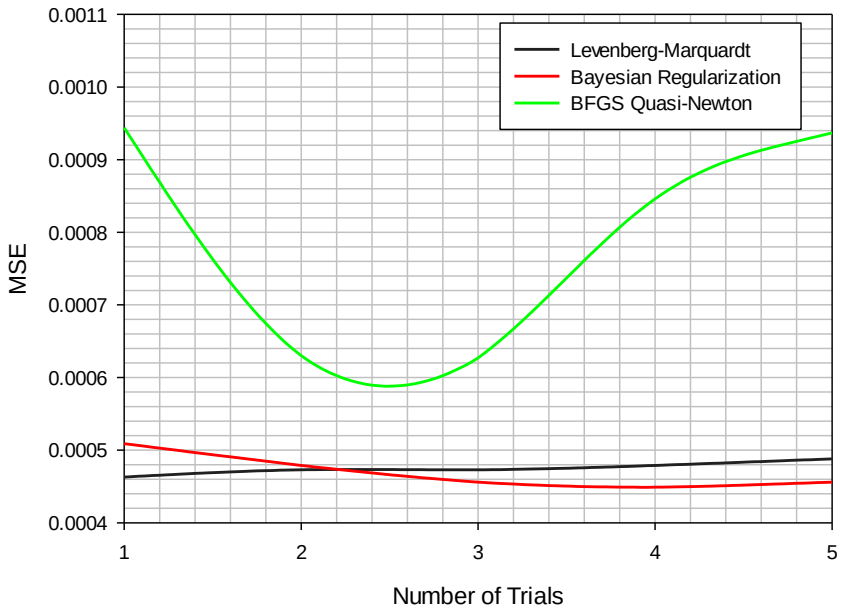

Figure 6.17: Full Vehicle Neural Network Performance with Training Algorithm

The results in figure 6.17 show that both the Levenberg-Marquardt and the Bayesian Regularization algorithms produce good network performance but the

performance of the Bayesian Regularization gives the best network performance compared with the other algorithms. The only constraint with using both the Levenberg-Marquardt and the Bayesian Regularization algorithms was the training time as well as the huge amount of computing memory they required. It was observed that the larger the training set, the larger the amount of computing memory both algorithms required for training the network. It was observed that the BFGS Quasi-Newton algorithm produced a fairly good result as well and required much less computing memory to train the network compared with the other training algorithms.

6.4.3.2 Number of Input Delays

The number of input delays is optimised by investigating the performance of the number of input delays on the performance of the network.

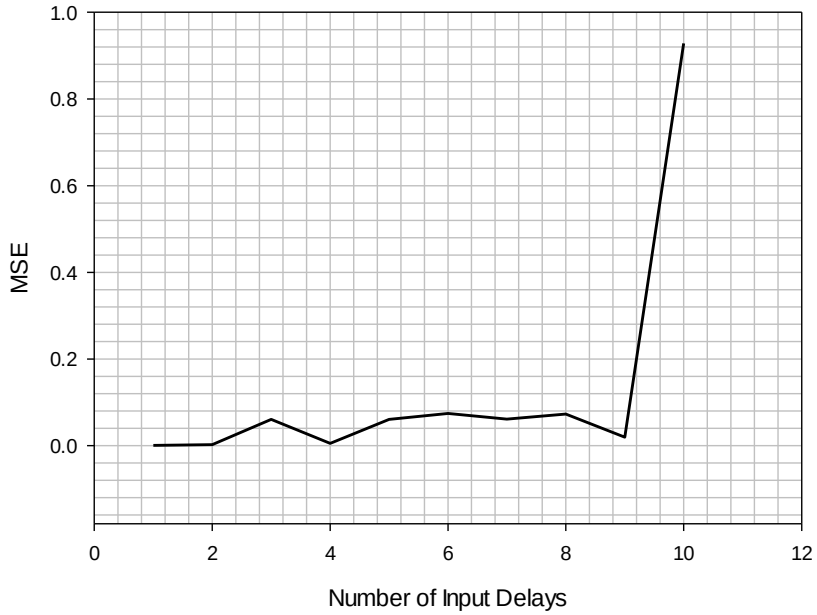

Figure 6.18: Full Vehicle NARX Network Performance with Number of Input Delay

The results from the quarter vehicle input delays optimisation (figure 6.5) showed that one input delay produced a better result than a larger number of input delays and this is confirmed again from the results in figure 6.18 for the full vehicle neural network.

6.4.3.3 Number of Feedback Delays

The initial investigation into the effects of the number of feedback delays in figure 6.6 revealed that the minimum number of feedback delays should be two and thereafter, the MSE of the network performance declined at a very small rate as the number of feedback delays increased. The results from the same investigation for the full vehicle ANN revealed a similar result as shown in figure 6.19.

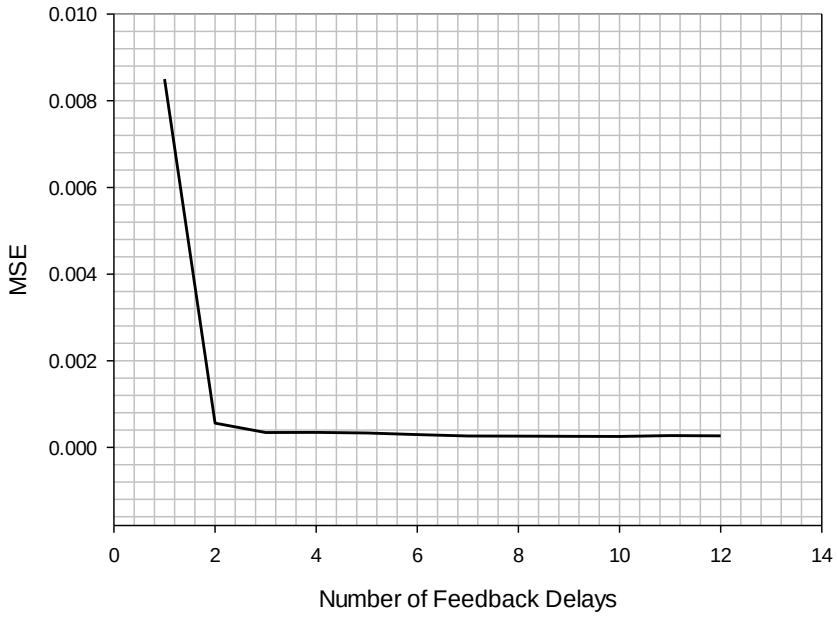

Figure 6.19: Full Vehicle NARX Network Performance with Number of Feedback Delays

6.4.3.4 Size of Hidden Layer

In investigating the effect of the size of the hidden layer, the results from the quarter vehicle ANN development did not reveal any particular trend though the size which produced the smallest MSE was observed. In developing the ANN for the full vehicle application, the results of the investigation into the effect of the size of the hidden layer shows an interesting trend as shown in figure 6.20.

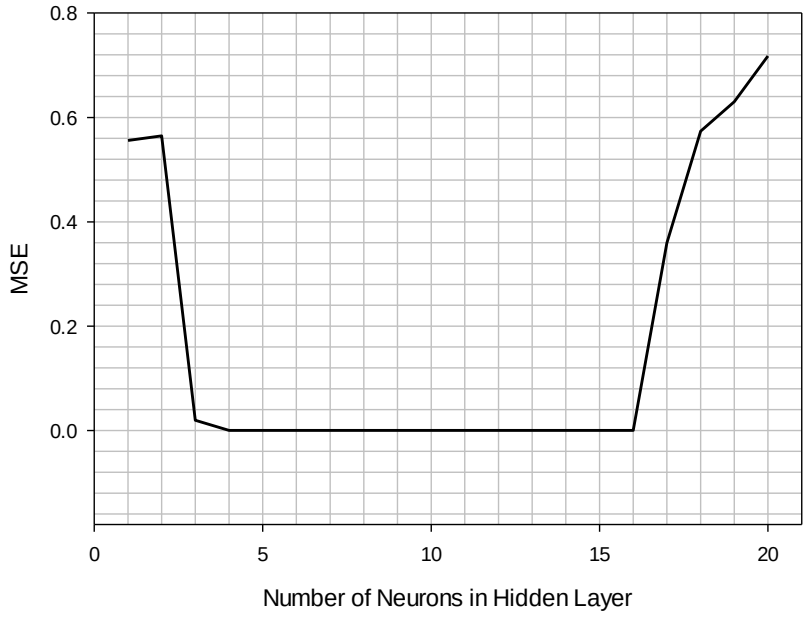

Figure 6.20: Full Vehicle NARX Network Performance with Size of Hidden Layer

The results show an initial decline in the mean squared error as the size of the hidden layer increased up to a layer size of 5 after which the mean squared error remains fairly constant. An increase in the MSE can be observed just after the layer size of 16 which indicates that the network would provide reliable results provided the number of neurons in the hidden layer is not more than 15.

6.4.3.5 General Data Processing

The data processing methods applied in the case of the quarter vehicle ANN development were again applied to determine the most suitable data processing method.

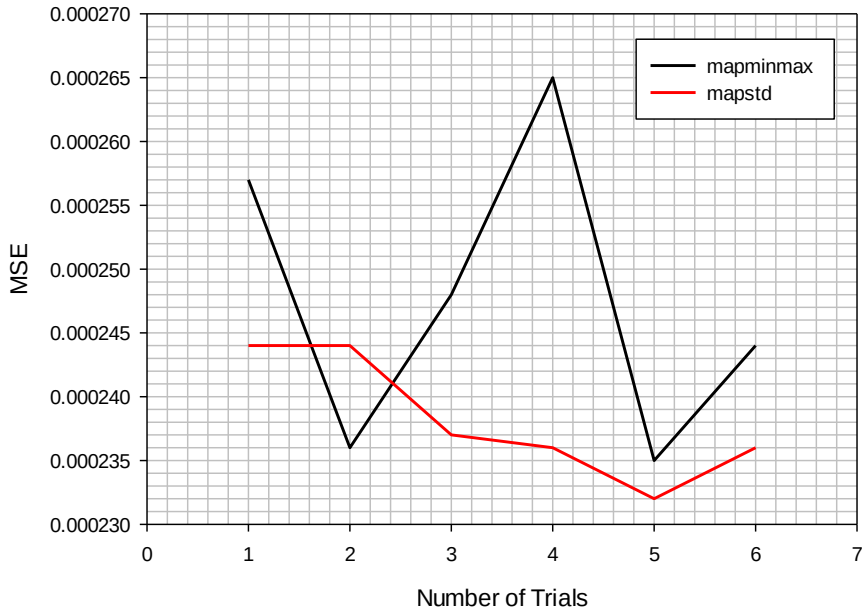

Figure 6.21: Full Vehicle NARX Network Performance with Data Processing Methods

The results in figure 6.21 indicate again that the *mapstd* produces a better network performance in five cases out of 6 trials compared with the performance of the *mapminmax* method. The results of the other methods of data processing were excluded for the sake of clarify.

6.4.4 Deployment and Testing of the Full Vehicle Artificial Road Input Tool

With the completion of the optimisation of the NARX network configuration parameters, the recommended configuration for the network was implemented, trained and tested.

6.4.4.1 Full Vehicle Artificial Neural Network Configuration

The NARX network for the deployment of the full vehicle ANN was trained with the Bayesian Regularisation algorithm based on the results in figure 6.17. The number of input delays selected was one based on the network performance as shown in figure 6.18 and one being the smallest number of input delays to produce an acceptable network performance. The number of feedback delays is selected as three. This was chosen on the basis of that it is the minimum number of input delays to produce a good network performance. The size of the hidden layer is once again chosen as six, similar to that of the quarter vehicle ANN development, on the basis of being the smallest number of hidden layer neurons to produce a good network performance. Finally, "*mapstd*" is selected as the general data processing method from the results observed in figure 6.21. The Full vehicle NARX configuration is compiled in the table 6.9.

Table 6.10: NARX Network Configuration

Configuration Parameter	
Training Algorithm	Bayesian Regularisation
Number of Input Delays	1
Number of Feedback Delays	3
Size of Hidden Layer	6
General Data Processing Method	Mapstd

6.4.4.2 Network Training and Testing

The final artificial neural network configuration as stated in table 6.10 above is trained once again with the data collected from the MBD simulation and QanTiM drive signal iteration. The results of the network's performance are as follows:

Training Performance (MSE): *2.9930e-4*

Test Performance (MSE): 2.9559e-4

The testing of the deployed neural network is carried out using the two different vehicle variants. The configurations of the variants are listed in the table 6.11.

Table 6.11: Full Vehicle Parameters for Neural Network Input

Full Vehicle Variant Number	Chassis Mass (kg)	Front Damping Factor	Rear Damping Factor	Front Spring Stiffness (kN/m)	Rear Spring Stiffness (kN/m)
1	2000	1.00	0.75	29	31
2	2500	1.00	1.00	35	31

The drive signal output from the neural network for each of the vehicle variants in table 6.11 were compared to the iterated drive signal output from QanTiM and the results show a very good correlation similar to what was obtained in the case of the quarter vehicle ARIT.

6.4.4.3 Full Vehicle Artificial Road Input Tool Testing Results

This section comprises the comparison of the ARIT's output drive signal with the iterated drive signal from QanTiM as well as the comparison of the results from running the MBDS model with both drive signals. The correlation coefficient for each of the results is also collated in order to examine the quality of the similarities in the drive signals and acceleration response in the MBD simulation.

6.4.4.3.1 Full Vehicle Variant 1

The results of the comparison of the drive signals and acceleration response signals for the full vehicle variant 1 are shown in figures 6.22 to 6.25 and figures 6.26 to

6.29 respectively. The table 6.12 shows the calculated correlation coefficients for both the drive and response signals.

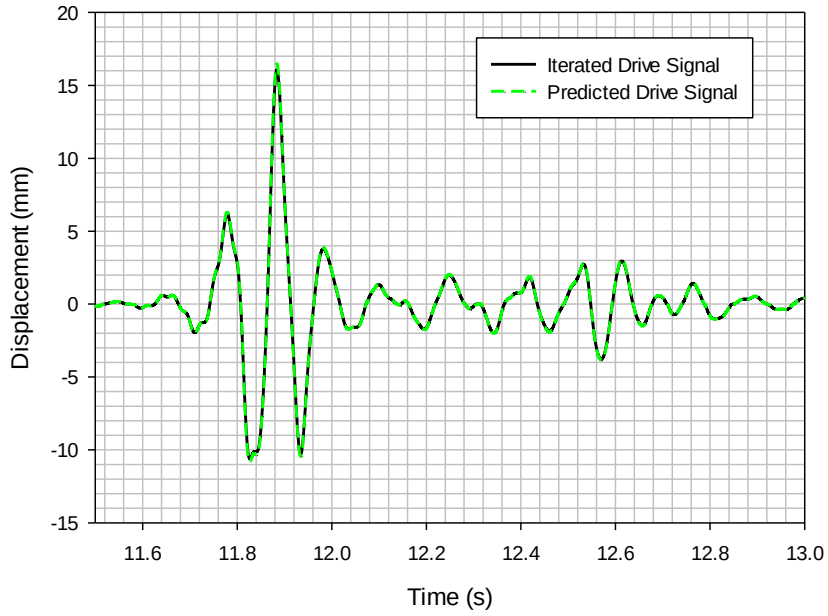

Figure 6.22: LHF Drive Signal for Full Vehicle Variant 1

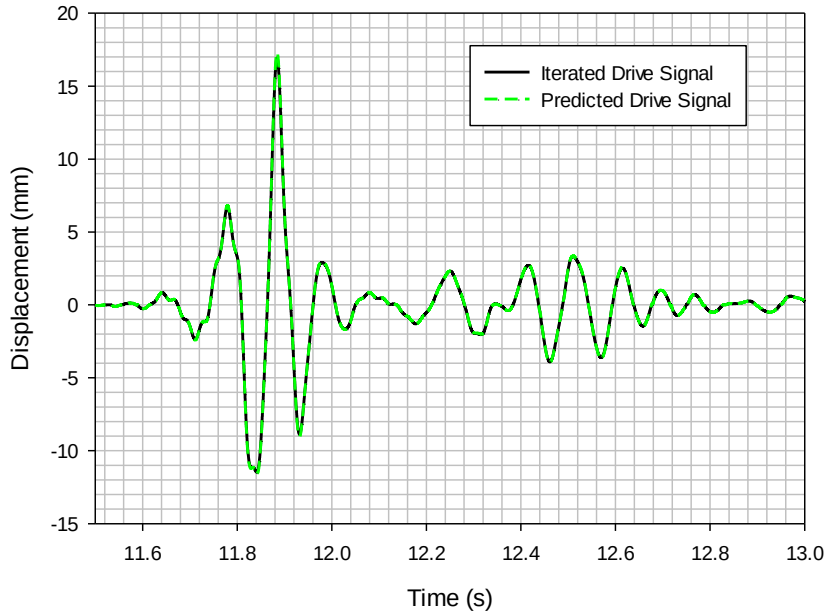

Figure 6.23: RHF Drive Signal for Full Vehicle Variant 1

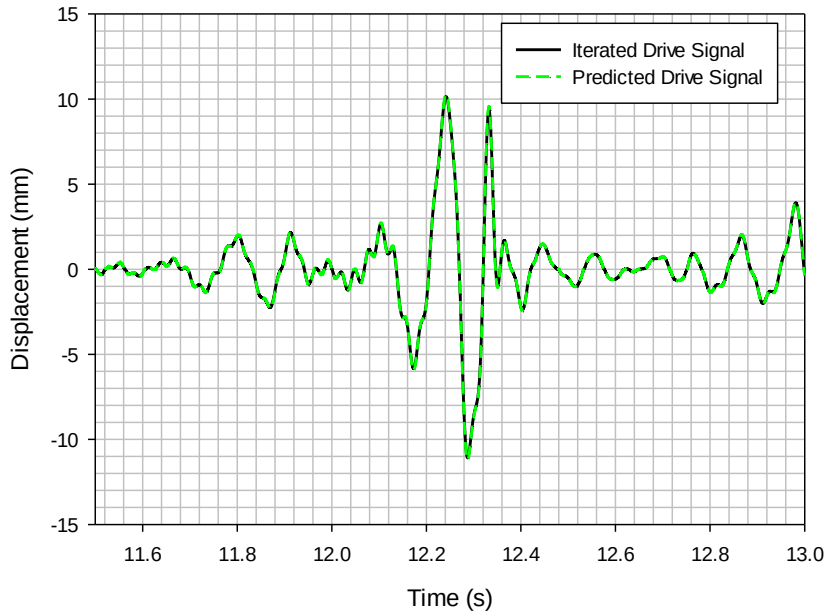

Figure 6.24: LHR Drive Signal for Full Vehicle Variant 1

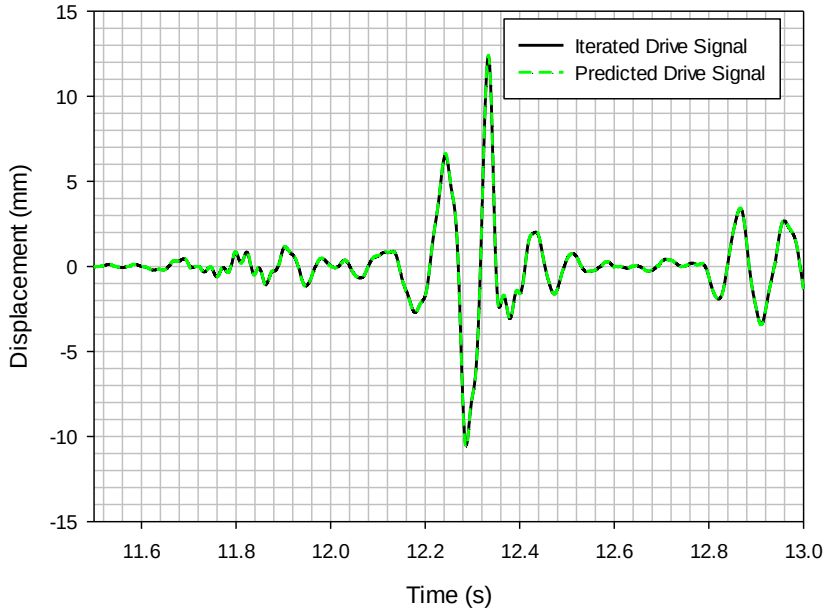

Figure 6.25: RHR Drive Signal for Full Vehicle Variant 1

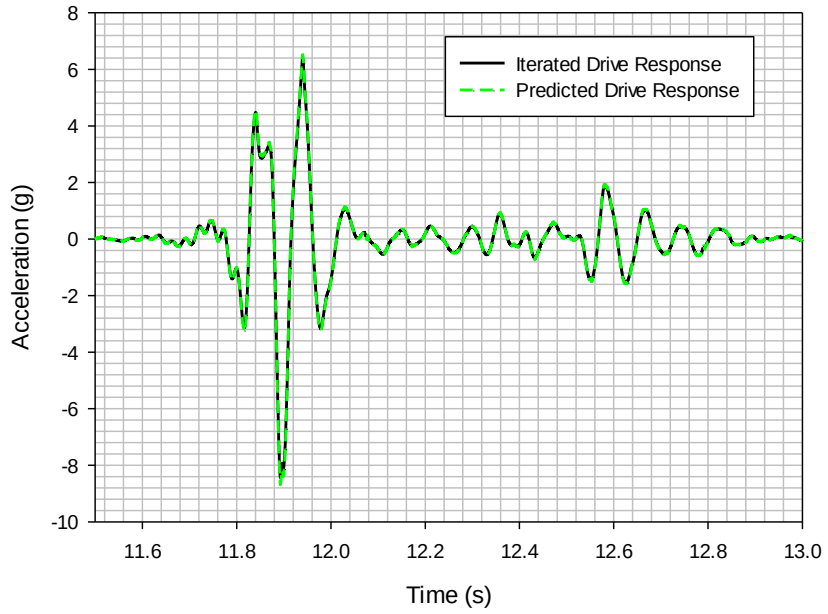

Figure 6.26: LHF Response Signal for Full Vehicle Variant 1

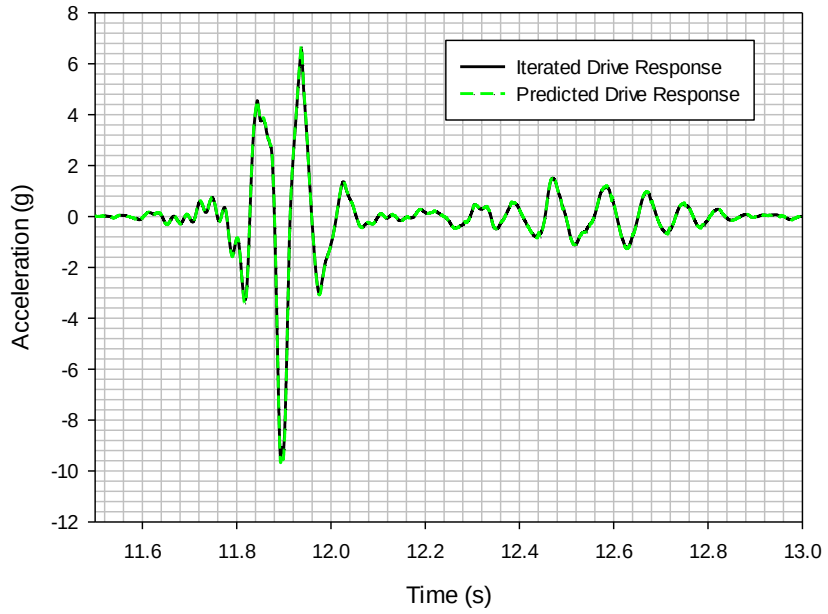

Figure 6.27: RHF Response Signal for Full Vehicle Variant 1

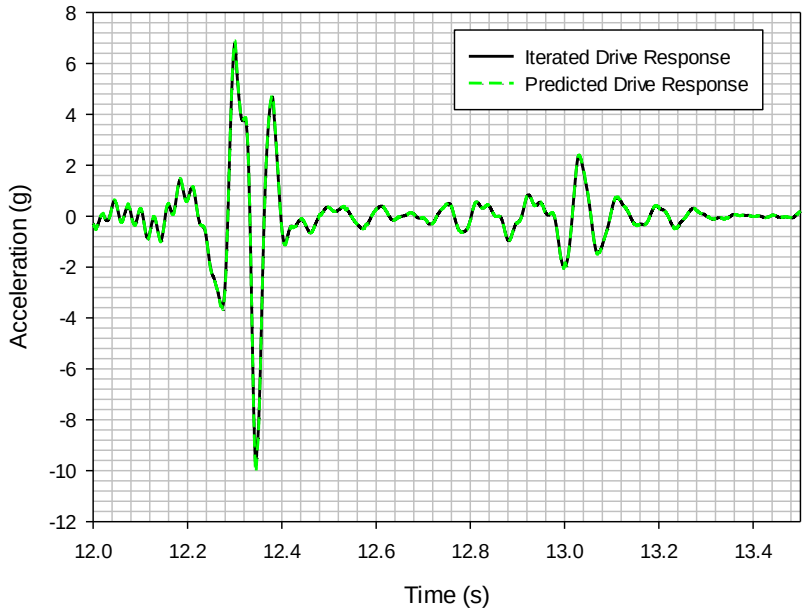

Figure 6.28: LHR Response Signal for Full Vehicle Variant 1

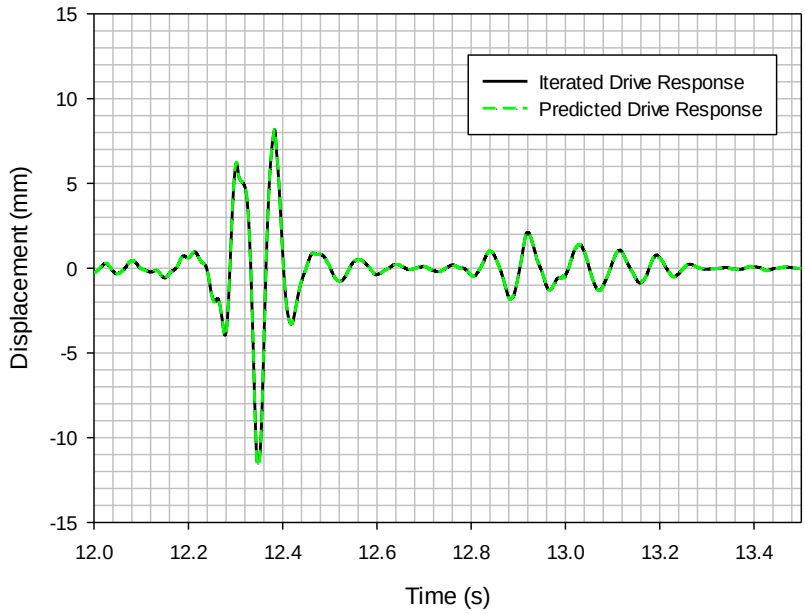

Figure 6.29: RHR Response Signal for Full Vehicle Variant 1

Table 6.12: Correlation Coefficient for Full Vehicle Variant 1

	Drive Signal	Response Signal
Left Hand Front (LHF)	0.999945	0.999859
Right Hand Front (RHF)	0.999929	0.999831
Left Hand Rear (LHR)	0.999861	0.999826
Right Hand Rear (RHR)	0.999873	0.999908

The results of the ARIT shown in figures 6.22 to 6.25 show a very good correlation with those iterated from QanTiM. The correlation coefficients shown in table 6.12 confirm that the ARIT's performance with the variation in the vehicle parameter is as good as iterating the drive signal from the actual vehicle variant. In addition, the response signal comparison results shown in figure 6.26 to 6.29 show a very good correlation as shown in table 6.12; the comparison of the variation in the response of the full vehicle to the ARIT's output is very similar to that from QanTiM's iterated drive signal. The results generally show, from table 6.12, that the ARIT's predictions are 99.9% accurate.

6.4.4.3.2 Full Vehicle Variant 2

In order to further test the accuracy and reliability of the ARIT, it is used to predict the drive signal for a second full vehicle variant and the correlation coefficients are

calculated. The result of the comparison of the drive signals are shown in figures 6.30 to 6.33 while the response signals are shown in figures 6.34 to 6.37. The correlation coefficients are shown in table 6.13.

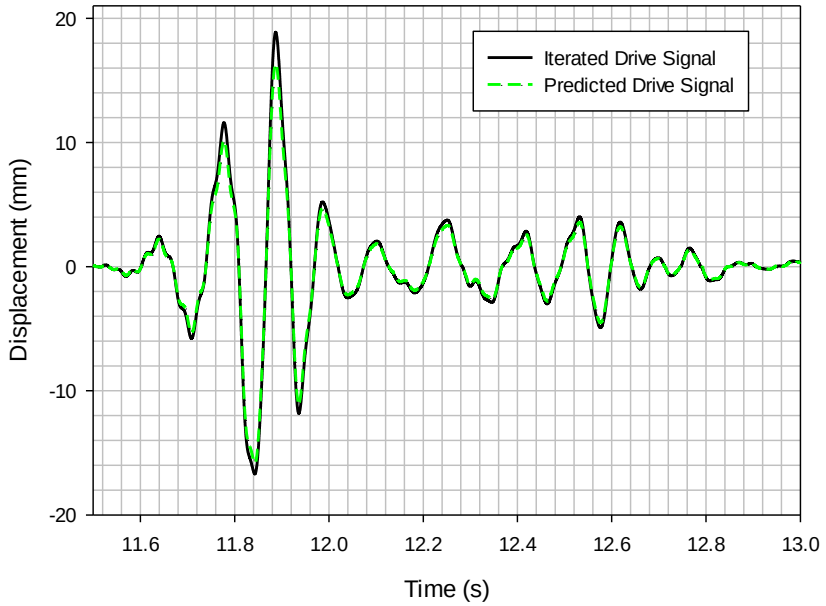

Figure 6.30: LHF Drive Signal for Full Vehicle Variant 2

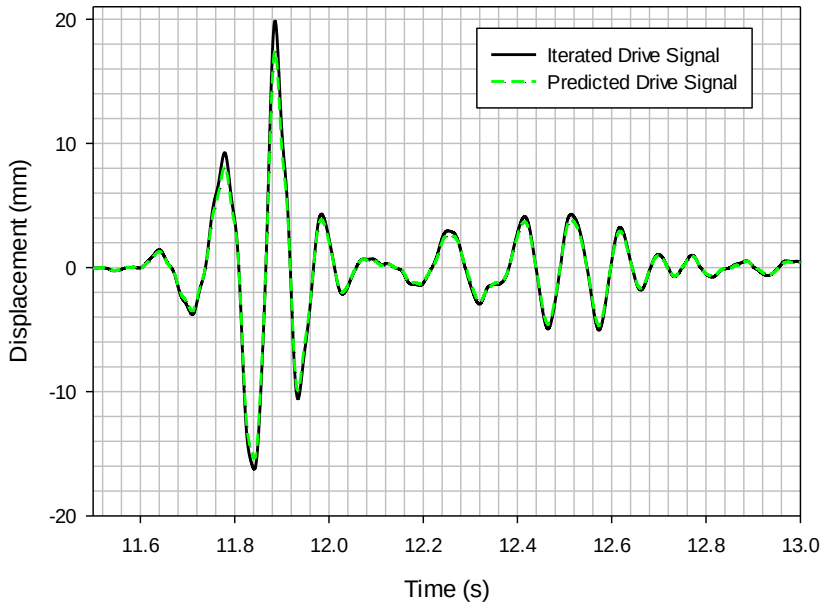

Figure 6.31: RHF Drive Signal for Full Vehicle Variant 2

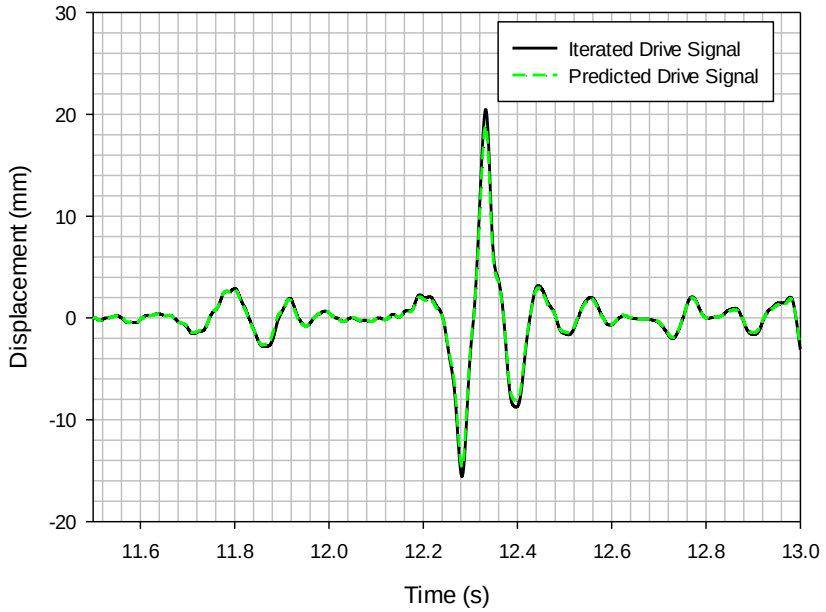

Figure 6.32: LHR Drive Signal for Full Vehicle Variant 2

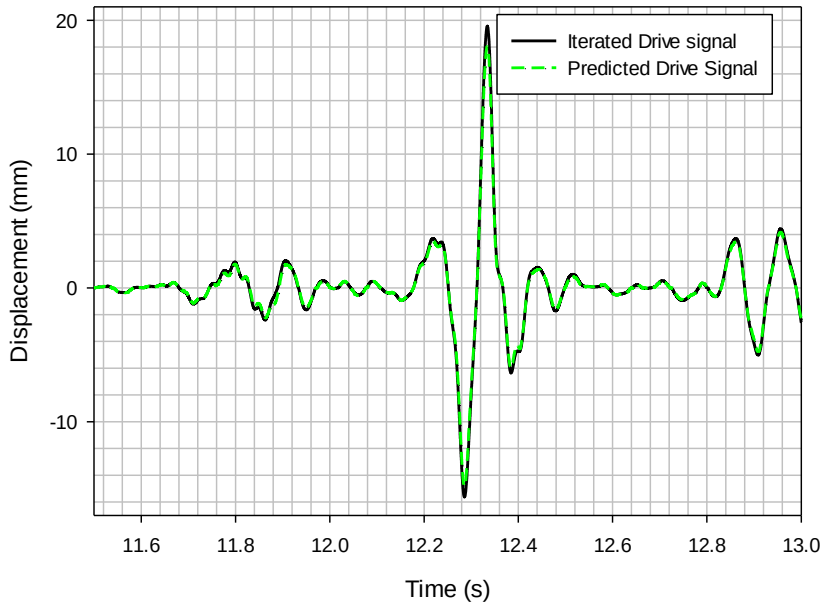

Figure 6.33: RHR Drive Signal for Full Vehicle Variant 2

Figure 6.34: LHF Response Signal for Full Vehicle Variant 2

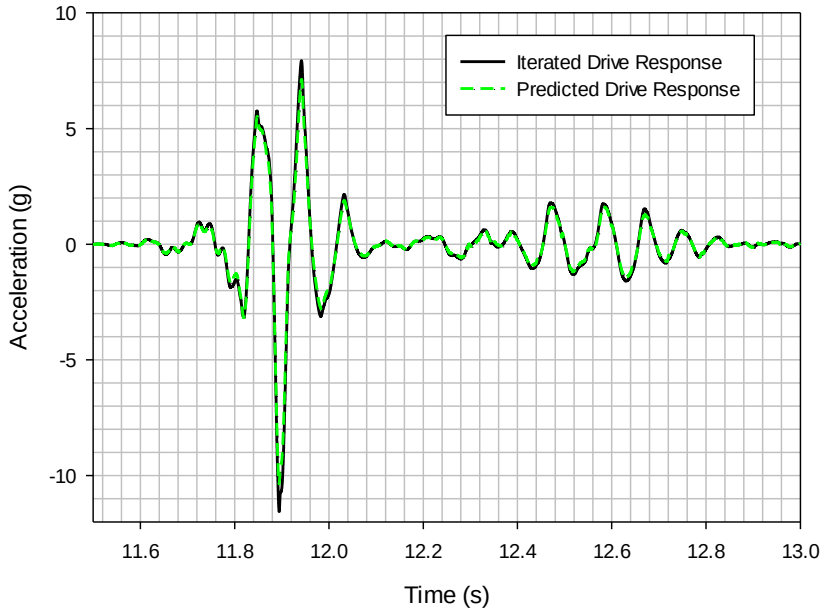

Figure 6.35: RHF Response Signal for Full Vehicle Variant 2

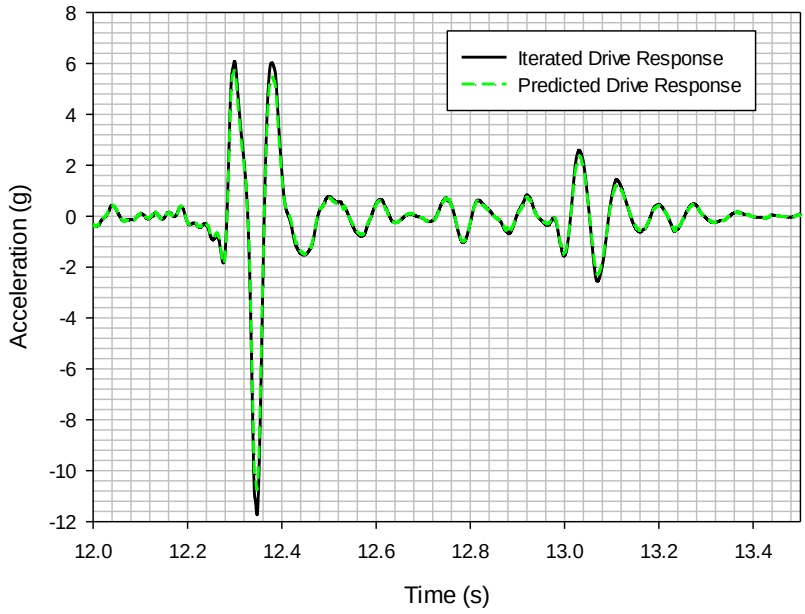

Figure 6.36: LHR Response Signal for Full Vehicle Variant 2

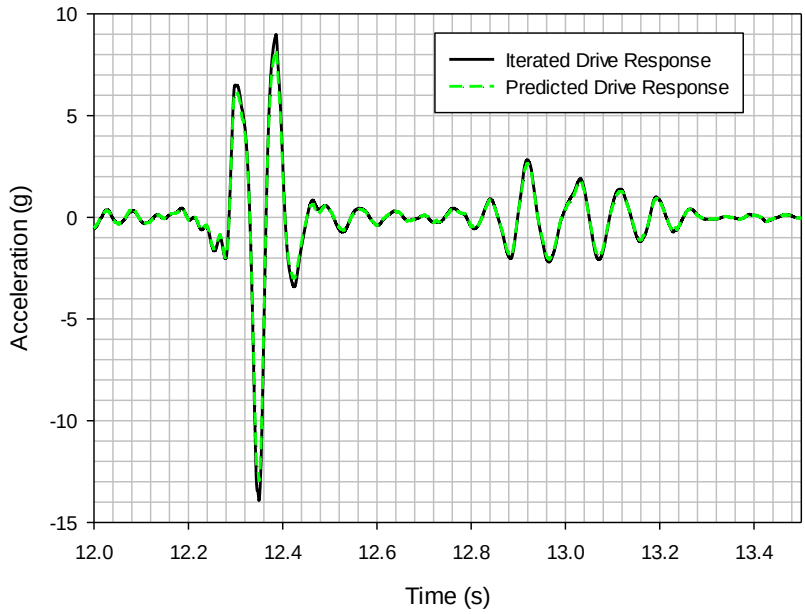

Figure 6.37: RHR Response Signal for Full Vehicle Variant 2

Table 6.13: Correlation Coefficient for Full Vehicle Variant 2

	Drive Signal	Response Signal
Left Hand Front (LHF)	0.999389	0.997743
Right Hand Front (RHF)	0.999497	0.998608
Left Hand Rear (LHR)	0.999628	0.999394
Right Hand Rear (RHR)	0.999487	0.999508

The results shown in figures 6.30 to 6.37 further endorse the accuracy of the ARIT. A simple visual inspection of the results show a very good correlation and this is corroborated by the correlation coefficients in table 6.13 which indicate that the ARIT's performance is at least 99.94% accurate.

6.5 CONCLUSION

The results in figures 6.11 to 6.16 and 6.21 to 6.37 for the Quarter Vehicle and Full Vehicle Artificial Road Input Tool (ARIT) deployment respectively indicate a very good performance of the artificial neural network in predicting the drive signals for the variations in vehicle configuration parameters. The results of the responses to the drive signal in the MBD simulation also corroborate the effectiveness of the ARIT. Though the results presented in this chapter are each about four seconds long, it is believed that the Artificial Road Input Tool, with sufficient training data, can produce a much longer representative vehicle usage time history which can be used

to drive MBS simulations from the early stages in the vehicle design programme. With the level of accuracy obtained from the ARIT, it would be possible for design engineers and teams to carry out realistic durability and fatigue testing on various components in the vehicle using the output of the ARIT as the drive signal. As highlighted earlier in this chapter, the fidelity of the training data is very important to the accuracy of the output of the ARIT. Hence, a pre-processing method for the training data is very important in guaranteeing the reliability of the ARIT's output.

6.6 SUMMARY

An Artificial Neural Network was developed and optimised for the prediction of road input for driving MBD simulation models for the quarter vehicle and full vehicle variants. The resulting Artificial Road Input Tool was tested for both the Quarter Vehicle and Full Vehicle and the results of the comparison of the predicted drive and response signals showed a very good correlation. These results of the correlation of the drive signal from the Artificial Road Input Tool shows the capability of the artificial neural network method in modelling the relationship between the input drive signal and the vehicle parameters.

CHAPTER SEVEN: PROJECT CONCLUSIONS AND FUTURE WORKS

7.1 INTRODUCTION

Following the development of the Artificial Road Input Tool, the project conclusions and recommendations for future work from this current research project are presented in this chapter.

7.2 PROJECT CONCLUSION

In this study, a review of the existing literature on road load data acquisition and application revealed the importance of road load data for the optimisation of the durability performance of a vehicle particularly in the early stage of the vehicle programme when modifications are more cost effective. Also, the literature survey showed that there are currently no methods for generating virtual road input data which take into consideration the variation in vehicle configuration parameters; the existing methods of road load prediction involved cost intensive methods. With the aforementioned in mind, this current research introduced a method of artificial intelligence for the prediction of the road load which was able to transform existing road load data for use in a newer vehicle development programme. Hence, the contributions resulting from this research are summarised as follows:

1. The efficiency of a simple tyre model for the accurate determination of the vertical acceleration response of a quarter vehicle in the multi-body dynamics (MBD) simulation environment was established. This showed that a simple

tyre model could effectively replace a complex tyre model for the vehicle excitation and response in the vertical direction.

2. A method of characterising road load data from MBD simulation as vehicle parameters changes in order to understand the effect of the varying vehicle parameters on the vehicle's behaviour to a realistic road input was developed. This method was reported in a technical paper at the Society of Automotive Engineers (SAE) Congress [93].
3. A novel method of artificial neural networks was used to design an artificial road input tool (ARIT) which was capable of using collected road load data and some vehicle suspension parameters of the vehicle from which the data was collected to generate a road input signal to drive the MBDS model of a variant of the chosen vehicle. The result of the implementation of this tool was published and presented at the Society of Automotive Engineers (SAE) Congress [99].
4. The accuracy of the ARIT for the vehicle parameters considered is a precursor to the further use of artificial intelligence in accurately predicting road loads for vehicles in the pre-prototype stage of a vehicle programme. Though a few vehicle parameters have been used in this current research, the method presented for selection and optimisation of a neural network can be used in determining the road input for a larger selection of vehicle parameters.

7.3 RECOMMENDATIONS FOR FUTURE RESEARCH

Although the work carried out in this current research for the development of the ARIT demonstrated very good results for predicting the road input for the generation of road load data, there are still a good number of improvements that can be made to increase the robustness of the ARIT. These recommendations are as follows:

1. The ARIT developed in this project was used for the prediction of just the vertical input to the vehicle. Hence, further work should be carried out to modify it for predicting road input in the three axes of vehicle motion. This would make the tool robust and ready for deployment in a real vehicle programme environment.
2. The ARIT should be tested on a more complex vehicle model with a larger number of non-linear components such as bushes, active shock absorbers, flexible body chassis etc. to expand on the capacity of the tool. This may require the use of other neural network types, configuration, training algorithms or data processing.
3. A method for optimising the training of the neural network should be investigated. It was discovered in the course of developing the full vehicle ARIT, which had more training data than the quarter vehicle ARIT, that the computer memory requirement of the neural network training algorithms was proportional to the amount of data used for the training. This could pose a challenge in the event that a very large amount of training data is presented to the neural network.
4. A programme with a user friendly graphical interface for the implementation of the ARIT should be designed. The current implementation of the ARIT

requires a good knowledge of the MATLAB programme and is implemented in a text-based user environment. The user friendly graphical interface would enable the ARIT to be used by anyone without the need to have background knowledge of MATLAB or neural network design. This programme should be able to pre-process the network training data, implement a neural network architecture, train the network, optimise the network and thereafter deploy the neural network for use. The programme should be able to store the configurations of the ARIT for different applications and call them up when needed. It would also be a good addition if the programme is able to directly load, read and extract data from the industry standard RPC® III file format as that is the file format in which most acquired road load data are stored.

5. Based on the successful implementation of the ARIT using data from MBD simulation, a real life implementation of this tool should be considered for application in a vehicle programme of an original equipment manufacturer (OEM). This should be carried out by developing a road load database from the proving ground and customer usage road load data acquisition exercises carried out in the past by the OEM and applying the methods highlighted in this thesis for the implementation of an artificial road input tool. This method can be implemented as a pilot programme to predict the road input on a component basis and thereafter expanded to the entire vehicle durability testing.

LIST OF REFERENCES

1. Lolas, S. and O.A. Olatunbosun, *Prediction of vehicle reliability performance using artificial neural networks.* Expert Systems with Applications, 2008. **34**(4): p. 2360-2369.

2. Reed, M.J. and M.R. Trivedi, *CAE-An Approach to a Shorter Product Design Cycle Time*. 1988, SAE International.

3. da Cruz, J.M., I.L. do Espírito Santo, and A.A. de Oliveira, *A Semi-Analytical Method to Generate Load Cases For CAE Durability Using Virtual Vehicle Prototypes*. 2003, SAE International.

4. Londhe, A. and S. Kangde, *Virtual Road Approach for Vehicle Durability Simulations.* SAE Int. J. Passeng. Cars - Mech. Syst., 2013. **6**(2).

5. Roy, N. and M. Villaire, *Virtual Road Load Data Acquisition using Full Vehicle Simulations*. 2013, SAE International.

6. Kim, D. and S. Joo, *Generation of 3-D Virtual Block Belgian Road for Prediction of Road Load*. 2011, The Automotive Research Association of India.

7. Schudt, J.A., et al., *Virtual Road Load Data Acquisition in Practice at General Motors*. 2011, SAE International.

8. Hong, H.-J. and S.D. Strumpfer, *Virtual Road Load Data Acquisition for Twist Axle Rear Suspension*. 2011, SAE International.

9. Scime, S., *Conducting Tire-Coupled (4-Post) Durability Simulations without Road Load Data Acquisition*. 2011, SAE International.

10. Schmeitz, A., W. Versteden, and T. Eguchi, *Road Load Simulation using the MF-Swift Tire and OpenCRG Road Model*. 2011, SAE International.

11. Pham, D.T. and P.T.N. Pham, *Artificial intelligence in engineering.* International Journal of Machine Tools and Manufacture, 1999. **39**(6): p. 937-949.

12. Bäcker, M., et al., *Load Identification for CAE Based Fatigue Life Prediction of a New Bus Type.* 2007.

13. Haq, S., et al., *Vehicle Road Simulation Testing, Correlation and Variability.* 2005.

14. Reddy, C.V.R., et al., *Analysis of Road Load Data to Extract Statistical Trends in Spindle Loads for Vehicles with Variants.* 2005.

15. Babu, H.S., P.A. Thakare, and A. Shirguppe, *Design Optimization of a Mini-Truck Hydraulic Power Steering System Based on Road Load Data (RLD)*. 2010, SAE International.

16. Dodds, C.J. and A.R. Plummer, *Laboratory Road Simulation for Full Vehicle Testing: A Review*. 2001, The Automotive Research Association of India.

17. Xu, P., et al., *Road Test Simulation Technology in Light Vehicle Development and Durability Evaluation.* 2005.

18. Yang, X., Y. Men, and M.N. Rowley, *Back-Calculated Spindle Loads Sensitivity to Suspension Component Loads Availability*. 2008, SAE International.

19. Kim, J.C., S.Y. Cheong, and Y.M. Cheong, *Prediction of cumulative damage by analysis of automatic transmission endurance test mode.* SAE, 2000. **2000**: p. F2000A080.

20. You, S. and S.-G. Joo, *Virtual Testing and Correlation with Spindle Coupled Full Vehicle Testing System*. 2006, SAE International.

21. Ludes, R. and B. Steeples, *Road Load and Customer Data from the Vehicle Data Bus - A New Approach for Quality Improvement*. 1999, SAE International.

22. Aoki, T., et al., *A Study of Development Indices Established Quantification of Road Load*. 2003, SAE International.

23. Lin, S.H., et al., *CAE Analyses for Suspension System and Full Vehicle under Durability Road Load Conditions*. 2007, SAE International.

24. Lin, S.H., et al., *Experiments and CAE Analyses for Suspension under Durability Road Load Conditions*. 2006, SAE International.

25. Zhang, L., et al., *Component Load Predication from Wheel Force Transducer Measurements*. 2011, SAE International.

26. Bäcker, M., et al., *The Hybrid Road Approach for Durability Loads Prediction.* 2005.

27. Lima, I., G.M. Kato, and J.C. Parrilla, *CAE Approach for Light Truck Frame Durability Evaluation Due to Payload Increase*. 2004, SAE International.

28. Olatunbosun, O.A. and J.W. Dunn, *A Simulation Model for Passive Suspension Ride Performance Optimization*, in *Automotive Simulation '91*, M. Heller, Editor. 1991, Springer Berlin Heidelberg. p. 131-142.

29. Sun, T., Y. Zhang, and P. Barak, *Quarter Vehicle Ride Model*. 2002, SAE International.

30. Andersen, E.R., C. Sandu, and S. Southward, *Multibody Dynamics Modeling and System Identification of a Quarter-Car Test Rig with McPherson Strut Suspension*. 2007, SAE International.

31. dos Santos, R., et al., *Optimization of New Plastic Bracket NVH Characteristics using CAE*. 2012, SAE International.

32. Franco, J.M.V. and G. Schaefer, *Validation off an SUV Model for Vehicle Dynamics Simulation*. 2007, SAE International.

33. Budynas, R.G. and J.K. Nisbett, *Shigley's mechanical engineering design*. 9th ed. McGraw-Hill series in mechanical engineering. 2011, New York: McGraw-Hill. xxi, 1082 p.

34. Zhang, Y., et al., *Full Vehicle Finite Element Model 4-Post Durability Analysis.* 2005.

35. Shahidi, B., et al., *System Level Durability Engineering in CAE*. 2006, SAE International.

36. Bakir, M., M. Siktas, and S. Atamer, *Comprehensive Durability Assessment of Leaf Springs with CAE Methods*. 2014, SAE International.

37. Yang, X. and P. Xu, *Chapter 1 - Road Load Analysis Techniques in Automotive Engineering*, in *Metal Fatigue Analysis Handbook*, Y.-L. Lee, M.E. Barkey, and H.-T. Kang, Editors. 2012, Butterworth-Heinemann: Boston. p. 1-60.

38. Behrens, B.A., et al., *Fatigue analysis of a mechanical press by means of the hybrid multi-body simulation.* Production Engineering, 2012. **6**(4-5): p. 421-430.

39. Andrews, G.C. and H.K. Kesavan, *Vector-Network Model - New Approach to Vector Dynamics.* Mechanism and Machine Theory, 1975. **10**(1): p. 57-75.

40. Agrawal, O.P. and A.A. Shabana, *Dynamic Analysis of Multibody Systems Using Component Modes.* Computers & Structures, 1985. **21**(6): p. 1303-1312.

41. Zeid, A. and D. Chang, *Simulation of Multibody Systems for the Computer-Aided Design of Vehicle Dynamic Controls*. 1991, SAE International.

42. Chan, B., *Development of a Mass-Customizable Medium-Duty Vocational Commercial Vehicle Using Multibody Dynamics*. 2013, SAE International.

43. Subramanyam, V., V. Monkaba, and T. Alexander, *A Unique Approach to All-Wheel Drive Vehicle Dynamics Model Simulation and Correlation*. 2000, SAE International.

44. Dannbauer, H., et al., *Integrating Virtual Test Methods and Physical Testing to Assure Accuracy and to Reduce Effort and Time*. 2006, SAE International.

45. Wong, J.Y., *Theory of ground vehicles*. 3rd ed. 2001, New York: John Wiley. xxxii, 528 p.

46. Li, B., X. Yang, and J. Yang, *Tire Model Application and Parameter Identification-A Literature Review.* SAE Int. J. Passeng. Cars - Mech. Syst., 2014. **7**(1).

47. Mousseau, C.W. and S.K. Clark, *An Analytical and Experimental Study of a Tire Rolling Over a Stepped Obstacle at Low Velocity.* Tire Science and Technology, 1994. **22**(3): p. 162-181.

48. Mousseau, C.W. and G.M. Hulbert, *An efficient tire model for the analysis of spindle forces produced by a tire impacting large obstacles.* Computer Methods in Applied Mechanics and Engineering, 1996. **135**(1–2): p. 15-34.

49. Zegelaar, P.W.A. and H.B. Pacejka, *The In-Plane Dynamics of Tyres on Uneven Roads.* Vehicle System Dynamics, 1996. **25**(sup1): p. 714-730.

50. Oertel, C. and A. Fandre, *Ride comfort simulations and steps towards life time calculations: RMOD-K tyre model and ADAMS*. 1999.

51. Kao, B.G., *A Three-Dimensional Dynamic Tire Model for Vehicle Dynamic Simulations.* Tire Science and Technology, 2000. **28**(2): p. 72-95.

52. Schmeitz, A.J.C., et al., *Application of a semi-empirical dynamic tyre model for rolling over arbitrary road profiles.* International Journal of Vehicle Design, 2004. **36**(2): p. 194-215.

53. Lugner, P., H. Pacejka, and M. Plöchl, *Recent advances in tyre models and testing procedures.* Vehicle System Dynamics, 2005. **43**(6-7): p. 413-426.

54. Gipser, M., *FTire: a physically based application-oriented tyre model for use with detailed MBS and finite-element suspension models.* Vehicle System Dynamics, 2005. **43**(sup1): p. 76-91.

55. Gallrein, A. and M. Bäcker, *CDTire : a tire model for comfort and durability applications.* Tire Model Performance Test (TMPT), 2007: p. 69-77.

56. Baecker, M., A. Gallrein, and H. Haga, *A Tire Model for Very Large Tire Deformations and its Application in Very Severe Events.* SAE Int. J. Mater. Manuf., 2010. **3**(1): p. 142-151.

57. Ansari Ardeh, H., et al., *An Expeditious High Fidelity ABAQUS-Based Surrogate Tire Model for Full Vehicle Durability Analysis in ADAMS.* SAE Int. J. Mater. Manuf., 2011. **4**(1): p. 263-277.

58. Schudt, J.A., et al., *Supplementation of Measured Vehicle Road Loads to Study Vehicle Configuration Changes.* 2005.

59. Liu, L., X. Ran, and L. Li, *Hybrid Vehicle Road Loads Simulation and Correlation*. 2007, SAE International.

60. Rui, Y., F. Saleem, and J.H. Zhou, *Road Load Simulation Using Effective Road Profile*. 1997, SAE International.

61. Kang, D., S. Heo, and H. Kim, *Virtual Road Profile Modeling Using Equivalent Damage Method For VPG Simulation*. 2009, SAE International.

62. Tasci, M., et al., *Development of 3-D Digital Proving Ground Profiles for Use in Virtual Prediction of Vehicle System/Sub-System Loads*. 2011, SAE International.

63. S, S., S. S, and N. Saravanan, *Durability Test Sequence and Target Generation for Variants among Commercial Vehicles*. 2013, SAE International.

64. Kasabov, N.K., *Foundations of Neural Networks, Fuzzy Systems, and Knowledge Engineering*. 1996: MIT Press.

65. Hagan, M.T., H.B. Demuth, and M.H. Beale, *Neural network design*. 1st ed. 1996, Boston: PWS Pub.

66. McCulloch, W. and W. Pitts, *A logical calculus of the ideas immanent in nervous activity.* The bulletin of mathematical biophysics, 1943. **5**(4): p. 115-133.

67. *Hebb, D. O. Organization of behavior. New York: Wiley, 1949, pp. 335, $4.00.* Journal of Clinical Psychology, 1950. **6**(3): p. 307-307.

68. Rosenblatt, F., *The perceptron: A probabilistic model for information storage and organization in the brain.* Psychological Review, 1958. **65**(6): p. 386-408.

69. Widrow, B. and M. Hoff. *Adaptive Switching Circuits*. in *1960 {IRE} {WESCON} Convention Record, Part 4*. 1960: {IRE}.

70. Minsky, M. and P. Seymour, *Perceptrons*. 1969, Oxford, England: M.I.T. Press.

71. Kohonen, T., *Correlation Matrix Memories.* IEEE Trans. Comput., 1972. **21**(4): p. 353-359.

72. Rumelhart, D., J.L. McClelland, and P.R. Group, *Parallel Distributed Processing: Explorations in the Microstructure of Cognition: Psychological and Biological Models, Vol. 2*. 1986, Cambridge: MIT Press.

73. Downes, A.W., *The use of artificial neural network techniques in cold roll-forming process design / by Anthony William Downes*. 2006, Thesis (PhD.)--University of Birmingham, School of Engineering, Department of Mechanical and Manufacturing Engineering, 2007.: Birmingham.

74. Lee, J.A., D.P. Almond, and B. Harris, *The use of neural networks for the prediction of fatigue lives of composite materials.* Composites Part A: Applied Science and Manufacturing, 1999. **30**(10): p. 1159-1169.

75. Banerjee, P., et al., *Artificial neural network model as a potential alternative for groundwater salinity forecasting.* Journal of Hydrology, 2011. **398**(3–4): p. 212-220.

76. Adibifard, M., S.A.R. Tabatabaei-Nejad, and E. Khodapanah, *Artificial Neural Network (ANN) to estimate reservoir parameters in Naturally Fractured Reservoirs using well test data.* Journal of Petroleum Science and Engineering, 2014. **122**(0): p. 585-594.

77. Beale, M.H., M.T. Hagan, and H.B. Demuth, *Neural Network Toolbox™ User's Guide*. R2014a ed. 1992 - 2014.

78. Dan Foresee, F. and M.T. Hagan. *Gauss-Newton approximation to Bayesian learning*. in *Neural Networks,1997., International Conference on*. 1997.

79. Lolas, S., *Development of a Reliability Imporvement Expert System using Artificial Intelligence Techniques*, in *Mechanical Engineering*. 2008, University of Birmingham: Brimingham.

80. Kurniawan, W.H., et al., *The Development of Artificial Neural Network for Prediction of Performance and Emissions in a Compressed Natural Gas Engine with Direct Injection System*. 2007, SAE International.

81. Johrendt, J.L., P.R. Frise, and M.A. Malik, *Improving Virtual Durability Simulation with Neural Network Modeling Techniques.* 2005.

82. Leser, C., T.E. Renner, and D.C. Salmon, *Accurate Shock Absorber Load Modeling in an All Terrain Vehicle using Black Box Neural Network Techniques*. 2002, SAE International.

83. Balakrishnan, S., et al., *Accurate Estimation of Time Histories for Improved Durability Prediction Using Artificial Neural Networks.* 2012.

84. Raath, A.D. and C.C.V. Waveren, *A time domain approach to load reconstruction for durability testing.* Engineering Failure Analysis, 1998. **5**(2): p. 113-119.

85. CaTs[3], *QanTiM®* – *Simulation Theory and Application Notes*. 2004.

86. SIMPACK-AG, *SIMPACK 9.6 Documentation*. 2001 - 2014.

87. MathWorks, *MATLAB Documentation*. 1994-2014.

88. Takuya, Y. and N. Toshiaki, *The Improvement of Accuracy of Road Load Input Prediction for Durability.* 2006.

89. Dannbauer, H., et al., *Integrating Virtual Test Methods and Physical Testing to Assure Accuracy and to Reduce Effort and Time.* 2006.

90. Bolarinwa, E.O., *Investigation of The Dynamic Characteristics of Radial Tyre Using the Finite Element Method*, in *School of Mechanical Engineering*. 2004, University of Birmingham.

91. Olatunbosun, O.A., *Automotive Engineering Lecture Notes*. 2010, University of Birmingham.

92. Gillespie, T.D., *Fundamentals of Vehicle Dynamics*. 1992: Society of Automotive Engineers.

93. Ogunoiki, A. and O.A. Olatunbosun, *Characterisation of the Effects of Vehicle Parameter Variations on Vehicle Road Load Data*, in *SAE 2015 World Congress & Exhibition*. 2015, SAE International: Detroit.

94. Minitab, *Minitab 17 Statistical Software [Computer software]*. 2010: State College, PA.

95. Mohsen, B.-E. and T.R. Mohammad, *Application of Bayesian ANN and RJMCMC to predict the grain size of hot strip low carbon steels.* Journal of the Serbian Chemical Society, 2012. **77**(7).

96. Abdulkadir, S.J. and Y. Suet-Peng. *Empirical analysis of parallel-NARX recurrent network for long-term chaotic financial forecasting*. in *Computer and Information Sciences (ICCOINS), 2014 International Conference on*. 2014.

97. Kheirkhah, A., et al., *Improved estimation of electricity demand function by using of artificial neural network, principal component analysis and data envelopment analysis.* Computers & Industrial Engineering, 2013. **64**(1): p. 425-441.

98. Choudhury, T., N. Hosseinzadeh, and C. Berndt, *Improving the generalization ability of an artificial neural network in predicting in-flight particle characteristics of an atmospheric plasma spray process.* Journal of thermal spray technology, 2012. **21**(5): p. 935-949.

99. Ogunoiki, A. and O.A. Olatunbosun, *Artificial Road Load Data Generation using Artificial Neural Networks*, in *SAE 2015 World Congress & Exhibition*. 2015, SAE International: Detroit.